University of Modena and Reggio Emilia

Department of Engineering “Enzo Ferrari

PhD “Enzo Ferrari” in Industrial and Environmental Engineering

XXXV Cycle

SUSTAINABILITY AND DECARBONIZATION OF CEMENTITIOUS CONSTRUCTION MATERIALS

Supervisor:
Prof. Cristina Siligardi

Candidate:
Beatrice Malchiodi

Co-Supervisor:
Prof. Paolo Pozzi

Coordinator of the PhD Program:
Prof. Alberto Muscio

AY 2021-2022

Abstract

Concrete, and more generally cementitious construction materials (mortars, concretes, grouts etc.), is the most widely used material worldwide, being second only to water. Although the CO_2 footprint per kilogram is lower than other construction materials (i.e., asphalt, steel, plastics, glass, etc.), the massive consumption results in the overall contribution of cementitious construction materials to 8% of global CO_2 emissions. In addition, a significant growth in the demand for cementitious building materials is expected in the coming years to meet population growth in emerging countries such as India, Latin America, and Africa and the consequent need for new structures and infrastructures. As a result, CO_2 emissions from cementitious building materials are set to increase.

To reduce the overall environmental impact of the construction sector, there is an urgent need for new and more sustainable construction materials based on recycled materials, alternative raw materials or with optimized properties that allow for minimizing the amount of material used.

This thesis displays different solutions to increase the sustainability of cementitious construction materials while maintaining the performance required for their application. The suggested solutions can be grouped into three classes, namely, (i) reduction of non-renewable resources by using secondary raw materials, (ii) performance optimization of polypropylene fiber-reinforced concrete through the application of surface treatments aimed to improve the fiber-to-matrix adhesion, (iii) use of low-carbon binders with low clinker content.

The first scenario aims both to increase the sustainability of building materials and to address the rising issue of waste management by finding alternatives to disposal in landfills. The use of recycled concrete aggregates (RCA) from Construction and Demolition Waste (CDW) is proposed as a partial replacement for natural aggregates (NA) in producing structural concrete with R_{ck} 30 MPa. Despite the severe limitations of their use prescribed by the Italian construction code, it was observed that both fine and coarse RCA could be successfully used as substitutes for NA. In addition, the prescribed maximum percentage of use (30%) was largely exceeded (up to 90%) while maintaining mechanical performance consistent with the strength class of the designed concrete.
Cork waste from the manufacturing of cork bottle caps was used up to 5 wt.% (65 vol.%) as filler within mortars. It provided lightening and aesthetic properties to mortars without penalizing the mechanical and thermal insulation properties. In fact, despite the poor mechanical properties of cork, it improved the mechanical properties of mortar through the gradual release of water and reduction in mortar porosity. Recycling textile waste microfibers as reinforcement in cement allowed to remediate the equivalent amount of daily microplastic runoff in Paris per ton of fiber-reinforced cement produced. Composite materials with greater toughness, durability and thermal insulation were obtained. 100% replacement of distilled water by microfiltered wastewater was considered to manufacture sustainable mortars. The wastewater was generated during the industrial washing of concrete mixers and later microfiltered to remove aggregates and cementitious sludges. The microfiltered wastewater was characterized and its beneficial influence on workability, setting time and compressive strength test of mortars was assessed.

For the second approach, sustainable surface treatments such as UV-LED, picosecond UV-LASER, and corona discharge treatments were considered in the optimization of polypropylene-fiber reinforced cementitious composites. All treatments provided greater adhesion between PP fibers and cementitious matrices, thus encouraging the use of fiber-reinforced composite materials with PP fibers (lightweight, cost-effective, and durable) rather than those more commonly used in steel.

Finally, highly sustainable structural concretes were designed using innovative low-clinker binders (LC^3). By reducing both the clinker content in the binder and the binder content in concrete, it has been demonstrated how it is possible to cut CO_2 emissions without penalizing the designed mechanical properties.

Riassunto

Il calcestruzzo, e più in generale i materiali da costruzione a matrice cementizia (malte, calcestruzzi ecc.), è il materiale più utilizzato al mondo, secondo solo all'acqua. Anche se l'impatto ambientale dei materiali cementizi per kg di materiale è il più basso di tutti gli altri (asfalto, acciaio, plastica, vetro ecc.), il loro massiccio consumo fa sì che esso contribuisca globalmente all'8% di emissioni di CO_2. Il loro utilizzo, e quindi le loro emissioni di CO_2, subirà un significativo incremento per far fronte alla crescita demografica in Paesi emergenti quali India, America Latina e Africa ed al conseguente bisogno di nuove strutture ed infrastrutture.

Per abbassare globalmente l'impatto ambientale del settore delle costruzioni, c'è un urgente bisogno di nuovi materiali da costruzione sostenibili basati su materie prime alternative o dalle proprietà ottimizzate che ne permettano di ridurne i quantitativi a parità di prestazioni.

Il presente lavoro di tesi propone differenti soluzioni per aumentare la sostenibilità dei materiali da costruzione cementizi mantenendone le prestazioni necessarie alla finalità d'uso. Le soluzioni proposte si raggruppano in tre classi, ossia, (i) riduzione dell'utilizzo di materie prime esauribili tramite impiego di materie prime seconde (ii) ottimizzazione delle prestazioni di calcestruzzi fibrorinforzati (FRC) con fibre in polipropilene (PP) tramite l'applicazione di trattamenti superficiali atti a migliorare l'adesione tra fibra e matrice, (iii) impiego di leganti idraulici sostenibili a ridotto contenuto di clinker.

La prima classe si propone il duplice obiettivo di aumentare la sostenibilità dei materiali da costruzione e di far fronte alla crescente problematica della gestione dei rifiuti, trovando soluzioni alternative al conferimento in discarica. L'uso di aggregati di riciclo derivanti da rifiuti di costruzione e demolizione viene proposto in sostituzione parziale agli aggregati naturali per la produzione di calcestruzzi strutturali con R_{ck} 30MPa. Contrariamente alle forti limitazioni d'uso prescritte dalla normativa italiana, si è osservato che sia gli aggregati fini che grossolani potessero essere impiegati con successo in sostituzione a quelli naturali. In aggiunta, che la percentuale massima prescritta di impiego (30%) potesse essere largamente superata (fino al 90%) mantenendo prestazioni meccaniche soddisfacenti alla classe di resistenza di progetto. Sfridi della produzione di tappi in sughero sono stati impiegati come riempitivi all'interno di malte a base di calce fino al 5% in massa (65% in volume) ed hanno contribuito ad alleggerire le malte e a conferirne proprietà estetiche aggiunte senza penalizzare le proprietà meccaniche di isolamento termico. Il riciclo di microfibre tessili di scarto come rinforzo in cementi ha permesso di riciclare, per tonnellata di cemento FRC, l'equivalente delle microplastiche che piovono ogni giorno a Parigi. Si sono ottenuti prodotti con maggior tenacità, durabilità ed isolamento termico. Una sostituzione del 100% di acqua distillata con acque reflue microfiltrate è stata valutata per la produzione di malte. Le acque reflue sono state generate durante il lavaggio industriale delle betoniere e successivamente microfiltrate per rimuovere aggregati e fanghi cementizi. L'acqua microfiltrata è stata caratterizzata e ne è stata valutata l'influenza positiva sulla lavorabilità, tempo di presa e resistenza alla compressione delle malte.

Per il secondo approccio sono stati considerati ricoprimenti tramite tecnica sol-gel a differenti condizioni di pH, ma anche trattamenti più sostenibili, senza l'impiego di reagenti chimici, quali UV-LED, UV-LASER e scarica corona. Essi hanno permesso di ottenere una maggior adesione tra fibre in PP e matrici cementizie, favorendo così l'impiego di FRC con fibre in PP (leggere, economiche e durevoli) piuttosto che quelle più comunemente impiegate in acciaio.

Infine, calcestruzzi strutturali altamente sostenibili sono stati realizzati tramite l'impiego di innovativi leganti a basso contenuto di clinker (LC^3). Riducendo sia il contenuto di clinker nel legante che il contenuto di legante nel calcestruzzo, è stato dimostrato come sia possibile ridurre le emissioni di CO_2 per area edificata in calcestruzzo senza penalizzare le proprietà meccaniche di progetto.

Contents

List of figures

10. Annex A: Cementitious sludges

11. Annex B: Particle size distribution of the binder components

List of tables

1.Introduction

Climate change, about which we have been warned in the past decades without much follow-up, is beginning to affect our lives. It occurs globally and is intensifying and spreading rapidly. The year 2022 recorded extreme weather events caused by climate change all over the world: severe droughts (Africa and Mexico), hurricanes (Caribbean and Atlantic), destructive floods (South Africa, Australia and Pakistan), and deadly heat waves (Europe, USA, India, Pakistan). As reflected in the uneven distribution of the major catastrophic events, the negative impacts of climate change mainly affect countries that have least affected the environment in the past. Concerningly, the environmental disasters caused by climate change represent the main source of threat for 75% of respondents from all over the world. [1]
The influence of human actions on the environment can no longer be ignored and decisive actions must be taken to limit environmental damage in the future. Global measures and commitments have recently been agreed upon to limit climate damage. The Paris Agreement of 2015 set the goal of keeping global warming below 2°C (compared to the pre-industrial value of the '90s) and targeted to limit it to 1.5°C. Accordingly to the Intergovernmental Panel on Climate Change (IPCC, 2018), this goal could be achieved by halving carbon emissions by 2030 and reaching carbon neutrality by 2050. In this framework, the European Union announced in July 2021 to cut CO_2 emissions by at least 55% by 2030. While globally, during the COP27 (annual United Nations Climate Change Conference) held in Egypt in 2022, it was established that to maintain the 1.5°C target, a 43% reduction in CO_2 emissions by 2030 compared to 2019 must be addressed. [1-3]. As a further indication of the commitment to these goals, philanthropic funding for climate change mitigation research has increased by 25% in 2022. [1]

Regardless of these commitments, a global warming of 2.4° C is occurring nowadays, and prompt and effective solutions must be adopted. [1] Considering that the cement and concrete sector has a major role in the European economy, reducing the emissions related to constructions can be a key contribution in achieving the goals of the Paris Agreement. [2,3]

20% of global annual anthropogenic emissions, or Green House Gas emissions (GHG), come from the embodied GHG emissions of the construction sector [3,4]. Mostly (for around ¾), these emissions are related to concrete and steel because of their high exploitation for structural purposes [3]. The production of cement alone accounts for a quarter to a half of these emissions (5-10% global GHG).
On the other hand, all the operational and maintenance emissions related to the construction sector stand for an additional 30% of global GHG (Figure 1), while operational and embodied ones for 40% of global energy-related GHG emissions. [3,4]
The reduction in energy-related emissions has been successfully addressed recently due to an improvement in the building efficiency and supply of more sustainable energy sources. Contrarily, embodied emissions have been decreased slightly. [3]

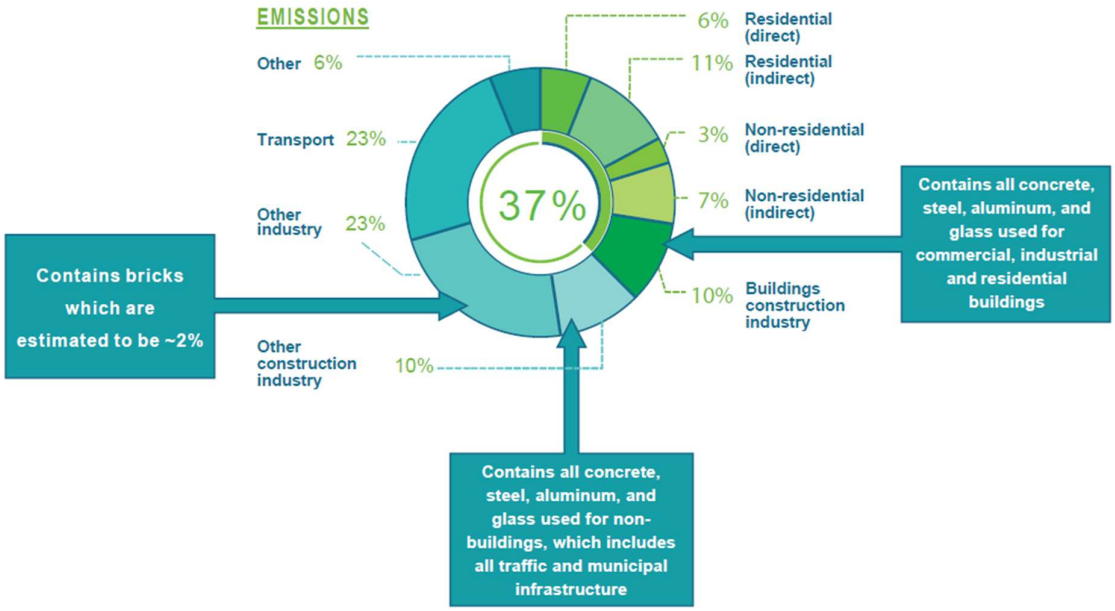

Figure 1. CO_2 emissions in the construction sector [3].

The emissions related to the construction sector are even expected to increase in the future mainly to face the demand for structures and infrastructures in the Global South (including Africa, Latin America, Rest of Asia excluding India and China). There, indeed, the economy and population growth are leading to a fast-developing urbanization and, as a consequence, the request for more construction. [2,3,5,6].

This phenomenon started during the 80s when a shift in global cement demand from the Global North to the Global South/China/India occurred (Figure 2). The demand for cement is expected to increase further during the next decades with clear consequences in terms of GHG emissions if no fast and effective measures will be taken. From now to 2050, 5 billion m^2 of built-up area will be requested each year. Remarkably, this amount corresponds to +150% of the existing built area and 85% of it will occur in the Global South. As an estimation, India and Africa will increase by 50% and 80% respectively in the amount of structures and infrastructures by 2050. On the other hand, the lack of available building areas in the Global North (Europe, North America, Russia and Japan) will encourage the rehabilitation and maintenance of existing buildings and infrastructures, still contributing to 10% of global cement production. [3,4]

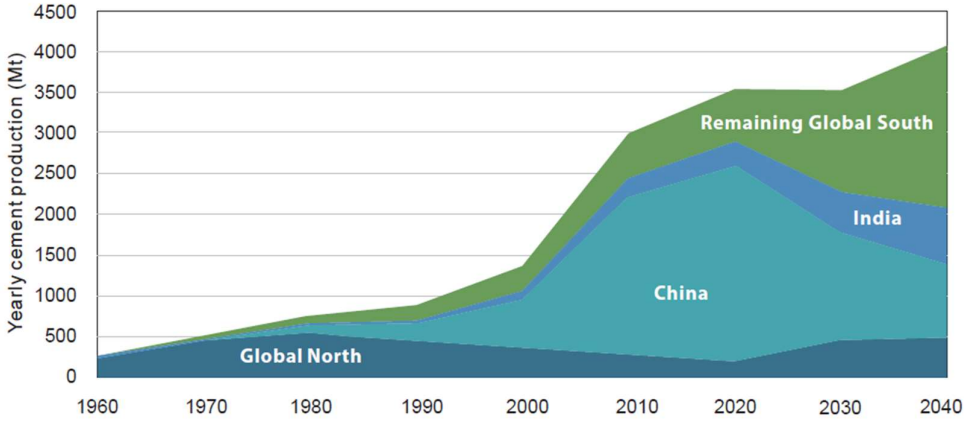

Figure 2. Forecast of the annual cement production over time and Countries.

The rising global demand for construction (Figure 2) can only be met by using cementitious construction materials. Not only because of their exceptional properties, but also because of the easy availability of raw materials, low cost and low-skilled manpower required. Moreover, they are the only ones capable to respond to such a large quantity of construction materials demanded on a global scale. There are other sustainable building materials (timber, biobased materials, materials containing by-products) but in most cases they must be considered for local rather than global demand. Indeed, their availability is localized and limited (by-products) or requires a lot of space and time for cultivation (timber, biobased materials). Moreover, these materials do not always provide suitable mechanical properties like cement-based materials [3].

Achieving sustainability in the construction sector requires ensuring that it does not exhaust natural resources or cause irreversible damage to the quality of the environment, both on a local and global scale. Nowadays, the construction sector is a long way from sustainability.
To limit the annual global warming to 1.5°C, immediate actions must be taken to face the rising demand for constructions. These actions must be easily applicable worldwide, regardless of cultural, geographical, and economic circumstances [3, 4].
It was proven that almost 50% of construction embodied GHG can be reduced by using already available technologies, while a decrease of 80% can be achieved by 2050 considering better practices in the entire construction chain [2,3].
Overall, GHG emissions from constructions can be reduced following these criteria [3,4]:

- Develop low-embodied GHG materials.
- Minimize the exploitation of natural resources and the consumption of manufacturing energy by recycling construction waste and reusing structural elements.
- Minimize the amount of construction materials needed for the structures and infrastructures by optimizing the structural design (-50% GHG).
- Reduce the demand for construction materials by enhancing the durability of structures and infrastructures.

Since cementitious materials stand for greater than 50% of all manufactured materials and will be the ones to meet the construction growing demand, these will play a key role in decarbonizing the construction sector [6]. Specific best practices are suggested to decarbonize the concrete industry and include the reduction of CO_2 emissions at different stages, namely [2]:

- At the clinker production scale: promoting the use of alternative low-CO_2 emitting fuels and increasing the thermal efficiency of the clinker rotary kilns.
- At the cement level: reducing the clinker content in the cement by replacing it with supplementary cementitious materials (SCMs)
- At the concrete level: reducing the cement content in the concrete by optimizing the mix design of concrete.
- At the structure level: reducing the concrete in the structure by optimizing the material mechanical properties or the shape of the structural elements.

However, these good practices can only be effectively implemented if there is a cooperation between all the parties involved in the construction field (scientists, engineers, industries, governments and regulators). Importantly, an impulse for sustainability research funding and a change in regulations should be implemented to promote and fasten this necessary change.
The current regulations, developed when climate change was not an issue, must be reconsidered to include GHG emissions on the same level as safety and functionality [3,4]. As a second reason to change them, the current codes and standards inhibit the adoption of sustainable materials and practices (optimization of the element shape and cross-section) because they are mainly driven by tradition, economic and time constraints, and conservative prescriptions. Moreover, their complexity and numerosity discourage the engineer to adopt sustainable measures and use innovative materials. Finally, it is common knowledge that regulations and codes take many years (even up to 20 years) before they can be updated [3,4]. As a result, they do not reflect contemporary social reality and do not reflect technological and scientific advances [4].

Therefore, the standards need to be (i) reshaped on the GHG emission reduction to reflect the current concerning issues (ii) simplified to allow more freedom in decision-making, and (iii) updated to allow the use of new technologies and sustainable materials. For the latter, a performed-based approach rather than a conservative approach is suggested [3].
Considering the high influence of construction standards and codes (especially for the industry and structural design), their change is expected to cut GHG emissions from the construction sector by up to 50%.

All the suggested criteria are individually effective in reducing the GHG emissions from the construction sector. Nevertheless, the decarbonization of the construction sector can only be achieved by 2050 if all of these are applied simultaneously and if all parties are committed to cooperating. In particular, the role of scientists is to provide evidence that innovative low-carbon materials and materials containing secondary raw materials perform as well as traditional ones, thus supplying enough results for the necessary updating of standards and codes.

References

[1] H. Desanlis, T. Lau, K. Janik, S. Suttenberg, S. Menon, *Funding trends 2022: Climate change mitigation philanthropy,* Climateworks global intelligence.

[2] A. Favier, C. De Wolf, K. Scrivener, G. Habert, A sustainable future for the European cement and concrete industry: Technology assessment for full decarbonisation of the industry by 2050, https://doi.org/10.3929/ethz-b-000301843, 2018

[3] Joint Committee on the Globe Consensus, DECARBONISING GLOBAL CONSTRUCTION, GLOBE - Global Consensus on Sustainability in the Built Environment

[4] GLOBE - Global Consensus on Sustainability in the Built Environment, RILEM. https://www.rilem.net/globe

[5] United Nations, World Urbanization Prospects, the 2011 Revision, (2011). http://esa.un.org/unup/

[6] K.L. Scrivener, V.M. John, E.M. Gartner, Eco-efficient cements: Potential, economically viable solutions for a low-CO2, cement-based materials industry, United Nations Environment Program, 2016.

2. Goal and structure of the thesis

The present thesis work aims to provide different scenarios to achieve the decarbonization of cementitious construction material, thus contributing to the achievement of the global targets fixed by 2050 for the carbon neutrality of the construction sector.

Several performed-based solutions are investigated and proposed as data-driven contributions for the upgrading of construction standards and codes.

The first scenario involves the recycling of waste generated by the construction sector to promote a circular economy and reduce landfilling. This includes the recycling of recycled concrete aggregate from Construction and Demolition waste (CDW), and cementitious sludge and wastewater from the washing of concrete mixers.
Despite the Italian prescriptions for the manufacturing of structural concrete, a replacement ratio of up to 90% of natural aggregate with recycled concrete aggregate (RCA) is investigated and both fine and coarse fractions of RCA are considered. A thorough characterization of RCA is carried out following the reference standards and the resulting properties are used for the mix design of sustainable structural concrete with R_{ck} 30 MPa. Slump test at the fresh state, and apparent density and compressive strength test at the hardened state are used to test the designed sustainable concrete mixes. The main goal is to provide performance-based evidence that the actual code restrictions should be reconsidered to promote recycling and sustainability while reducing the exploitation of natural resources and landfilling.
Cementitious sludges and microfiltered wastewaters are chemically/physically characterized to validate their use as secondary raw materials in new cementitious materials. The microfiltered wastewaters are used in 100% replacement of distilled water to manufacture cementitious mortars and their influence on mechanical performance is assessed by standard compressive strength test.

A second approach to waste management is displayed and involves the reuse of by-products from other manufacturing processes as secondary resources for cementitious construction materials. Cork waste from the manufacturing of cork bottle caps and textile microfibers waste from the finishing of fabrics are considered. Both are investigated in a two-fold strategy to reduce the landfilling of waste and enhance the performance and sustainability of the resulting cementitious composite materials.
Cork waste is added as a filler up to 65 vol.% to reduce the use of cementitious mortars while maintaining the workability, thermal conductivity, and mechanical properties (three-point bending and compressive strength) of the cementitious matrix. A morphological, chemical, physical, and thermal characterization of the cork waste is preliminarily performed, and the resulting properties are used to adjust the mix design of the composite materials.
On the other hand, blend textile microfiber waste is used as fiber reinforcement in Portland cement (fiber-reinforced cementitious composite) and allows for the mitigation of the concerning release of microplastics into the environment. Fiber contents up to 4 wt.% are considered to increase the resistance to crack formation and propagation, and toughness (crack bridging effect). This phenomenon is shown to increase mechanical performance and durability, thus enhancing the sustainability of the final construction material. The apparent density, water absorption and desorption over time of the microfibers are used to design the reinforced composite materials which are later characterized through hydraulic linear shrinkage, three-point bending test and thermal conductance. An estimate of the amount of microplastics (synthetic microfibers) not released into the environment and which contribute to optimizing the properties of construction materials is made.

The third scenario focuses on optimizing the performance of cementitious materials to reduce the amount of construction material used in the structure and make it more durable, thus increasing sustainability at material and structure levels. Fiber-reinforced cementitious materials (FRCC) are considered for this purpose, and precisely, polypropylene (PP) fibers are suggested as a more

sustainable reinforcing alternative to steel fibers. Although the advantages of using PP fibers instead of steel fibers are several, the a-polar surface of PP fibers prevents a good adhesion with the cementitious matrix reducing its attractiveness. Three sustainable functionalizing treatments are considered to promote the fiber-to-matrix adhesion in PP-FRCC, thus the valuable use of PP fibers for structural purposes. As opposed to the chemical treatments proposed in the literature, UV-LED, picosecond LASER and corona discharge sustainable treatments are considered to increase the hydrophilicity of the PP surface. Indeed, besides the effective functionalization provided to the PP surface, these treatments are suggested as faster, no-chemical added, cost-effective and industrially scalable solutions. Different treatment setups and operating conditions are considered. The best treatment conditions are identified as the most effective in increasing hydrophilicity (optical contact angle measurements, OCA) and surface functionalization (Fourier-transformed infrared spectroscopy, FTIR). Later, the effectiveness in increasing the PP-to-matrix adhesion is investigated by considering the pullout test of treated-PP dog-bone samples from lime-based and cement-based mortars. The first cracking strength, residual strength and deformation energy are considered as main mechanical performance indicators; and the behavior of treated-PP composites is compared to untreated-PP composites. Scanning electron microscopy is used to support mechanical evidence.

The fourth scenario suggests a highly promising solution to reduce CO_2 emissions of structural concrete based on the use of a low-clinker blended cement: Limestone Calcined Clay Cement (LC^3). The project has a two-fold strategy to reduce $C0_2$ emissions: (i) reduce the clinker content in concrete considering LC^3 as a binder, (ii) reduce the binder content in concrete considering an optimized particle size distribution of the aggregate. Different clinker contents are considered in LC^3 (25, 35, 50, 60 and 100 wt.%) and different binder contents are considered in concrete (250, 275 and 300 kg/m^3). The raw materials are thoroughly characterized, and the resulting features are used as input data for the concrete mix design. Density measurement, moisture content and water absorption are considered for this purpose. The particle size distribution of the aggregates is optimized considering four fractions (0/4 mm, 4/8 mm, 8/16 mm, 16/22.4 mm) and finding their optimum relative proportion allowing for greater particle size, thus lowering the binder demanded to cover them. High attention is paid to keeping a high-quality aggregate by sieving, washing and drying. Fifteen concrete mixes are prepared and characterized through slump test, 7- and 28-day compressive strength test, 7- and 28-day elastic modulus and rapid chloride penetration test (RCPT). An LCA analysis is finally proposed to see the effective CO_2 saving for each mix.

3. Recycled Concrete Aggregates from CDW as aggregates for structural concrete

Note: This chapter is based on a published conference paper and a journal paper under review in a peer reviewed journal.

Submission title-Conference paper: Recycled Aggregate from Construction and Demolition Waste: characterization and use in sustainable concretes.

B. Malchiodi, V. Barbieri, L. Lanzoni, P. Pozzi, C. Siligardi

Published in ACI Special publication by American Concrete Institute.

DOI: 10.14359/51736046

Contribution of the candidate: experimental design, conduction of the experiments, writing and reviewing, corresponding author.

The use of RCA (Recycled Concrete Aggregate) from CDW (Construction and Demolition Waste) in new concrete production is a promising solution to reduce the exploitation of non-renewable resources and landfill waste. Nowadays, only a small part of CDW is recycled due to severe regulatory restrictions in this field. Specifically, Italian standards enable the use of solely coarse RCA and limit by 30% its replacement rate to natural aggregate for structural concrete >C20/25 and ≤C30/37. In the present paper, concrete waste resulting from a selective demolition procedure was fully characterized and the high potential to develop green structural concrete using high RCA content (both coarse and fine fraction) was outlined. Replacement ratios of 30, 60 and 90 vol.% of natural aggregate by RCA were evaluated and special attention was paid to the concrete mix design based on the specific properties of the aggregate involved. Compressive strength tests following 3, 7 and 28 days of curing outlined the possibility to develop highly sustainable concrete of strength class C25/30, suggesting a viable and sustainable valorisation approach of all particle size fractions of the involved RCA, as well as the necessity of more permissive regulations based on the quality of the RCA used.

3.1. Introduction

The European building sector uses about 3 billion tons of aggregates every year [1] and is a major contributor to the voluminous streams of waste generated, about 35% in mass of the total [2]. These Construction and Demolition Waste (CDW) typically comprise large quantities of concrete rubbles due to the widespread use of concrete as construction material, in addition to bricks, bituminous materials, soil, steel, wood and gypsum. The composition is highly variable and depends on the source and the applied separation techniques [3].

In order to mitigate the fast-increasing CDW stream in landfills and barriers to materials recovery, many standards [4-8], policies, protocols [4] and EU-funded projects (e.g. [5]) have been focused on the incorporation of CDW in construction practice and thus close the loop of the supply chain in line with the principles of the circular economy.

In the last decade, several scientific papers highlighted the high potential for recycling CDW as aggregate [6, 7], finding an alternative to natural resources for new concrete production with multiple benefits (reduction of CO_2 emissions, waste disposal costs, consumption of virgin aggregates) [8].

As extensively documented [3], after crushing and undergoing beneficiation in certified recycling plants, the resulting aggregates from CDW may be assigned to one of the four following categories

depending on their composition: Recycled Concrete Aggregate (RCA); Recycled Masonry Aggregate (RMA); Mixed Recycled Aggregate (MRA) and Construction and Demolition Recycled Aggregate (CDRA). Among all, the RCA (composed of a minimum of 90 wt.% of Portland cement-based fragments and NA) is the most compatible for concrete production since it is obtained from a product with similar characteristics. However, literature data concerning concrete made with RCA are highly variable [9] due to aggregates heterogeneous physical and chemical properties [10]. In fact, RCA quality mostly depends on the parent demolished concrete; a complete characterization is thus needed every time that CDW is used as RA in the mix design of new concretes.

So far, most of the literature studies carried out focused on the use of coarse RCA (particle size > 4mm) as a partial or even complete substitute for coarse Natural Aggregate (NA) in new structural concrete [9-13]. Despite the promising results obtained from academic research, a safe/conservative approach is adopted in regulations currently in use in many EU countries. In particular, the tight constraints for RA quality and maximum recycling rate prevent a wide RA use in real practice [14-17]. In Italy, the maximum allowed replacement rate of coarse NA by RCA is 30% for concrete greater than C20/25 up to C30/37, and 60% for C20/25 maximum concrete class [16].

The use of fine recycled fractions (particle size < 4mm) in concrete products is not yet widely accepted, and regulations in some countries (i.e., Italy, Germany, Spain, France, Portugal, UK) forbid their use in concretes for structural purposes [18]. These limitations are motivated by the discouraging results of early research works that evidenced several issues in both fresh and hardened properties of new concretes due to the high-water absorption and contaminant content in fine RCA [19]. In this context, the studies and practical experiences on proper treatment and fine RA utilization are limited and/or inconclusive. Additionally, only a few researchers report the use of fine RA as a substitute for fine NA in structural concretes [20-22]. However, they mainly evaluate fine RCA from laboratory crushed mortars or concretes that could present differences from the recycled concrete from industrial processes. Therefore, fine RCA is currently used in low-grade applications such as substitutes for natural sand in cementitious renderings and masonry mortars [23], road constructions [24] and as filling material for geo-synthetic reinforced structures and soil stabilization [25].

The use of fine RCA has recently achieved great international interest, mainly because of i) economic implications related to the shortage of natural sands suitable for concrete production; ii) the environmental damage caused by extraction of fine natural aggregate from rivers and seas; iii) the high availability of fine RCA which represent about half of the total CDW weight [19].

In the present work, concrete waste deriving from the demolition of buildings located in the north of Italy was investigated as suitable RCA to produce high-quality concrete for structural applications. The crushed concrete particles of all grades (fine and coarse) resulted from a selective demolition procedure operated by a local company that works in the field of waste disposal, reclamation, and environmental management. In order to obtain CE marking of the RCA produced, all material was thoroughly characterized following regulatory prescriptions [16,17,26-28] evaluating the proprieties of both fine and coarse fractions.

Italian regulation [16] forbids the use of fine RCA in new structural concretes and tightly limits the coarse NA replacement rate with coarse RCA. Conversely, in this work both fine and coarse RCA were studied as possible substitutes of NA in structural concrete mixtures, underling the possibility of using both fractions if suitable characteristics of aggregates are verified. To strengthen the concept of sustainability in civil constructions, the present work combines the use of coarse and fine RCA in high percentages to produce structural concrete with a low environmental impact and suggests more permissive regulations based on the quality and characteristics of the RCA involved.

Considering this final objective, three sustainable concrete mixtures were designed with replacement rates of 30, 60 and 90 vol.% of coarse and fine NA by RCA. A commercial superplasticizer was also

employed in concrete mix design to maintain the same workability for all mixes and reduce water demand. Furthermore, a sulphate-resistant cement type was chosen based on the chemical results of RA characterizations. Compressive strength tests following 3, 7 and 28 days of curing showed the high potential to obtain structural concretes with high RCA content (till 90 vol.% of NA replacement), highlighting a viable and sustainable valorization approach for all particle size fractions of the CDW characterized in the present work.

3.2. Materials

Locally available RCA (in this work renamed as RA for simplicity) resulting from a selective demolition procedure of a concrete building located in northern Italy was involved in the present work. Additionally, NA suitable for structural concrete production was considered and proportionally combined with RA in the concrete mix design. Both aggregates displayed a 0/32 mm particle size distribution and were supplied by A.C.R. S.p.A, a local company engaged in the C&D field and waste disposal. A sulphate-resistant CEM-III/A 42.5R from Cementerie Aldo Barbetti of Ravenna (IT) was employed for the preparation of concrete samples for compression test. Moreover, a commercial superplasticizer (Compactcrete 39T 75R Sika) was employed in the concrete mix design to enhance workability and reduce water demand.

Manufacturing of the concrete specimens

Three sustainable concrete mixtures were considered and aimed at replacing NA with increasing volume percentage of RA, namely Mixture_30% (30%RA-70%NA), Mixture_60% (60%RA-40%NA), Mixture_90% (90%RA-10%NA). Fresh concrete consistency, hardened concrete strength and exposure class were set as desired reference requirements and as input data for the mix design method. In addition, data deriving from aggregates characterization were also involved in this step (Table 1).

Table 1. Mix design of concrete mixtures, input data

Parameter	Target
Concrete consistency class	S4
Concrete strength class	C25/30
Concrete exposure class	XC1/XC2
Cement type	CEMIII/A 42.5 R
Max. particle size	32mm
A parameter (Bolomey curve)	14

Depending on the cement type and required compressive strength at 28 days, the w_{eff}/c ratio (effective water over cement ratio) was evaluated using experimental curves as derived by Abrams's equation for mix design method, which correlates the mean compressive strength (Rm=Rck+3.5MPa) with the w_{eff}/c ratio (see for instance [29]). Hence, considering a CEMIII/A 42.5R and a R_{ck}=30MPa at 28 days, a w_{eff}/c ratio of about 0.59 was graphically extracted. It must be displayed that this value is lower than the corresponding of Prospectus F.1 [17] and so more conservative to set. Indeed, considering the desired exposure class, namely XC1/XC2, a maximum w_{eff}/c of 0.6 is established.

Furthermore, Lyse's correlation between consistency class and maximum particle size allowed to determine the effective water content (w_{eff}) and, consequently, the cement content (c) of the concrete mixture. Since the resulting cement content largely departed from the minimum amount required in Prospectus F.1 [17], then the addition of a superplasticizer was demanded to optimize it. Hence, the minimum allowed cement content of 280 kg/m^3 was considered, the water content was derived as 165 kg/m^3, and the amount of 1.02% of superplasticizer (s) was computed (Table 2). However, these theoretical formulations were adopted solely for Mixture_30%. For Mixture_60% and Mixture_90%,

both w_{eff}/c ratio and superplasticizer content were increased (Table 2) based on experimental attempts to reproduce S4 fresh mixtures. Indeed, the fresh concrete workability tends to decrease at increasing RA percentage, due to aggregate water absorption and morphology [6,19,20,23].

The aggregates volume (V_i) was evaluated as $V_i=1000-w_{eff}-c-10a'-s$ with a' designed air content. Following the RA:NA proportion in Mixture_30%, Mixtue_60% and Mixture_90%, V_i was further divided into RA and NA volumetric content (Table 2). Then the mean bulk density of both RA and NA was considered in dry conditions (as derived from aggregate physical characterization) and used to obtain the total mass of RA and NA for each mix (Table 3). A particle size distribution adjustment of solid fractions (cement and aggregates) was required to optimize concrete compaction and was performed for the designed concrete mixes by referring to the Bolomey reference curve (Fig. 1). Additionally, Table 3 reports, for the designed mixes, a wt.% distinction between fine and coarse fractions of RA and NA. Considering the aggregates water absorption capacity (as obtained from aggregate characterization) and the aggregates content (Table 3), an extra water content (w_{extra}) was involved to theoretically reach the aggregate saturated surface-dry condition. Finally, the mix formulations of the designed concrete mixtures are reported in Table 2.

Table 2. Mix design of concrete mixtures, output data.

Parameter	Unit	Mixture_30%	Mixture_60%	Mixture_90%
w_{eff}/c	-	0.59	0.63	0.63
Effective water (w_{eff})	kg/m^3	165	175	175
Extra water (w_{extra}) [1]	kg/m^3	44	71	100
Cement, CEM III/A 42.5R (c)	kg/m^3	280	280	280
Recycled Aggregate (RA)[2]	kg/m^3	491	968	1457
Natural Aggregate (NA) [2]	kg/m^3	1325	747	187
Superplasticizer (s)	vol/c %	1.02	1.05	1.63
	kg/m^3	3.1	3.2	5.0
Theoretical air content (a')	%	1.5	1.5	1.5

[1] extra water necessary to reach the saturated surface-dry condition of aggregates, [2] dry conditions.

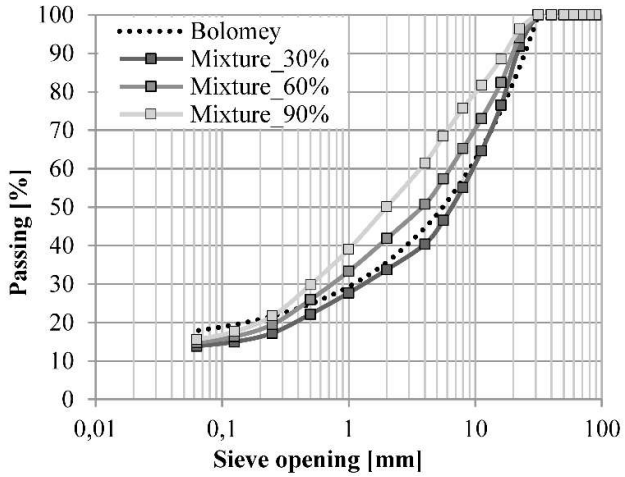

Figure 1. Particle size distribution (cement + aggregates) of the designed concrete mixtures, in comparison with the Bolomey reference curve.

Table 3. Aggregates proportion in concrete mixtures.

Mixture	RA				NA			
	Tot vol. [vol.%]	Tot mass [wt. %]	Fine [wt.%]	Coarse [wt.%]	Tot vol. [vol.%]	Tot mass [wt.%]	Fine [wt.%]	Coarse [wt.%]
Mixture_30%	**30**	27.0	16.1	10.9	**70**	73.0	14.9	58.1
Mixture_60%	**60**	56.4	33.6	22.8	**40**	43.6	8.9	34.7
Mixture_90%	**90**	88.6	52.8	35.8	**10**	11.4	2.3	9.1

To control the concrete production, aggregates were wetted the day before their use and covered with a plastic sheet to maintain the humidity level until the concrete mixing phase. A recommended moisture level equal to the 80% of aggregates absorption capacity (80% of w_{extra}) was pursued [30] to reduce aggregates water absorption capacity in concrete during the cement hydration process [31]. However, recycled aggregates should not be saturated before mixing [32], as that would probably result in the failure of an effective interfacial transition zone between the saturated recycled coarse aggregate and the new cement paste. In line with these recommendations, Poon et al. [31] discovered that the compressive strength of concrete made with saturated aggregate was affected by the bleeding phenomenon.

Firstly cement, superplasticizer, effective water and 20% of extra water were mixed. Then the aggregates, pre-soaked with 80% of w_{extra}, were added to the mixture. The fresh concrete workability was tested at 7 minutes through slump test [33] and provided a lowering of 160 mm for all three mixtures involved. Therefore, the desired input parameter of fresh concrete consistency (S4) was achieved; thus, the mixes resulting from the mix design were properly identified.

Finally, five concrete cubic samples (150mm size) were cast and cured for 7, 14 and 28 days at 20±1°C and RH 95%, for physical and mechanical tests [34].

3.3. Methods

Characterization of RCA

The RA was thoroughly characterized (both fine and coarse fractions) to state the feasibility of its use in new structural concretes. The goal was pursued by following the general prescriptions for aggregates [16,17,28], and the specific requirements for coarse recycled aggregates [26,27] employed in structural concrete. Since the use of RA is prescribed and governed solely for coarse fraction [16], the fine RA properties were evaluated following those required for the use of fine NA [16,17,28].

A mechanical dry sieving test was performed [35,36] to obtain the RA particle size distribution. The considered sieve opening sizes, and so the aggregates fractions derived, were 0.063 mm, 0.125 mm, 0.250 mm, 0.500 mm, 1 mm, 2 mm, 4 mm, 8 mm, 16 mm, 32 mm. Since fillers (<0.063 mm) could significantly influence the RA behavior, their content was computed through the Sand Equivalent test [37] and Methylene Blue test [38]. The Sand Equivalent was determined by the mean of SE_i coefficients, related to two RA samples, where $SE_i=100 \cdot h_2/h_1$ with h_2 sedimentation height and h_1 total height [37]. The Methylene Blue value, corresponding to the absorbed amount of a solution containing methylene blue, was computed as $MB=10 \cdot V_1/M_1$, with V_1 total volume of the injected coloring solution and M_1 sample mass [38].

The surface texture and grain morphology were further detected, for coarse and fine fractions, through optical microscopy (for fractions ≥ 0.250 mm) and Environmental Scanning Electron Microscopy (ESEM Quanta-200 Fei Company, Oxford Instruments, for fractions < 0.250 mm). The evaluation of the Flakiness Index (FI) and Shape Index (SI) allowed defining the geometry of coarse RA [39,40]. The Flakiness Index test quantified the percentage of particles that own one cross-

dimension 0.6 times lower than the average dimension of their particle size class; it was computed as $FI=100 \cdot M_2/M_1$, with M_1 total sample mass and M_2 passing mass through $Ri=Di/2$ bars opening [39]. The Shape Index test quantified the percentage of particles that own a dimensional ratio L/E >3, with particle length L and thickness E; it was computed as $SI=100 \cdot M_2/M_1$, with M_2 mass of particles exceeding the dimensional limit of L/E >3 and M_1 mass of particles under investigation [40].

Furthermore, the examination of physical properties was achieved through bulk density and water absorption evaluation. The parameters were obtained following the Standard's procedure [41] but involving uncleaned RA; thus, detecting the aggregate properties in real application conditions. Besides, the coarse RA mechanical properties were highlighted through the resistance to fragmentation test [42] and by computing the Los Angeles coefficient as $(M_1-M_2)/50$, with M_1 initial mass and M_2 retained mass at the interposed sieve.

Moreover, the lithological composition was investigated through a detailed petrographic analysis and, as normatively required, confirmed by X-Ray Powder Diffraction (XRPD, X'Pert PRO PANAlytical using Bragg-Brentano geometry and Cu Ka radiation) analysis [27]. The petrographic analysis was particularly relevant to detect and quantify potentially alkali-silica reactive components, thus, to classify the potential alkali-silica reactivity of RA in concrete. As prescribed by Standards [27,43], two thin sections were prepared (one for 1/2 mm and one for 2/4 mm fraction) for both fine and ground coarse RA and analyzed using a petrographic microscope with polarized light transmitted and a 4x magnitude lens. A semi-quantitative analysis was performed following method A and employing comparative tables of Appendix F [43].

Finally, a chemical investigation [44] was performed to reveal the content of chemicals potentially contributing to the early degradation of concrete and reinforcing bars. Whereas a leaching test was performed, following environmental regulations [45], on fine RA fraction (1000 g) to simulate the RA real application conditions and detect the possible release of contaminants when in contact with rainwater. A leaching portion of 154 g and an eluent volume of 1.5 L were considered.

Characterization of concrete mixes containing RCA

A mechanical investigation of the three concrete mixtures was achieved by performing a compression test on cubic samples (150mm size) as regulatory prescribed [46]. The compressive strength and hardened concrete apparent density were registered at 3, 7 and 28 days of curing following the test standards [34].

3.4. Results

Particle size distribution and filler content

The particle size distribution of RA was determined as regulatory prescribed [16,35] and reported in Fig. 2 in comparison with the NA one. A prevalence of the fine fraction (around 60 wt.%) was detected for RA, conversely 80 wt.% of coarse fraction was determined for NA. Additionally, the dry mechanical sieving was required to separate the aggregates into particle size fractions, thus, to allow their simpler recombination following the optimized grading curves (see Fig. 1).

Moreover, as reported in Table 4 and Table 5, the RA filler content was considered as not negatively affecting the quality of RA because it satisfied both the regulatory limits of the Sand Equivalent test (SE >70%) and Methylene Blue test (MB ≤1.5 g/kg) [27,37,38].

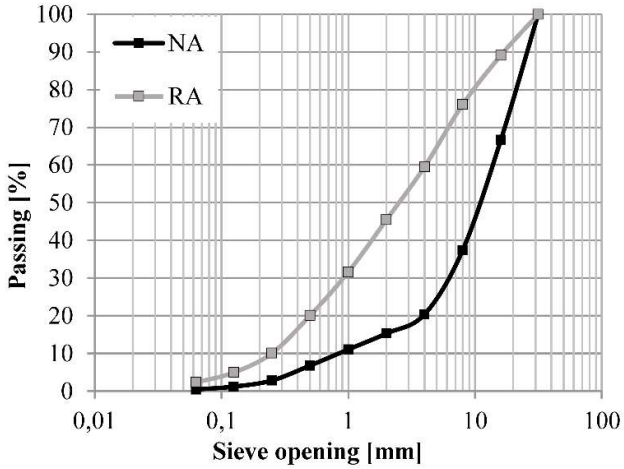

Figure 2. Particle size distributions of NA and RA

Table 4. Sand Equivalent test

Parameter	Unit	Sample 1	Sample 2
h_1	mm	118	123
h_2	mm	87	91
SE_i	%	73.7	74.0
Sand Equivalent SE	%	**74.0**	

h_1 total height, h_2 sedimentation height

Table 5. Methylene Blue test

Parameter	Unit	Value
M_1	g	205
V_1	mm^3	1.5
Methylene Blue value (MB)	g/kg	**0.7**

M_1 sample mass, V_1 total volume of the injected solution

Surface properties and geometry

Differences in texture and grain morphology were observed between RA and NA for all the particle size fractions through optical microscopy (≥ 0.250 mm fractions) and scanning electron microscopy (< 0.250 mm). As reported for the 2/4 mm fraction (Fig. 3) in the representation of all fractions, RA displayed a rougher surface and an angular morphology (Fig. 3a) compared to smooth and rounded NA (Fig. 3b). This evidence confirmed literature data [6,20,24] and must be attributed to the aggregate origin and production process [3,19]. Indeed, the rough surface texture was conferred to RA by the residual porous mortar on grains, while the crashing demolition phase was responsible for the RA angular morphology.

Flakiness Index and Shape Index values (Table 6 and Table 7), resulted in determining an almost ideal cubic geometry of RA and fitting [24] or even exceeding [9,47] the values from the literature. Therefore, this particle geometry is highly suitable for concrete production because it avoids preferable orientation during fresh concrete compaction. Finally, since the average FI and SI were less than 15% (Table 6 and Table 7), then the RA could be classified as FI_{15} and as SI_{15} [17,39,40].

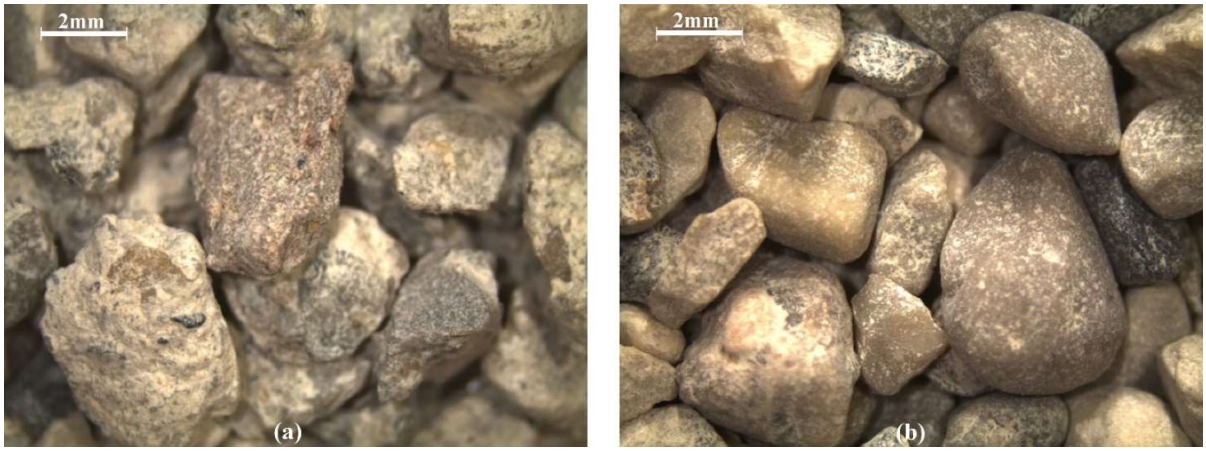

Figure 3. Optical microscopy images of a) RA b) NA

Table 6. Flakiness Index of coarse RA

Sieve opening size [mm]	M_1 [g]	Bar opening size [mm]	M_2 [g]	FI_j [%]
32	182.7	20	0	0
25	78.7	16	0	0
20	441.8	12.5	31.4	7.1
16	1261.9	10	56.6	4.5
12.5	1949.5	8	87.5	4.5
10	1936.6	6.3	119.8	6.2
8	703.6	5	43.5	6.2
6.3	1756.4	4	112.6	6.4
5	2236.3	3.15	158.9	7.1
4	1354.5	2.5	104.4	7.7
Total	11902	Total	714.7	**6.0**

M_1 total sample mass, M_2 mass passing through $R_i=D_i/2$ bars opening

Table 7. Shape Index of coarse RA.

Sieve opening size [mm]	M_1 [g]	M_2 [g]	SI_j [%]
32	182.7	0	0
25	78.7	0	0
20	441.8	69.3	15.7
16	1261.9	31.5	2.5
12.5	1949.5	84.3	4.3
10	1936.6	65.2	3.4
8	703.6	85.6	12.2
6.3	1756.4	84.5	4.8
5	2236.3	155.6	7.0
4	1354.5	107.3	7.9
Total	11902	683.3	**5.7**

M_1 particles mass under investigation, M_2 particles mass exceeding the dimensional limit.

Physical properties

The dry bulk density (ρ_{rd}) and water absorption after 24h of immersion (WA_{24}) are reported for both RA and NA in Table 8. As a direct consequence of the more significant amount of residual porous mortar on the fine fraction, the fine RA displayed a lower density and higher water absorption than

the coarse one [6,8,10,22,24]. Additionally, the RA displayed a significantly lower density and water absorption in comparison with NA. This evidence perfectly reflects the literature findings and matches the typical ρ_{rd} and WA_{24} values of RA [9,10,19-22,24,47].

Besides, referring to Los Angeles resistance to fragmentation in Table 9, the coarse RA could be classified as LA_{30} and, theoretically, be used for structural concrete greater than C50/60 [27,42]. Compared to literature data [21,24,47], the RA under investigation resulted in more resistance to fragmentation, so potentially in a higher feasibility of use for high-performance structural concrete.

Table 8. Dry bulk density and water absorption of RA and NA

Parameter	Unit	RA			NA		
		Fine	Coarse	Mean*	Fine	Coarse	Mean*
ρ_{rd}	kg/m³	2110	2350	2270	2570	2650	2630
	St. dev.	60	30	40	30	5	13
WA_{24}	%	9.4	5.4	6.7	0.6	1	0.8
	St. dev.	0.6	0.8	0.7	0.3	0.1	0.2

**weighted mean depending on the percentage of fine and coarse fractions in RA and NA*

Table 9. Resistance to fragmentation (LA coefficient) of RA

Parameter	Unit	Value
Particle size fraction	mm	4-8
Interposed sieve	mm	6.3
Passing	%	60-70
Spherical abrasive charge	n	8
Initial mass (M_1)	g	5000
Retained mass (M_2)	g	3747
Mass loss percentage (LA)	%	**25.1**

Lithological-mineralogical composition and potential alkali-aggregate reactivity

As reported in Table 10 and Figure 4, the petrographic analysis identified seven lithological components: two of them were crushed recycled concrete composed of residual mortar and original virgin aggregate (i.e. mortar containing feldspathic-quartz aggregate and mortar containing carbonate aggregate, Fig. 4a and Fig. 4b respectively), the others were original virgin aggregates (i.e. carbonate aggregate - Fig. 4c, feldspathic-quartz aggregate - Fig. 4d, microcrystalline glassy aggregate - Fig. 4e, metamorphic marble aggregate - Fig. 4f and polycrystalline quartz aggregate - Fig. 4g). The mean percentage of each lithological component was determined for both fine and coarse RA (see Table 10). For both fractions, the percentage of crushed recycled concrete exceeded the total amount of original virgin aggregates. Furthermore, the content of crushed recycled concrete is higher for fine RA; indeed, it represents around 80% of the fine fraction and 50% of the coarse fraction (see Table 10). It can be assumed that during the RA production, the crushing of parent concrete generated a particle size distribution linearly dependent on the RA lithological composition. Consequently, since the residual mortar adhering to crushed recycled concrete is more friable than the original virgin aggregate, it was expected that mortars should be present mainly in the fine fraction [3,6].

Moreover, since the primary lithological components were represented by crushed recycled concrete and carbonate original virgin aggregate, then silicate and carbonate minerals should be detected as RA main mineralogical phases by XRPD analysis. As reported in Table 11 and in Annex (Fig.7 and Fig.8), XRPD results validated the identification of the petrographic investigation. Indeed, the detected primary mineralogical phases were calcite, dolomite and quartz.

Following the definition of alkali-silica reactive constituents of Annex G [43], the microcrystalline glassy aggregate and polycrystalline quartz aggregate (see Table 10, Fig. 4e, Fig. 4g) could potentially develop an alkali-silica reaction in specific environmental conditions [43,47,48]. Table 10 displays that the two potentially reactive components were almost equally distributed in fine and coarse fractions and that their average amount in RA was around 4% with a prevalence of the microcrystalline glassy aggregate (around 3%). Considering these data and referring to the reactivity of Italian aggregates [43] and expert petrographer's assessment, the RA was classified as potentially reactive but with a low probability to develop an alkali-silica reaction (PR/B classification).

Table 10. Petrographic analysis, mean content of lithological components.

Lithological component [%]	Fine RA	Coarse RA	Average	AAR*
Mortar containing Feldspathic-quartz aggregate	40.7	20	30.3	no
Mortar containing carbonate aggregate	40.7	31.7	36.2	no
Carbonate aggregate	9.7	36.7	23.2	no
Feldspathic-quartz aggregate	5	3.7	4.3	no
Microcrystalline glassy aggregate	2.7	3	2.8	potential
Metamorphic marble aggregate	0	1	0.5	no
Polycrystalline quartz aggregate	1	1	1	potential

**AAR= Alkali-Aggregate-Reaction*

Table 11. Mineralogical composition of all RA fractions.

Sieve opening size [mm]	Primary phases			Secondary phases			
	Calcite	Dolomite	Quartz	Plagiocl.	Microcl.	Muscov/Illite	Kaolinite
32	•	•	•	•	•	•	•
16	•	•	•	•	•	-	-
8	•	•	•	•	•	•	•
4	•	•	•	•	•	-	-
2	•	•	•	•	•	•	-
1	•	•	•	•	•	-	-
0.500	•	•	•	•	•	•	•
0.250	•	•	•	•	•	•	•
0.125	•	•	•	•	•	•	•
0.063	•	•	•	•	•	•	•
<0.063	•	•	•	•	•	•	•

• Detected, - Not detected

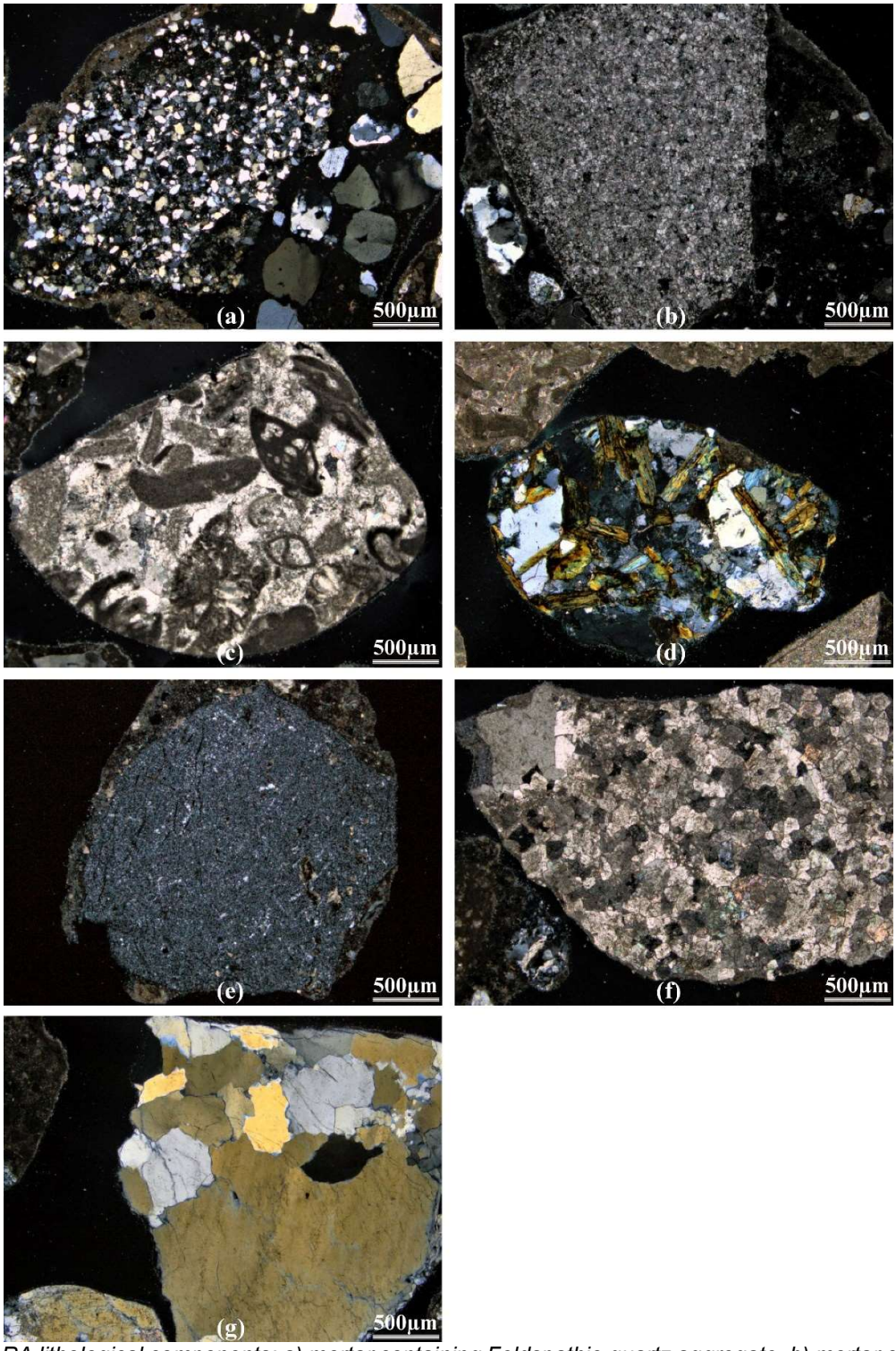

Figure 4. RA lithological components: a) mortar containing Feldspathic-quartz aggregate, b) mortar containing carbonate aggregate, c) carbonate aggregate, d) feldspathic-quartz aggregate, e) microcrystalline glassy aggregate, f) metamorphic marble aggregate g) polycrystalline quartz aggregate.

Chemical and leaching test

As reported in Table 12 and Table 13, RA met all the requirements of the chemical [17,27] and leaching test [45]. Hence, the use of the present RA in concrete mixtures does not contribute to early

concrete degradation or environmental contaminants release in leaching conditions, so the transition of RA status from waste to secondary raw material could be stated. Nevertheless, the results showed a content of acid-soluble sulphate greater than 0.2%. This requirement exceeding would restrict the RA use solely to its fine fraction [27]. So, even if the fine RA is regulatorily forbidden for structural concrete, it is the only one that fits the chemical requirements. Otherwise, the employment of a sulphate resistance cement could involve all the RA particle size assortment.

Table 12. Chemical analysis of RA.

Parameter	Method*	Unit	Limit	Value
Water-soluble Chloride (Cl, fine fraction)	par.7	%	0.03	0.0017
Water-soluble Chloride (Cl, coarse fraction)	par.7	%	0.03	0.0003
Water-soluble Sulphate (SO_4, fine fraction)	par.10	%	0.2	0.0034
Water-soluble Sulphate (SO_4, coarse fraction)	par.10	%	0.2	0.0068
Acid-soluble Sulphate (SO_4)	par.12	%	0.8[1]	0.5781
Total sulphur (S)	par.11	%	1.0[2]	0.1988

**following [44], [1]$AS_{0.8}$ class, [2]limit referred to natural aggregate*

Table 13. Leaching test of RA.

Parameter	Unit/l	Value	Limit
pH (20°C)	-	11.9	5.5-12
Nitrate (NO_3)	mg	4	50
Fluoride (Fl)	mg	0.4	1.5
Sulphate (SO_4)	mg	25	250
Chloride (Cl)	mg	<QL	100
Cyanides (CN)	µg	<QL	50
Barium (Ba)	mg	0.1	1
Copper (Cu)	mg	<QL	0.05
Zinc (Zn)	mg	<QL	3
Beryllium (Be)	µg	<QL	10
Cobalt (Co)	µg	<QL	250
Nickel (Ni)	µg	<QL	10
Vanadium (V)	µg	<QL	250
Arsenic (As)	µg	<QL	50
Cadmium (Cd)	µg	<QL	5
Total chrome (Cr)	µg	49	50
Total lead (Pb)	µg	<QL	50
Selenium (Se)	µg	<QL	10
Mercury (Hg)	µg	<QL	1
COD (O_2)	mg	29	30

QL=Quantification Limit, COD=Chemical Oxygen Demand

Apparent density of concrete

Quite similar values of mean apparent density were observed for Mixture_30% and Mixture_60%, being 2417 ±15 kg/m^3 and 2375 ±18 kg/m^3, respectively. Whereas slightly lower apparent density was found for Mixture_90% (i.e., 2280 ±19 kg/m^3) for all the observed times of curing. Indeed, the curing time appeared as not to affect the apparent density values of the considered hardened concretes.

In line with literature findings [8,20,22], a clear linear trend was found between RA content and a concrete apparent density (Fig. 5a). In detail, Mixture_60% and Mixture_90% displayed a concrete apparent density reduction by 1.7% and 5.7%, respectively, in comparison with Mixture_30%.

The RA content principally contributed to the apparent concrete density reduction. Indeed, since RA displayed a lower density than NA (ρ_{rd}, Table 8), the density of hardened concretes decreased with the increasing RA replacement rate in the mixture [8,20,22]. Moreover, as from mix design and

particle size adjustment of solid fraction (Fig. 1 and Table 3), greater fine fraction contents, lower in density than the coarse one, were considered in concretes with increasing RA percentage. Fig. 5b highlights a rapid linear reduction of total aggregates wt.% content for increasing RA vol.% in the mixture. Precisely, in comparison with Mixture_30%, a reduction of 5.6% for Mixture_60% and 9.5% for Mixture_90% was observed. Besides, a slower linear increase of total water (w_{eff} + w_{extra}) occurred for increasing RA replacement as from mix design results (see Table 3).

Theoretical concrete apparent densities by 2308 kg/m^3, 2244 kg/m^3, and 2204 kg/m^3 were computed for Mixture_30%, Mixture_60% and Mixture_90%, respectively, as the sum of aggregates, total water, cement and superplasticizer contents (see Table 2). Compared to Mixture_30%, reductions by 2.8% and 4.5% of theoretical apparent concrete density were detected for Mixture_60% and Mixture_90%, respectively. As an evidence, theoretical and real concrete apparent density displayed quite a similar reduction trend for increasing RA replacement rate and a relative mean shift (mean over theorical and real concrete apparent density values for 30, 60, 90%RA) by around 4.4%.

Nonetheless, from Mixture_30% to Mixture_90% a higher real apparent density reduction (-5.7%) was depicted compared to the theoretical one (-4.5%). Remarkably, for the real apparent density, this phenomenon principally occurred from Mixture_60% to Mixture_90%, being -4%; whereas the value for the theorical one was -1.8%. Thus, other influencing parameters might have influenced the reduction of the real apparent concrete density in comparison with the theorical one, especially for high RA vol.% content (Mixture_90%). Some works displayed that RA does not reach its theoretical water absorption capacity (WA_{24}, Table 8) during the mixing phase; thus, a portion of extra water (w_{extra}) intended for RA saturation is not effectively absorbed and contributes to modifying the designed w/c ratio, then in lowering the concrete density of Mixture_90% [6,22]. This aspect is emphasized for higher RA content and higher fine fraction as for Mixture_90%. Furthermore, the solid fraction of Mixture_90% showed a greater departure from the Bolomey reference curve (Fig. 1) and, as a result, could have involved a more porous structure so a lower real concrete apparent density.

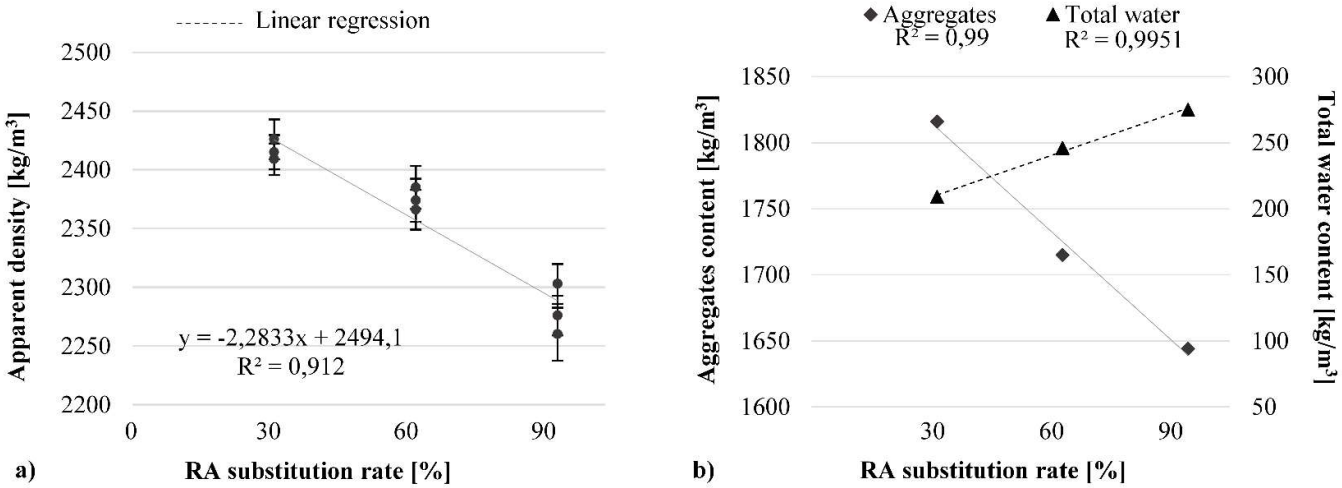

Figure 5. Variability with RA replacement rate of a) mean apparent density of the hardened concrete mixtures, b) aggregates and total water content.

Compression test

Fig. 6 shows compressive strength as a function of curing time (i.e. 3, 7 and 28 days) for Mixture_30%, Mixture_60% and Mixture_90%. As expected, all concrete mixtures increased their compressive strength over time due to the progressive hydration development of the cement matrix. In detail, several works identified the hydration reaction in the new interfacial transition zone,

between the new cement paste and RA, as the main cause of the strength development over time of recycled aggregate concretes [30,49,50].

However, in contrast to the most common results reported in the literature [51,52], no significant compressive strength reduction was observed with the increasing content of RA (i.e., from 30% to 90%) at 3 and 7 days of curing. Indeed, at both curing times, the compressive strength variation between the three types of hardened concretes was found to be lower than 10%. This could be partially justified by the use of the different amounts of superplasticizer and water in the designed concrete mixtures (see Table 2) that could have promoted different early strength development in the three hardened concretes [52, 53].

At 28 days of curing, Mixture_30% and Mixture_60% showed the highest values of mean compressive strength, being around 45MPa for both. Despite the slightly higher w_{eff}/c of the Mixture_60% (see Table 2), the similar performances observed for the two mixtures could be related to the good adhesion between the new cement matrix and the adhered mortar on RA as well as the high quality of RA itself. Indeed, the full RA characterization performed in Section 3.1, outlined not only the fulfilment of the regulatory requirements, but also some similarities to NA (e.g., Los Angeles resistance, shape index) that could positively affect the mechanical performances of the designed concretes [54]. Additionally, some studies [53,55] outlined the possibility to develop sustainable concretes with comparable or even enhanced mechanical performances than the traditional ones, through the use of high-quality RA in replacement to NA.

Compared to Mixture_30% and Mixture_60%, a lower mechanical performance (i.e. -17%) was observed for Mixture_90% which displayed a compressive strength of 37±1MPa at 28 days of curing. A reasonable explanation of this evidence could be the low amount of cement in the concrete mixture (i.e., 280 kg/m^3, see Table 2) to achieve medium-high strength (45-60 MPa). Indeed, to reach better performances at 28 days, some studies [30.56] report the necessity of increasing the amount of cement, and thus reducing the w_{eff}/c, for concrete with a high RA content (till 100%). Moreover, in comparison with Mixture_30% and Mixture_60%, a significant reduction of coarse fraction in Mixture_90% (see Fig. 1 and Table 3) might have contributed to decreasing the concrete mechanical strength assured by the solid fraction.

However, all concrete mixtures reached the required concrete strength for C25/30 class (Rck = 30 MPa) at 7 days yet. Hence, through a suitable concrete mix design and a good RA quality, the minimum regulatory strength could be achieved even by Mixture_90% and, thus, using the highest RA replacement rate.

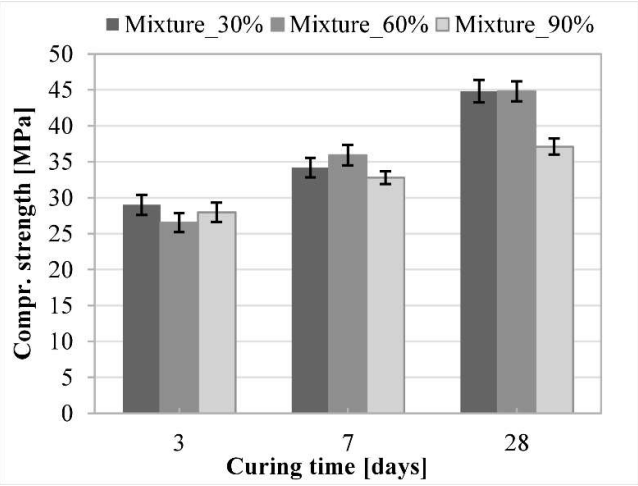

Figure 6. Mean compressive strength of the hardened concrete mixtures at 3, 7 and 28 days of curing.

3.5. Conclusion

Nowadays, the Italian standard (NTC2018) allows the use of RA (or RCA, Recycled Concrete Aggregate) for structural concrete solely in coarse fraction (>4mm). Additionally, for concrete strength class greater than C20/25 and up to C30/37, it limits by 30% the replacement rate of coarse NA with coarse RA. To overcome regulatory prescriptions, both fine and coarse RA were considered and highly sustainable concrete mixtures containing 30, 60, and 90 vol.% of RA were involved.

A thorough RA characterization was performed to establish its feasibility of use in new structural concrete and adequately perform a mix design for each concrete mixture (namely Mixture_30%, Mixture_60%, Mixture_90%). The mixtures were specifically designed to satisfy realistic requirements in terms of fresh concrete consistency (S4), hardened concrete strength (C25/30) and environmental exposure class (XC1/XC2). To achieve the desired workability even for a high RA replacement rate, a higher w/c ratio and superplasticizer content were required. Additionally, a sulphate-resistant cement CEMIII/A was selected due to acid-sulphate content greater than 0.2% in RA.

The principal conclusions resulting from this work are itemized as follows:

1. Coarse RA fulfilled the required conditions for coarse recycled aggregate for structural concrete.
2. Fine RA fulfilled the requirements that must be satisfied by the equivalent fine natural aggregate for structural concrete.
3. Potentially alkali-reactive components were identified to the restricted extent of around 4% and the RA was classified as potentially reactive but with a low probability to develop an alkali-silica reaction (PR/B classification).
4. At increasing RA replacement rate, the apparent concrete density linearly decreased mainly due to the low recycled aggregate density, increasing amount of extra water un-absorbed by the aggregate, higher fine fraction content, and higher departure of the solid fraction (cement+aggregates) from the Bolomey reference curve.
5. In comparison with the other mixtures, at 28 days of curing Mixture_90% displayed a reduction of 17% in compressive strength mainly due to the different mix design and particle size adjustment.
6. Mixture_60% and Mixture_90% reached the 30MPa minimum compressive strength, required for C25/30 class, already at 7 days of curing owing to a good RA quality. At 28 days, the Mixture_90% enhanced by 24% the minimum required strength.

In conclusion, the feasibility of using RA for new structural concrete was demonstrated for both fine and coarse fractions. Moreover, it was exhibited that increasing up to 90vol.% RA in concrete mixture allowed to obtain more sustainable concretes and equally overcome the minimum required compressive strength. The necessity of more permissive regulations based on the quality and characteristics of the RA involved was so underlined. Therefore, the high potential to develop sustainable structural concrete is outlined and proposed as a viable solution for concrete waste recovery and exploitation reduction of non-renewable natural resources.

References

[1] European Aggregates Association, 2020. UEPG Annual Review 2019 - 2020. UEPG 31.

[2] Eurostat, 2018. Waste statistics - Statistics Explained.

[3] Silva, R. V., De Brito, J., Dhir, R.K., 2014. Properties and composition of recycled aggregates from construction and demolition waste suitable for concrete production. Constr. Build. Mater. 65, 201–217. https://doi.org/10.1016/j.conbuildmat.2014.04.117

[4] European Commission, 2016. EU Construction & Demolition Waste Management Protocol. Off. J. Eur. Union.

[5] Interreg Europe, 2020. CONDEREFF [WWW Document]. URL https://www.interregeurope.eu/condereff/ (accessed 5.7.21).

[6] Kisku, N., Joshi, H., Ansari, M., Panda, S.K., Nayak, S., Dutta, S.C., 2017. A critical review and assessment for usage of recycled aggregate as sustainable construction material. Constr. Build. Mater. https://doi.org/10.1016/j.conbuildmat.2016.11.029

[7] Tam, V.W.Y., Soomro, M., Evangelista, A.C.J., 2018. A review of recycled aggregate in concrete applications (2000–2017). Constr. Build. Mater. 172, 272–292. https://doi.org/10.1016/j.conbuildmat.2018.03.240

[8] Zhang, L.W., Sojobi, A.O., Kodur, V.K.R., Liew, K.M., 2019. Effective utilization and recycling of mixed recycled aggregates for a greener environment. J. Clean. Prod. 236. https://doi.org/10.1016/j.jclepro.2019.07.075

[9] Pacheco, J., de Brito, J., Chastre, C., Evangelista, L., 2019. Experimental investigation on the variability of the main mechanical properties of concrete produced with coarse recycled concrete aggregates. Constr. Build. Mater. 201, 110–120. https://doi.org/10.1016/j.conbuildmat.2018.12.200

[10] Khoury, E., Ambrós, W., Cazacliu, B., Sampaio, C.H., Remond, S., 2018. Heterogeneity of recycled concrete aggregates, an intrinsic variability. Constr. Build. Mater. 175, 705–713. https://doi.org/10.1016/j.conbuildmat.2018.04.163

[11] Etxeberria, M., Vázquez, E., Marí, A., Barra, M., 2007. Influence of amount of recycled coarse aggregates and production process on properties of recycled aggregate concrete. Cem. Concr. Res. 37, 735–742. https://doi.org/10.1016/j.cemconres.2007.02.002

[12] Jalilifar, H., Sajedi, F., 2021. Micro-structural analysis of recycled concretes made with recycled coarse concrete aggregates. Constr. Build. Mater. 267. https://doi.org/10.1016/j.conbuildmat.2020.121041

[13] Trottier, C., Zahedi, A., Ziapour, R., Sanchez, L., Locati, F., 2021. Microscopic assessment of recycled concrete aggregate (RCA) mixtures affected by alkali-silica reaction (ASR). Constr. Build. Mater. 269. https://doi.org/10.1016/j.conbuildmat.2020.121250

[14] DIN 1045-2, 2008. Concrete reinforced and prestressed concrete structures-Part2: Concrete - specification, properties, production and conformity - Application rules for DIN EN 206-1.

[15] EHE08, 2008. Code on Structural Concrete.

[16] NTC18, 2018. Norme tecniche per le costruzioni, Decreto Ministeriale 17/01/2018.

[17] UNI EN 206, 2014. Concrete - Specification, performance, production and conformity.

[18] Gonçalves, P., De Brito, J., 2010. Recycled aggregate concrete (RAC) - Comparative analysis of existing specifications. Mag. Concr. Res. 62, 339–346. https://doi.org/10.1680/macr.2008.62.5.339

[19] Nedeljković, M., Visser, J., Šavija, B., Valcke, S., Schlangen, E., 2021. Use of fine recycled concrete aggregates in concrete: A critical review. J. Build. Eng. 38. https://doi.org/10.1016/j.jobe.2021.102196

[20] Manzi, S., Mazzotti, C., Bignozzi, M.C., 2013. Short and long-term behavior of structural concrete with recycled concrete aggregate. Cem. Concr. Compos. 37, 312–318. https://doi.org/10.1016/j.cemconcomp.2013.01.003

[21] Pedro, D., de Brito, J., Evangelista, L., 2017. Structural concrete with simultaneous incorporation of fine and coarse recycled concrete aggregates: Mechanical, durability and long-term properties. Constr. Build. Mater. 154, 294–309. https://doi.org/10.1016/j.conbuildmat.2017.07.215

[22] Puente de Andrade, G., de Castro Polisseni, G., Pepe, M., Toledo Filho, R.D., 2020. Design of structural concrete mixtures containing fine recycled concrete aggregate using packing model. Constr. Build. Mater. 252. https://doi.org/10.1016/j.conbuildmat.2020.119091

[23] Silva, R. V, De Brito, J., Dhir, R.K., 2016. Performance of cementitious renderings and masonry mortars containing recycled aggregates from construction and demolition wastes. Constr. Build. Mater. 105, 400–415. https://doi.org/10.1016/j.conbuildmat.2015.12.171

[24] Sanchez-Cotte, E.H., Fuentes, L., Martinez-Arguelles, G., Rondón Quintana, H.A., Walubita, L.F., Cantero-Durango, J.M., 2020. Influence of recycled concrete aggregates from different sources in hot mix asphalt design. Constr. Build. Mater. 259. https://doi.org/10.1016/j.conbuildmat.2020.120427

[25] Vieira, C.S., Pereira, P.M., Lopes, M.D.L., 2016. Recycled Construction and Demolition Wastes as filling material for geosynthetic reinforced structures. Interface properties. J. Clean. Prod. 1–13. https://doi.org/10.1016/j.jclepro.2016.02.115

[26] UNI 8520-1, 2015. Aggregates for concrete - Additional provisions for the application of EN 12620 - Part 1:Designation and conformity criteria.

[27] UNI 8520-2, 2016. Aggregates for concrete - Additional provisions for the application of EN 12620 - Part 2:Requirements.

[28] UNI EN 12620, 2013. Aggregates for concrete.

[29] Dewar, J., 2003. Concrete mix design, in: Advanced Concrete Technology. Elsevier, pp. 3–40. https://doi.org/10.1016/B978-075065686-3/50287-1

[30] Etxeberria, Miren, Vázquez, E., Mari, A.R., Etxeberria, M, Marí, A., 2006. Microstructure analysis of hardened recycled aggregate concrete. Mag. Concr. Res. 58, 683–690. https://doi.org/10.1680/macr.2006.58.10.683

[31] Poon, C.S., Shui, Z.H., Lam, L., Fok, H., Kou, S.C., 2004b. Influence of moisture states of natural and recycled aggregates on the slump and compressive strength of concrete. Cem. Concr. Res. 34, 31–36. https://doi.org/10.1016/S0008-8846(03)00186-8

[32] Barra, M., Vazquez, E., 1998. Properties of concretes with recycled aggregates: influence of properties of the aggregates and their interpretation, in: Proceeding of the International Symposium on Sustainable Construction:Use of Recycled Concrete Aggregate. London, UK, pp. 19–30.

[33] UNI EN 12350-2, 2019. Testing fresh concrete Part2: Slump test.

[34] UNI EN 12390-3, 2019. Testing hardened concrete Part3: Compressive strength of test specimens.

[35] UNI EN 933-1, 2012. Tests for geometrical properties of aggregates Part 1: Determination of particle size distribution - Sieving method.

[36] UNI EN 933-2, 2020. Tests for geometrical properties of aggregates Part 2: Test sieves, nominal size of apertures.

[37] UNI EN 933-8, 2015. Tests for geometrical properties of aggregates Part 8: Assessment of fines - Sand Equivalent Test.

[38] UNI EN 933-9, 2013. Tests for geometrical properties of aggregates Part 9: Assessment of fines - Methylene blue test.

[39] UNI EN 933-3, 2012. Tests for geometrical properties of aggregates Part 3: Determination of particle shape - Flakiness Index.

[40] UNI EN 933-4, 2008. Tests for geometrical properties of aggregates Part 4: Determination of particle shape - Shape index.

[41] UNI EN 1097-6, 2013. Tests for mechanical and physical properties of aggregates Part6: Determination of particle density and water absorption.

[42] UNI EN 1097-2, 2020. Test for mechanical and physical properties of aggregates - Part 2:Methods for the determination of resistance to fragmentation.

[43] UNI 11530, 2014. Detection of potential alkali-reactivity of aggregates for concrete - Detailed petrographic examination to detect potentially alkali-reactive constituents of aggregates.

[44] UNI EN 1744-1, 2013. Tests for chemical properties of aggregates Part1: Chemical analysis.

[45] D.M. 15/02/1998, 1998. Individuazione dei rifiuti non pericolosi sottoposti alle procedure semplificate di recupero ai sensi degli articoli 31 e 33 del decreto legislativo 5 febbraio 1997, n. 22.

[46] UNI EN 12390-1, 2012. Shape, dimensions and other requirements for specimens and moulds.

[47] Barreto Santos, Miguel, de Brito, J., Santos Silva, A., Hasan Ahmed, H., 2020. Study of ASR in concrete with recycled aggregates: Influence of aggregate reactivity potential and cement type. Constr. Build. Mater. 265, 120743. https://doi.org/10.1016/j.conbuildmat.2020.120743

[48] Barreto Santos, M, de Brito, J., Santos Silva, A., Hawreen, A., 2020. Effect of the source concrete with ASR degradation on the mechanical and physical properties of coarse recycled aggregate. Cem. Concr. Compos. 111.

[49] Poon, C.S., Shui, Z.H., Lam, L., 2004a. Effect of microstructure of ITZ on compressive strength of concrete prepared with recycled aggregates. Constr. Build. Mater. 18, 461–468. https://doi.org/10.1016/j.conbuildmat.2004.03.005

[50] Tam, V.W.Y., Gao, X.F., Tam, C.M., 2005. Microstructural analysis of recycled aggregate concrete produced from two-stage mixing approach. Cem. Concr. Res. 35, 1195–1203. https://doi.org/10.1016/j.cemconres.2004.10.025

[51] Kou, S.C., Poon, C.S., 2012. Enhancing the durability properties of concrete prepared with coarse recycled aggregate. Constr. Build. Mater. 35, 69–76. https://doi.org/10.1016/j.conbuildmat.2012.02.032

[52] Rashid, K., Ul, M., Brito, J. De, Ghafoor, H., 2020. Multi-criteria optimization of recycled aggregate concrete mixes. J. Clean. Prod. 276, 124316. https://doi.org/10.1016/j.jclepro.2020.124316

[53] Soares, D., De Brito, J., Ferreira, J., Pacheco, J., 2014. Use of coarse recycled aggregates from precast concrete rejects: Mechanical and durability performance. Constr. Build. Mater. 71, 263–272. https://doi.org/10.1016/j.conbuildmat.2014.08.034

[54] Tunc, E.T., Alyamac, K.E., 2020. Determination of the relationship between the Los Angeles abrasion values of aggregates and concrete strength using the Response Surface Methodology. Constr. Build. Mater. 260, 119850. https://doi.org/10.1016/j.conbuildmat.2020.119850

[55] Manzi, S., Mazzotti, C., Bignozzi, M.C., 2017. Self-compacting concrete with recycled concrete aggregate: Study of the long-term properties. Constr. Build. Mater. 157, 582–590. https://doi.org/10.1016/j.conbuildmat.2017.09.129

[56] González-Fonteboa, B., Martínez-Abella, F., 2008. Concretes with aggregates from demolition waste and silica fume. Materials and mechanical properties. Build. Environ. 43, 429–437. https://doi.org/10.1016/j.buildenv.2007.01.008

4. Recycling of wastewater from the washing of concrete mixers as mixing water in mortars

Note: This chapter is based on a project with a local company.

Contribution of the candidate: experimental design, conduction of the experiments, writing and reviewing, project manager.

The present work aimed to characterize sludge and wastewater obtained from the washing of concrete mixers to assess the possibility of reusing them to manufacture new cementitious products. This allows for the effective recovery of waste that otherwise would need to be carefully disposed due to its hazardousness. By using sludge (as filler) and wastewater (as mixing water), a significant reduction in the use of virgin natural resources could be achieved, thus succeeding in setting up a circular economy perspective. The project involved the use of sludge and wastewater from two different plants (Milano and Trento): the Milano sludge was supplied after an air-curing process, while the Trento sludge was in the form of liquid slurry. On the other hand, the wastewater was micro-filtered. Various characterization techniques were carried out on sludges and microfiltered wastewaters to assess whether they were suitable for obtaining new cementitious materials and to understand their influence on the properties of the finished product. The microfiltered wastewater was used as mixing water to manufacture mortars. Workability, setting time and compressive strength were analyzed and compared to those of control mortars containing distilled water.

4.1. Introduction

According to Federbeton, world cement consumption in 2020 amounted to 4 billion 138 million tons, substantially in line with the previous year (-0.2%): China, with its 2.4 billion tons of cement (+2% compared to 2019) remains the country with the most significant market in the world [1]. On the other hand, Europe saw a decrease in cement consumption in most countries in 2020, except for Germany (+4%) [1]. Globally, this industry accounts for about 5% of carbon dioxide emissions: the substantial increase in demand for cement is leading to a massive growth in energy consumption and CO2 emissions related to this sector [2].

The same applies to concrete. The intense construction activity, which has been accelerating in recent years, has led to a drastically increased demand for ready-mixed concrete, producing consequent and inevitable environmental pollution, with increasing emissions of carbon dioxide levels and leading to a progressive decrease in natural resources. In Italy, approximately 30 million cubic meters of ready-mixed concrete were produced in 2020, and the last two years have witnessed a further consolidation of consumption, especially due to incentives for building rehabilitation and the desire to boost infrastructures [3].

In this context, it is becoming increasingly important for the construction sector to think from a perspective of environmental and economic sustainability: the indiscriminate exploitation of natural raw materials and disposal in landfills at the end of life (linear economic model) are no longer sustainable and it is becoming increasingly necessary to move towards a circular system, which considers the recovery and reuse of resources in the production cycle a decisive criterion capable of generating further value, thus reducing consumption and polluting emissions [4]. The Federbeton 2019 Sustainability Report [5] shows how the concrete sector has full potential to adapt to the logic of a circular economy, i.e. to be able to integrate the use of recycled material into its production chain: replacing 30% of natural raw materials with recycled ones (over an annual production of 28

million cubic meters of concrete, as recorded in 2019) could save more than 15 million tons of virgin raw materials and, consequently, the percentage of special waste sent to landfill produced annually in Italy (154 million tons in 2019) [4].

In particular, there is much demand worldwide for ready-mixed concrete (the main destination of cement production), which has led to a significant increase in concrete batching plants, where the highest production activity of this building material is concentrated.

However, the lack of appropriate disposal technologies often leads to the concentration of large quantities of sludge and water from the washing of concrete mixers in these plants: as the wastewater is highly alkaline and the sludge is rich in cement, ash, dust and other hydraulic cement materials, it is potentially very polluting if disposed of inappropriately. Proper disposal would involve treatment aimed at eliminating all those substances potentially harmful to the environment and reducing the alkalinity of the water.

A ready-mix concrete plant generates different types of waste: fresh concrete residues, recovered aggregates, concrete slurry waste and wastewater. In Europe, it is estimated that waste concrete sludge, so-called CSW - Concrete Slurry Waste, is in the order of 1-4% by weight of the total processed concrete [6, 7]: from a sustainable development perspective, the possibility of reusing sludge and wastewater from the washing of concrete mixers would reduce the costs of both water treatment and solid waste disposal from mixing plants, thus helping to protect the environment and save water resources [8]. Water and sludge recovered from concrete mixing plants are highly hazardous and corrosive and, if landfilled, can cause a great deal of damage to the surrounding area and ecosystems due to their highly basic pH value and considerable concentration of heavy metals [6].
With this in mind, recent scientific studies have been conducted to understand how to recycle sludge and water. Above all, this was made to assess whether new cement products could be obtained with them, limiting the use of potable water, virgin natural aggregates and/or cement, thus reducing the environmental impact (in light of the ever-increasing demand for concrete and cement). It should be emphasized that this is a relatively recent area of interest: in fact, few articles can be found in the literature relating to the early 2000s, while a growing interest in the topic can be observed from 2014 onwards, peaking between 2019 and 2020 (Figure 1).

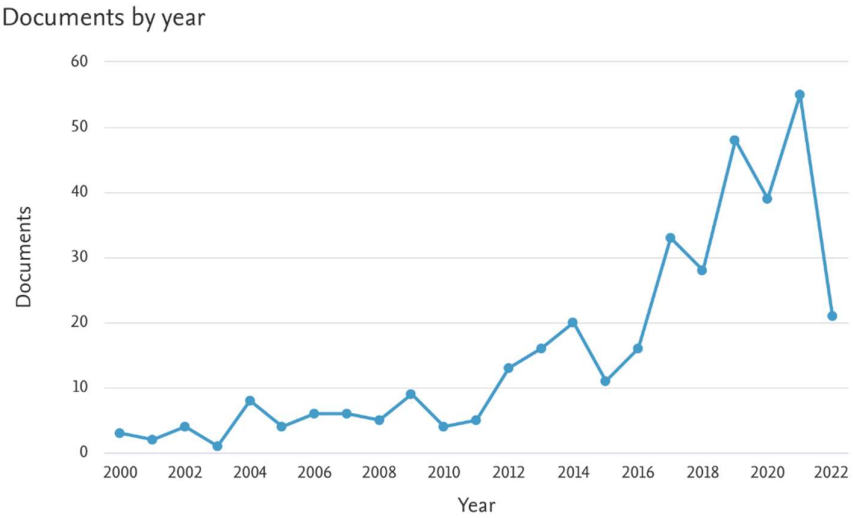

Figure 1. Number of documents published on the recycling of cement sludge and wastewater from 2000 to 2022 (Scopus.com).

In Xuan et al., for instance, adopting the technique of accelerated mineral carbonation, also known as 'CO2 curing', residual sludge was used as a cement binder to manufacture new construction

materials. This technique was used by exploiting the high concentrations of CaO and SiO_2 (>30%) in the residue as a result of cement hydration products [6].

In particular, it was observed that, after only one hour of carbonation, the pH values dropped from 13 to 9, thus reducing the alkalinity of the slurry. Moreover, the carbonated concrete mixtures showed rapid initial development of compressive strength and a reduction in shrinkage during drying compared to those non-carbonated [6]. In another study [9], the environmental sustainability of concrete sludge was assessed using LCA analysis to understand how to efficiently use this waste in producing concrete blocks for partition walls. It was shown that blocks prepared with residual sludge were more sustainable than conventional ones because they consumed less energy and reduced greenhouse gas emissions. In addition, the further use of accelerated carbonation allowed the environmental impact of the production of these blocks to be negligible, thus making them a zero-emission eco-product.

Furthermore, a study was carried out to test a new treatment technology, i.e., reusing wet-milled CSW as a partial substitute for cement [10]. The refined sludge with wet milling was used as a filler to densify the microstructure of the paste and accelerate the hydration processes. The grinding method involved the use of a mill filled with zirconium spheres, sludge and water, which, moving at a speed of 400 rpm, yielded a sludge with a certain viscosity called WCSW. The latter was then substituted in various percentages (from 1-15%) to cement, and the samples obtained were studied in comparison with the control sample (100% cement). The results showed that by increasing the slurry dosage, the initial and final setting time of the cement was significantly reduced. In addition, an improvement in compressive strength and pore distribution was observed, with a reduction in porosity. Therefore, these WCSWs can be considered a good substitute for cement because, besides providing improvements, they would also reduce energy and carbon emissions and cement production. Assuming that the amount of CSW sludge produced in a plant is approximately 0.8% of all the concrete produced, Keppert et al. [11] propose different strategies to recycle it, especially based on the fact that the portlandite and calcite content in these wastes is very high. In particular, the research focused on the use of CSW as a supplementary cementitious material instead of traditional Portland cement. From the results, it was observed that Portland cement could be replaced with 10% CSW slurry without any loss of strength. However, the considerable fineness of CSW required a higher contribution of water in the mix, reducing the strength of the concrete for higher dosages, a problem that could be solved by introducing an admixture to decrease water. Finally, it was observed that CSWs have a high chloride-binding capacity, an advantageous aspect for greater reinforcement protection.

Another significant study by Reiterman et al. investigated the recovery of concrete sludge for soil stabilization in the geotechnical field [12]. As already pointed out, the recovery of residual water is also very important because the water supply is becoming a concern and will have to be addressed by 2050, or a large part of the world's population will be without water [13,14]. The industrial sector is a major consumer of water and, in particular, the construction industry uses a significant amount of water for production processes and the washing of concrete mixers. Therefore, it is particularly necessary to find virtuous solutions for using residual water from the washing of concrete mixers, both to preserve water resources and to deal with disposal issues.

4.2. Sludge waste [Annex A]

The results obtained from the characterization of the cementitious sludges assessed their unfeasibility to be used as secondary raw materials into new cementitious materials due to their high content of chlorides and sulphates. The present section is fully reported in Annex A, chapter 10.

4.3. Microfiltered wastewater

Results

Macroscopic inspection and fixed residue

A macroscopic inspection was carried out for the two as-received samples of microfiltered wastewater called Milano and Trento. As shown in Figure 2, the two samples were transparent and without particle residues (neither floating nor sedimented).

Figure 2. Macroscopic inspection of the two as-received samples of microfiltered wastewater.

Representative samples of the two microfiltered wastewaters were heated at 110°C on a hot-magnetic plate while stirring until completely evaporating. The resulting powder was weight and the fixed residue was evaluated as in Table 1.

Table 1. Fixed residue in the Milano and Trento microfiltered wastewater samples.

	Sample [g]	Residue [g]	Water [g]	Residue %	Residue [mg/L]
Milano	188.39	3.9	184.49	2.07	21138.90
Trento	208.12	3.03	205.09	1.46	14774.07

Chemical-physical analysis

A chemical-physical analysis was carried out for the two microfiltered wastewaters following the main standard test for the characterization of water samples (see standard references in Table 8). The detection of the most relevant parameters and their comparison with the standard limits is shown in Table 2 and Table 3.

The limits selected for the comparison are those required to allow the discharge of wastewater into surface water flows and sewerage systems. Indeed, these are the most common methods for discharging wastewater deriving from the washing of concrete mixers in construction sites.

Table 2. Chemical-physical analysis of the Milano microfiltered wastewater.

PARAMETER	**Unit**	**Value**	**Limits** Surface water **D.Lgs. 152/06 Tab 3**	**Limits** Sewerage **D.Lgs.152/06 Tab 2**	**Test method**
pH	-	12,58	5,5 ÷ 9,5	5,5 ÷ 9,5	APAT CNR IRSA 2060 Man 29 2003
Conductivity	μScm^{-1}	13350	-	-	APAT CNR IRSA 2030 Man 29 2003

Hardness		°F	201,4	-	-	UNI EN ISO 11885:2009
Alkalinity*	$CaCO_3$	mg/l	n.d.	-	-	APAT CNR IRSA 2010 B Man 29 2003
Aluminum	Al	µg/l	6,7	1000	2000	UNI EN ISO 11885:2009
Cadmium	Cd	µg/l	< 1	20	20	UNI EN ISO 11885:2009
Lead	Pb	µg/l	18	200	300	UNI EN ISO 11885:2009
Zinc	Zn	µg/l	4,7	500	1000	UNI EN ISO 11885:2009
Arsenic	As	µg/l	1,3	500	500	UNI EN ISO 11885:2009
Chrome	Cr	µg/l	34	2000	4000	UNI EN ISO 11885:2009
Iron	Fe	µg/l	69	2000	4000	UNI EN ISO 11885:2009
Manganese	Mn	µg/l	< 1	2000	4000	UNI EN ISO 11885:2009
Mercury*	Hg	µg/l	< 1	5	5	UNI EN ISO 11885:2009
Copper	Cu	µg/l	165	100	400	UNI EN ISO 11885:2009
Nickel	Ni	µg/l	1,8	2000	4000	UNI EN ISO 11885:2009
Calcium	Ca	mg/l	800	-	-	UNI EN ISO 11885:2009
Magnesium	Mg	mg/l	0,45	-	-	UNI EN ISO 11885:2009
Sodium	Na	mg/l	169	-	-	UNI EN ISO 11885:2009
Potassium	K	mg/l	661	-	-	UNI EN ISO 11885:2009
Ammonia nitrogen	NH_4^+	mg/l	0,19	15	30	UNI 11669:2017
Sulfate	SO_4^{2-}	mg/l	6,0	1000	1000	UNI EN ISO 10304-1:2009
Chloride	Cl^-	mg/l	75	1200	1200	UNI EN ISO 10304-1:2009
Fluoride	F^-	mg/l	0,451	6	12	UNI EN ISO 10304-1:2009
Nitrate	NO_3^-	mg/l	18	-	-	UNI EN ISO 10304-1:2009
Nitrite	NO_2^-	mg/l	0,15	-	-	UNI EN ISO 10304-1:2009
Phosphate*	PO_4^{3-}	mg/l	< 0,6	-	-	UNI EN ISO 10304-1:2009

Silica* SiO_2	mg/l	0,09	-	-	APAT CNR IRSA 4130 Man 29 2003
Turbidity*	NTU	< 0,1	-	-	APAT CNR IRSA 2110 Man 29 2003
Suspended solids	mg/l	1	80	200	APAT CNR IRSA 2090 B Man 29 2003

Table 3. Chemical-physical analysis of the Trento microfiltered wastewater.

PARAMETER	**Unit**	**Value**	**Limits** Surface water D.Lgs. 152/06 Tab 3	**Limits** Sewerage D.Lgs.152/06 Tab 2	**Test method**
pH	-	12,58	5,5 ÷ 9,5	5,5 ÷ 9,5	APAT CNR IRSA 2060 Man 29 2003
Conductivity	μScm^{-1}	12400			APAT CNR IRSA 2030 Man 29 2003
Hardness	°F	239,0	-	-	UNI EN ISO 11885:2009
Alkalinity* $CaCO_3$	mg/l	n.d.	-	-	APAT CNR IRSA 2010 B Man 29 2003
Aluminum Al	µg/l	3,0	1000	2000	UNI EN ISO 11885:2009
Cadmium Cd	µg/l	< 1	20	20	UNI EN ISO 11885:2009
Lead Pb	µg/l	6,9	200	300	UNI EN ISO 11885:2009
Zinc Zn	µg/l	10	500	1000	UNI EN ISO 11885:2009
Arsenic As	µg/l	1,8	500	500	UNI EN ISO 11885:2009
Chrome Cr	µg/l	84	2000	4000	UNI EN ISO 11885:2009
Iron Fe	µg/l	49	2000	4000	UNI EN ISO 11885:2009
Manganese Mn	µg/l	< 1	2000	4000	UNI EN ISO 11885:2009
Mercury* Hg	µg/l	< 1	5	5	UNI EN ISO 11885:2009
Copper Cu	µg/l	87	100	400	UNI EN ISO 11885:2009
Nickel Ni	µg/l	2,4	2000	4000	UNI EN ISO 11885:2009
Calcium Ca	mg/l	950	-	-	UNI EN ISO 11885:2009
Magnesium Mg	mg/l	0,25	-	-	UNI EN ISO 11885:2009

Sodium	Na	mg/l	95	-	-	UNI EN ISO 11885:2009
Potassium	K	mg/l	321	-	-	UNI EN ISO 11885:2009
Ammonia nitrogen	NH_4^+	mg/l	0,11	15	30	UNI 11669:2017
Sulfate	SO_4^{2-}	mg/l	15	1000	1000	UNI EN ISO 10304-1:2009
Chloride	Cl^-	mg/l	24	1200	1200	UNI EN ISO 10304-1:2009
Fluoride	F^-	mg/l	0,225	6	12	UNI EN ISO 10304-1:2009
Nitrate	NO_3^-	mg/l	13	-	-	UNI EN ISO 10304-1:2009
Nitrite	NO_2^-	mg/l	0,058	-	-	UNI EN ISO 10304-1:2009
Phosphate*	PO_4^{3-}	mg/l	5,0	-	-	UNI EN ISO 10304-1:2009
Silica*	SiO_2	mg/l	0,06	-	-	APAT CNR IRSA 4130 Man 29 2003
Turbidity*		NTU	< 0,1	-	-	APAT CNR IRSA 2110 Man 29 2003
Suspended solids		mg/l	1	80	200	APAT CNR IRSA 2090 B Man 29 2003

Characterization of the residue

The powder residue obtained after the heating of the wastewater until complete drying was characterized in terms of mineralogic composition and particle size distribution.

The qualitative mineralogical composition was studied using X-ray diffractometry (XRD). The X'Pert PRO Diffractometer, PANAlytical was used for this analysis. The results showed that, as found in the Milano sludge, the residue obtained from the Milano microfiltered wastewater was rich in Calcite and Quartz phases (Figure 3). Other potassium-based compounds were very abundant and supported the high alkalinity of the Milano water. Calcite and potassium-based compounds were also found in the residue from the Trento microfiltered wastewater, but Portlandite was additionally found and supported the results from the Trento sludge (Figure 4).

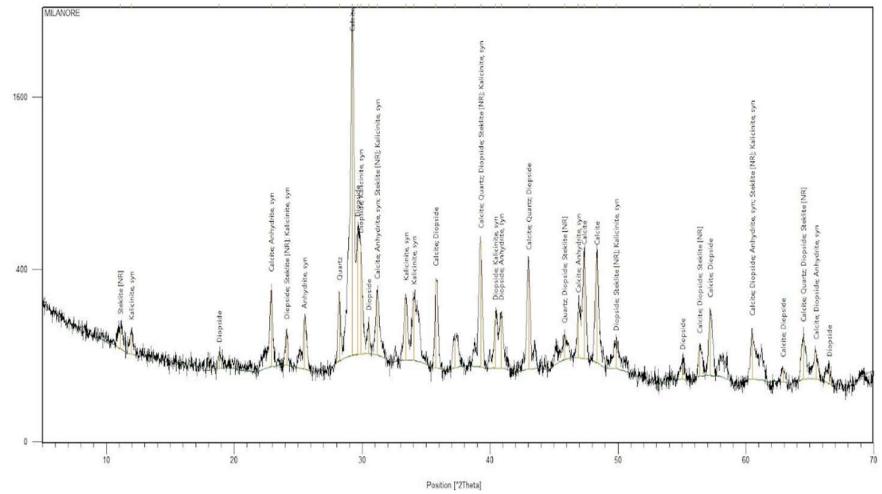

Figure 3. Particle size distribution of the residue from the Milano microfiltered wastewater.

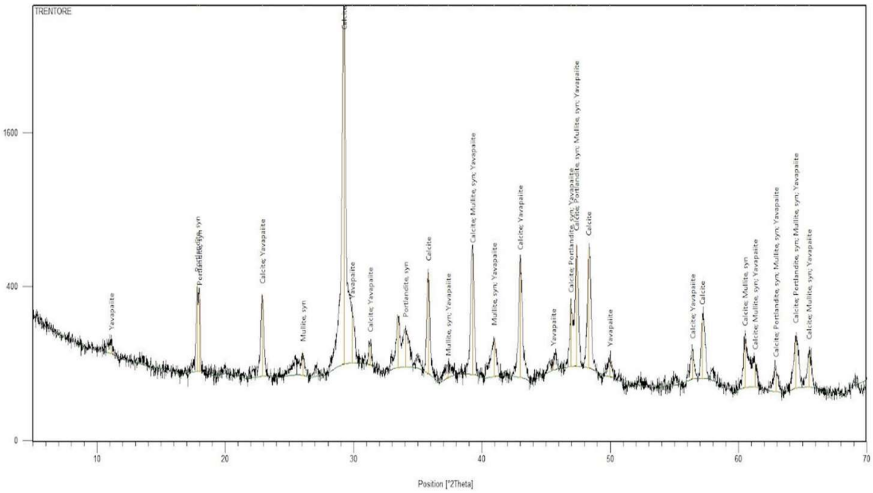

Figure 4. Particle size distribution of the residue from the Trento microfiltered wastewater.

Moreover, a particle size distribution analysis of the two samples was carried out using a Malvern Mastersizer Laser Granulometer 0.1-2000 µm. The residues obtained by both the Milano and Trento microfiltered wastewaters displayed a monomodal trend and comparable d_{10}, d_{50}, and d_{90} values (Figure 5 and Figure 6).

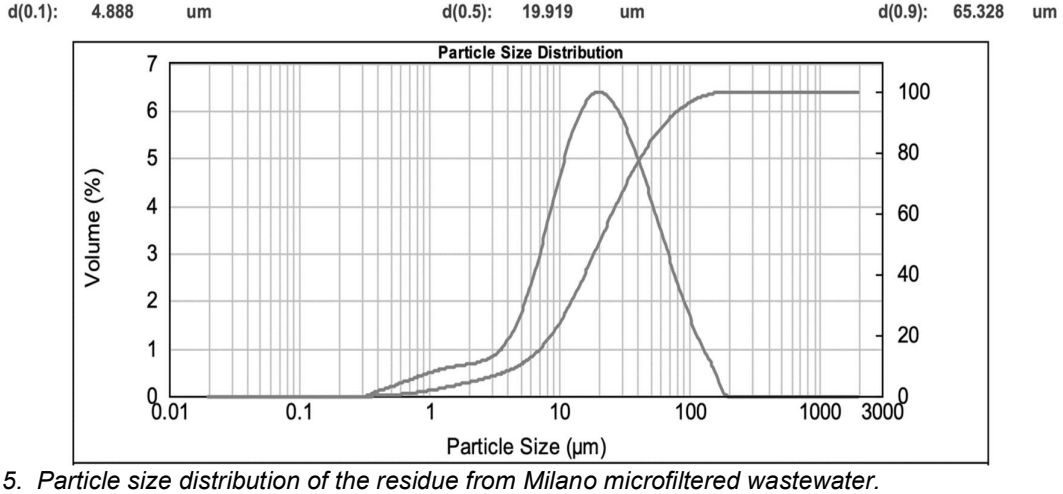

Figure 5. Particle size distribution of the residue from Milano microfiltered wastewater.

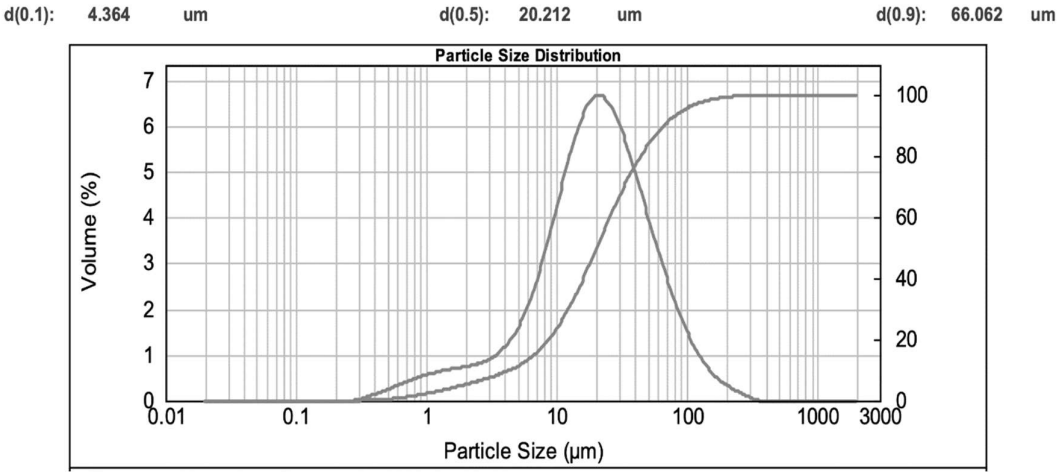

Figure 6. Particle size distribution of the residue from Trento microfiltered wastewater.

4.4. Cementitious mortars

Preparation of the specimens

Cementitious mortars were manufactured using (i) distilled water), (ii) Milano microfiltered wastewater and (iii) Trento microfiltered wastewater. Moreover, the following type of cement (a) CEM IIA 42.5R (b) CEM IVA 42.5R, (c) CEM IIB 32.5R and (d) CEM IVB 32.5R-SR were considered for a total of 12 mixes (Table 9). The cements were provided by Italcementi.

The mixes were manufactured according to UNI EN 196-1 and considering a water/cement ratio of 0.5. Although the relative proportions of the components prescribed by the standard were followed, four specimens (instead of three as from the standard) were produced for each mix. Consequently, 600g cement, 300 water and 1800 normalized sand were considered for each mix.

The mortars were mixed, cast, and vibrated following the standard procedures from the UNI EN 196-1. Mortar specimens of 40x40x160 mm^3 were produced and cured at T° = 25°C ± 2, UR = 60% ± 5% for 2 days and 7 days. Two prismatic specimens for each mix were split through bending test to obtain the 4 specimens of 40x40x80 mm^2 intended for the 2-day compressive strength test. The other two prismatic specimens were split through bending test to obtain the 4 specimens of 40x40x80 mm^2 intended for the 28-day compressive strength test.

Results

Workability

The workability of the mortars, described in Figure 7, was assessed using a flow table and following the requirements of UNI EN 459-2. The average spreading diameter (d_m) was calculated as the average of two orthogonal diameters and rounded to the nearest 1mm. A digital gauge was used to measure the two diameters.
When varying the type of water used (distilled, Trento, Milano), no clear trend in the variation of average spreading value (d_m) is observed. Instead, the variation of this value is influenced more by the type of cement used. In general, it can be stated that the use of microfiltered wastewater provides better workability than distilled water.

For cement type IVA 42.5R and IIB 32.5R, the mixes containing the Trento water displayed higher d_m values than distilled and Milano water. For cement types IIA 42.5R and IVB 32.5R-SR, on the other hand, the mix containing the Milano water had the best workability.

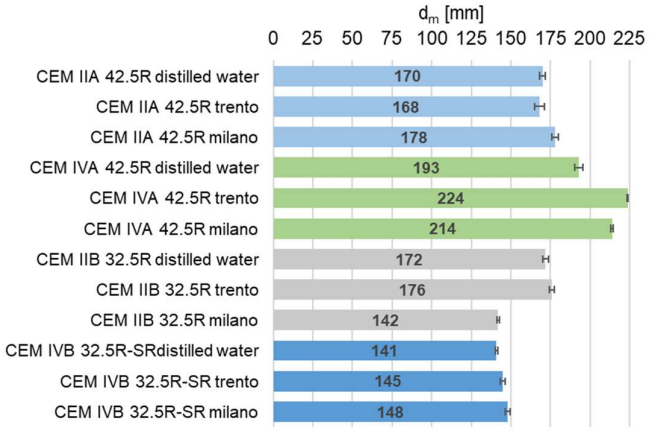

Figure 7. Workability of cementitious mortars containing microfiltered wastewater compared to those containing distilled water.

Setting time

The setting time of the mortars was evaluated using the Vicat needle test (UNI EN 196-3) and measuring the penetration of the needle within the twelve cement pastes of normalized consistency. The results are shown in Table 4. According to the standard, the start of setting time was calculated as the time required to reach a distance between the needle and base plate of 6±3 mm, i.e., at the penetration of the needle to a depth of 33 mm. The end of setting time, on the other hand, was considered as the time in which the needle penetrates the specimen for only 0.5 mm.

A comparison of the results in Table 4 shows, as for the workability test, a dependence of the setting time on the type of cement used. The CEM IIA 42.5R samples showed a shorter setting time (approximately 2 hours) than the others. In contrast, the CEM IVB 32.5R-SR samples displayed the longest setting times.
Overall, shorter starting times (t_0) are noted for samples manufactured with distilled water, except for the samples containing CEM IVA 42.5R for which Trento and Milano microfiltered wastewater promote earlier starting setting times. For all mixes except those containing CEM IVA 42.5R, the Trento and Milano microfiltered wastewaters delayed the start of the setting by a minimum of 20 min (CEM IIA 42.5R, IIB 32.5R) and a maximum of 51 min (CEM IVB 32.5R-SR). The Trento water seems to have the greatest influence on this delay.

The setting time (t) of the mixes ranged between 27 and 69 minutes. The Milano microfiltered wastewater promoted a rapid setting time for the mixtures CEM IIA 42.5R (18min) and CEM IVA 42.5R (27min), compared to the control mixes containing distilled water, 42min and 54min respectively.
In contrast, the Trento microfiltered wastewater promoted almost equivalent setting times to the same control mixtures (48 vs. 42min and 57 vs. 54min).
On the other hand, for the mixtures containing CEM IIB 32.5R, the Milano microfiltered wastewater had similar a setting time to the control (57min vs 51min), while Trento water promoted a longer setting time (69min vs 51min).
For the mixes containing CEM IVB 32.5R-SR, both microfiltered wastewaters showed a lower setting time than the reference with distilled water (about 15min).
Finally, it can be seen that all the mixes complied with the requirements of Table 3 of UNI EN 197-1 in terms of setting time: ≥ 75 min for CEM 32.5R and ≥ 60 min for CEM 42.5R.

Table 4. Vicat needle test of cementitious pastes containing microfiltered wastewater or distilled water. The values refer to t_0 = start of the setting time, t_f = end of the setting time, t = setting time, Δ = difference between the setting time of samples containing microfiltered wastewater and those containing distilled water.

Cement-Water type	t_o [h]	t_f [h]	t [h]	Δ [min]
CEM IIA 42.5R – Distilled water	2:00	2:42	0:42	ref
CEM IIA 42.5R – Trento water	2:19	3:07	0:48	+6
CEM IIA 42.5R – Milano water	2:31	2:49	0:18	-24
CEM IVA 42.5R – Distilled water	3:42	4:36	0:54	ref
CEM IVA 42.5R – Trento water	3:30	4:27	0:57	+3
CEM IVA 42.5R – Milano water	3:20	3:47	0:27	-27
CEM IIB 32.5R – Distilled water	2:50	3:41	0:51	ref
CEM IIB 32.5R – Trento water	3:19	4:28	1:09	+18
CEM IIB 32.5R – Milano water	3:10	4:07	0:57	+6
CEM IVB 32.5R-SR – Distilled water	3:30	4:35	1:05	ref
CEM IVB 32.5R-SR – Trento water	4:21	5:12	0:51	-14
CEM IVB 32.5R-SR – Milano water	4:17	5:05	0:48	-17

Compressive strength

Following the preparation and curing of the mortar samples, compressive strength tests were carried out following the UNI EN 197-1 part 3, at curing times of 2 and 28 days.Four 40 x 40 x 80 mm^3 specimens for each type of mortar and curing time were considered for the experimental mechanical compression testing campaign: for a total of ninety-six samples. The test was performed using UTM INSTRON under displacement control at a displacement rate of 1 mm/min.
Figure 8 and Figure 9 show the compressive strength values of the twelve mortar mixes at 2 and 28 days respectively. It is shown that the relative (compared to the reference sample) differences in compressive strength due to the use of different types of water (with the same type of cement) are the same at 2 and 28 days, except for the mixtures containing CEM IVB 32.5R-SR which are reversed.

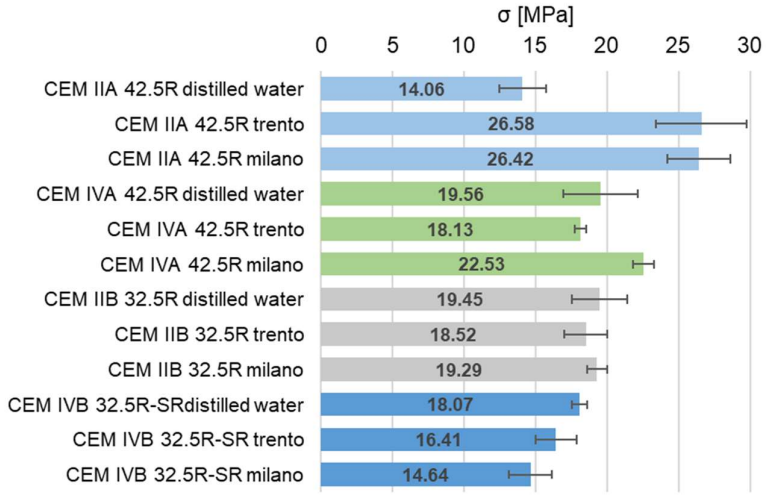

Figure 8. 2-day compressive strength for standard mortars containing microfiltered wastewater and distilled water.

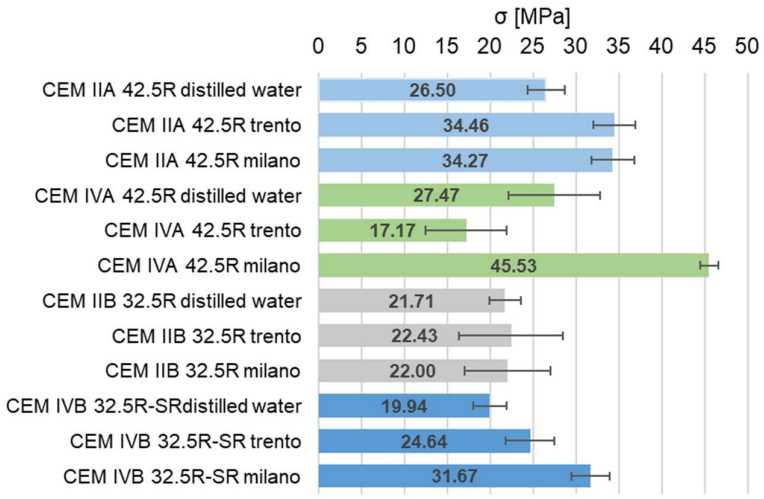

Figure 9. 28-day compressive strength for standard mortars containing microfiltered wastewater and distilled water.

At two days of curing, all the mixes containing CEM 32.5R met the requirements of Table 3, UNI EN 197-1: ≥ 10 MPa. For those containing CEM IIA 42.5R, only the mixes containing microfiltered wastewater achieved the 2-day strengths ≥ 20 MPa. For those containing CEM IVA 42.5R, the strengths were in the range of 20 MPa with the use of all three types of water. On the other hand, the mortars generally exhibited 28-day compressive strengths lower than those from UNI EN 197-1. Overall, the use of microfiltered wastewater did not decrease the mortar compressive strength compared to the use of distilled water, but rather improved it in most cases. Specifically, it was observed that for CEM IIB 32.5R the use of microfiltered wastewater performed equally to that of distilled water, both at 2- and 28-day curing. For the other cements, the use of microfiltered wastewater led to an improvement in mechanical properties, especially at the 28-day curing time and especially for Milano microfiltered wastewater (CEM IVA 42.5R and CEM IVB 32.5R-SR).

4.5. Conclusions

This research work aimed to recycle cement sludges and microfiltered wastewaters resulting from the washing of concrete mixers into new cementitious materials to avoid landfilling and, thus, make the industrial process more environmentally sustainable.

A thorough instrumental characterization highlighted the importance of seasoning the sludges to develop constant and comparable compositions and properties. However, it was concluded that the two sludge wastes under investigation were not suitable for the manufacturing of new cementitious material due to a high sulfates and chlorides content. This type of waste generated by concrete manufacturing, cannot be reused in the construction sector toward a circular economy but should be reused and recycled in other application fields.

Concerning the two microfiltered wastewaters, in general, they present similar properties, although the results of the chemical-physical analyses deviate somewhat from the limits admissible to authorize their discharge into surface waters and the sewerage system. A valorization of these microfiltered wastewaters within new, sustainable cement mixtures or other construction materials would therefore be a solution to the problem of their management and disposal. Conversely, it would be necessary to study solutions for neutralizing pH and lowering certain problematic chemical elements for discharge into surface water and the sewerage system. A first attempt to valorize microfiltered wastewater was conducted by using it as the mixing water in standard cementitious mortars. This solution would make it possible to reduce the use of water to produce mortars and, at

the same time, find an alternative use to discharge for the microfiltered wastewater generated by WAMGROUP's treatment of concrete mixers. Studies on the workability of mortars containing the microfiltered wastewater (composed of four different types of cement) showed comparable or in some cases better values than the same mortars mixed with distilled water. In general, microfiltered wastewaters, and more so Trento water, delay the setting time of mortars compared to distilled water. Depending on the type of cement used, the setting time is (i) kept approximately constant by Trento water and strongly reduced by Milano water, (ii) kept approximately constant by Milano water and prolonged by Trento water, and (iii) reduced by both. Furthermore, it was found that the use of microfiltered wastewater does not penalize the mechanical compressive strength of the mortars at 2 and 28 days of curing, but rather, in most cases, promotes it. Consequently, the use of microfiltered wastewater in the production of cement products constitutes a twofold advantage: it constitutes a solution to the difficult disposal of microfiltered wastewater in surface water and sewerage systems and represents a valorization of microfiltered wastewater for the production of a high-performance and sustainable end product.

References

[1] Federbeton Confindustria, “Rapporto di Sostenibilità 2020.”

[2] A. Hasanbeigi, L. Price, and E. Lin, “Emerging energy-efficiency and CO 2 emission-reduction technologies for cement and concrete production: A technical review,” Renewable and Sustainable Energy Reviews, vol. 16, no. 8. pp. 6220–6238, Oct. 2012. doi: 10.1016/j.rser.2012.07.019.

[3] P. Mezzi, “Edilizia circolare: il recupero del calcestruzzo di ritorno,” Materia Rinnovabile numero 38 / Edilizia circolare, Dec. 07, 2021.

[4] A. Diotti, L. Cominoli, G. Plizzari, and S. Sorlini, “Nuove opportunità dal recupero del calcestruzzo di risulta,” Ecomondo 2021, Oct. 25, 2021.

[5] Federbeton Confindustria, “Rapporto di Sostenibilità 2019.”

[6] D. Xuan, B. Zhan, C. S. Poon, and W. Zheng, “Innovative reuse of concrete slurry waste from ready-mixed concrete plants in construction products,” Journal of Hazardous Materials, vol. 312, pp. 65–72, Jul. 2016, doi: 10.1016/j.jhazmat.2016.03.036.

[7] S. L. Correia, F. L. Souza, G. Dienstmann, and A. M. Segadães, “Assessment of the recycling potential of fresh concrete waste using a factorial design of experiments,” Waste Management, vol. 29, no. 11, pp. 2886–2891, Nov. 2009, doi: 10.1016/j.wasman.2009.06.014.

[8] A. Raza, U. Rafique, and F. ul Haq, “Mechanical and durability behavior of recycled aggregate concrete made with different kinds of wastewater,” Journal of Building Engineering, vol. 34, Feb. 2021, doi: 10.1016/j.jobe.2020.101950.

[9] M. U. Hossain, D. Xuan, and C. S. Poon, “Sustainable management and utilisation of concrete slurry waste: A case study in Hong Kong,” Waste Management, vol. 61, pp. 397–404, Mar. 2017, doi: 10.1016/j.wasman.2017.01.038.

[10] X. He et al., “New treatment technology: The use of wet-milling concrete slurry waste to substitute cement,” Journal of Cleaner Production, vol. 242, Jan. 2020, doi: 10.1016/j.jclepro.2019.118347.

[11] M. Keppert, V. Davidová, B. Doušová, L. Scheinherrová, and P. Reiterman, “Recycling of fresh concrete slurry waste as supplementary cementing material: Characterization, application and leaching of selected elements,” Construction and Building Materials, vol. 300, Sep. 2021, doi: 10.1016/j.conbuildmat.2021.124061.

[12] P. Reiterman, P. Mondschein, B. Doušová, V. Davidová, and M. Keppert, “Utilization of concrete slurry waste for soil stabilization,” Case Studies in Construction Materials, vol. 16, Jun. 2022, doi: 10.1016/j.cscm.2022.e00900.

[13] M. G. Aboelkheir, K. Pal, V. A. Cardoso, R. Celestino, N. K. Yoshikawa, and M. M. Resende, “Influence of concrete mixer washing waste water on the chemical and mechanical properties of mortars,” Journal of Molecular Structure, vol. 1232, p. 3, 2021, doi: 10.1016/j.molstruc.2021.130.

[14] E. Gómez-Llanos, P. Durán-Barroso, and R. Robina-Ramírez, “Analysis of consumer awareness of sustainable water consumption by the water footprint concept,” Science of the Total Environment, vol. 721, Jun. 2020, doi: 10.1016/j.scitotenv.2020.137743.

5. Recycling of cork waste from cork bottle caps as a filler in mortars

Note: This chapter is based on a research paper published in a peer reviewed journal.

Submission title-Conference paper: Recovery of Cork Manufacturing Waste within Mortar and Polyurethane: Feasibility of Use and Physical, Mechanical, Thermal Insulating Properties of the Final Green Composite Construction Materials.

B. Malchiodi, R. Marchetti, L. Barbieri, P. Pozzi

Published in Applied Science, MDPI

DOI: https://doi.org/10.3390/app12083844

Contribution of the candidate: experimental design, conduction of the experiments, writing and reviewing, corresponding author.

The valorization of industrial waste is a hot topic toward circular economy and sustainability. Several wastes have been proposed as resources for different production processes; however, others are still disposed to landfill or waste-to-energy plants. For the first time, this work suggests a sustainable alternative to managing cork waste from bottle caps manufacturing; this is generated by a local company at about 220,000 m^3/year. The powder waste has a 0.063–1 mm particle size and is mainly composed of cork, polyurethane adhesive, and paraffin. Its valorization is proposed as filler in lime-based mortar (1–4 wt.%). Thermal, spectroscopic, and physical characterizations are performed on the cork waste, and mainly result in a low apparent density (340 kg/m^3) and high-water absorption (177%). Cork properties allow consideration of extra water in the mortar mix and improve lightness without significantly affecting compressive, bending strength, and thermal insulation. Considering the promising results, this study demonstrates the feasibility of using the manufacturing waste from cork bottle caps to produce green cementitious construction materials, thus upgrading it from waste to secondary raw material.

5.1. Introduction

The ongoing population growth, which deals with economic, social, and sustainability issues, has resulted in a significant increase in global solid waste generation, which is currently about 17 billion tons and is estimated to become 50 billion tons by 2050 [1].

Therefore, it becomes necessary to seek different solutions and new applications of waste materials, especially in the construction sector. This would reduce the environmental impact of the construction sector, which is responsible for producing 35% of global CO^2 emissions and 45–65% of waste disposed in landfills each year. [2]

Over the last few decades, attempts have been made to reduce the volume of waste in landfills by converting waste into secondary raw materials [3]. The principal construction materials that could benefit from introducing these secondary raw materials are mortar and concrete.

Currently, the most widely reused waste in mortar and concrete is construction and demolition waste (CDW), which seeks to solve the problem of natural aggregates exploitation and the increasing

production of CDW [4]. Glass waste [5], polymer waste [6], and natural fiber waste [7,8] are also involved in improving sustainability and lightness to the final product.

To avoid expensive disposal, several hazardous wastes which can be flammable, chemically reactive, or corrosive [9] are currently reused as a substitute for natural aggregates or cement (SCM) [10–13]. This also results in decreased demand for cement and natural resources and reduced CO^2 emissions [4]. In addition, it was displayed that some waste can promote the compressive strength of cementitious materials under elevated temperatures [14].

In the literature, some work has focused on the use of virgin cork and very few on cork waste in mortar and concrete. As a result of adding a lightweight material into a cementitious matrix, the introduction of cork is known to decrease the mechanical performance of the finished product. However, it has been shown not to affect it excessively, and the final products remain classifiable according to the strength classes of UNI EN 998-2 [15,16]. Density decreases and thermal conductivity depends on the sample curing conditions, thus on the presence of residual water within the cork [15,17].

In this framework, this paper proposes for the first time the valorization of cork waste from the manufacturing of cork bottle caps within lime-based mortar. Thus, this work aimed to fill the research gap of cork waste recycling, reduce the large volume of waste in landfills or waste-to-energy plants and provide sustainability to the most important construction material.

Cork is a natural material from the bark of the oak Quercus Suber L. and is mainly present in the western Mediterranean Sea area, including Sicily, Sardinia, Maremma of Grosseto, Corsica, Spain, and Portugal. The cork production involves about 20,000 km2 in the Mediterranean area for an annual extraction of 300,000 t [18]. Portugal is the first cork producer with about 52% of world production, followed by Spain (25%) and then all the other countries of the Mediterranean basin including Italy with 6%, concentrated for 4% in Sardinia [18].

Its primary use is in manufacturing wine bottle caps: globally, about 12 billion caps are produced per year [18]. In Italy, particularly in the Emilia Romagna region, and precisely in Reggio Emilia and Parma, cork factories have an ancient tradition.

Cork extraction and processing include several phases. The decortication is carried out between May and June when the bark is softer, and the damage to the plant is prevented. It is a delicate operation entrusted to specialized workers that allows the extraction of large sheets of bark called planks. The planks are then stored for seasoning and selected based on aesthetics. Cork planks with defects are milled and directly transformed into agglomerates for the building industry or agglomerated wine caps. On the other hand, cork planks without defects are used to produce high-quality cork caps. [18] During the cork trimming and cutting phase of high-quality cork caps, a large quantity of cork residue is generated, which is also used to produce agglomerated cork caps (micro agglomerated caps or pieces for sparkling wine caps).

The production of agglomerated cork caps first involves the selection of virgin cork residue (around 79 wt.%) depending on granulometry, then the mixing with a binder and other additives (around 21 wt.%, i.e., polyurethane glue and paraffin). The mixture is compressed and extruded at 95–105 °C to obtain the polymerization of the polymeric component. Alternatively, the mixture could be pressed and die-cut. Subsequently, a cutting phase occurs and provides agglomerated cork cylinders. Agglomerated caps may differ because of the residue granulometry, type of glue, compressive strength, etc. [19]. Finally, the caps are smoothed, and a large amount of fine cork waste is produced during this phase. This is usually delivered to waste-to-energy plants and not reused in cork manufacturing or other industrial processes.

The local company that supplied the cork waste under investigation produces about 240 t/year of cork residue, corresponding to 218,000 m^3. Since it cannot be reinserted within the same

manufacturing process, the most problematic residue is the one containing cork, polyurethane glue and paraffin deriving from the smoothing process of agglomerated bottle caps.

This work proposes a viable solution for the recycling of cork waste from the manufacturing of agglomerated bottle caps, considering its application as filler in traditional construction materials (i.e., mortar). This valorization approach is aimed to solve real waste management issues of the local company as well as contribute to the hot research topic on waste recycling. Since no evidence on cork waste has been registered by literature, this work assesses for the first time its properties and influence on those of the cementitious matrix in which it could be used as filler.

To this aim, a thorough preliminary characterization of the cork waste was performed, and morphological, chemical, physical, and thermal properties were investigated. Then, increasing cork waste content was considered in mortars to maximize the recycling effectiveness. Namely from 1 wt.% to 4 wt.% (from 16 vol.% to 65 vol.%) within lime-based mortar. Optical microscopy, colorimetry, apparent density, thermal conductivity, three-point bending, and compressive strength tests were carried out to detect the influence of cork addition on the properties of a commercial mortar. A curing of 35 days and drying at 50 °C for 12 h were considered for mortar samples to avoid the influence of cork humidity during testing.

5.2. Materials and Methods

Cork Waste

A cork waste from the manufacturing process of agglomerated cork bottle caps of a local company (Italsughero, Montecchio Emilia (RE), Italy) was considered. Precisely, this powder waste is generated during the smoothing phase of agglomerated cork caps and is directly collected through a cyclonic air-filtering system. The involved cork waste has a particle size distribution of 0.063 mm < d < 1 mm and contains polyurethane glue and paraffin which are industrially used as binders and additives for cork particles, respectively.

Simultaneous thermal analysis (STA 449 F3 Jupiter, Netzsch-Gerätebau GMBH, Selb, Germany) was considered for thermal characterization and composition description of cork waste. This technique allowed the merging of differential scanning calorimetry (DSC) and thermal gravimetric analysis (TGA) in the same measurement. Thus, it allowed relating each thermal transformation of the material to the corresponding mass loss. The test was performed considering a heating ramp from 0 °C to 900 °C at 10 °C/min heating rate, a silicon furnace (heating up to 1500°C), and aluminum crucibles. Data analysis was carried out through Proteus software (Netzsch Proteus Thermal Analysis, Proteus 6.1.0, Netzsch-Gerätebau GmbH, Selb, Germany), resulting in a combined plot of DSC, TGA and the first derivative of TGA (DTGA). The composition of cork waste was also detected through attenuated total reflectance Fourier transformation infrared spectroscopy (ATR-FT-IR analysis, FTIR VERTEX 70, Bruker Optics, Germany). A transmittance range between 400–4000 cm^{-1}, 32 scans, and a resolution of 4 cm^{-1} was considered, while FTIR spectra were analyzed through OPUS software (OPUS 6.5, Bruker Optics GmbH, Selb, Germany).

A laser particle sizer (Malvern Mastersizer 2000, Malvern Panalytical Ltd., Malvern, UK) was used to determine the particle size distribution of cork waste particles. Optical microscopy (LEICA EZ4D, Leica Microsystems) with 8×, 20× and 35× magnitude was considered for the morphological description of cork waste particles.

According to UNI EN 1079-6 2013, water absorption (WA) and apparent density (ρ_{rd}) values were evaluated by performing a 24 h water absorption test. Finally, real density was measured through a helium pycnometer (Micrometrics Accupyc 1330, Micrometrics Instruments).

Mortars

The first attempt to valorize the cork waste involved its use as filler within mortars. A commercially available mortar (GeoCalce Antisismico G by Kerakoll S.p.A., Sassuolo - MO, Italy) for historical buildings restoring and improving seismic resistance was considered. The binder is mainly composed of natural hydraulic lime NHL 3.5 and Portland cement. While the aggregate has a particle size between 0 mm and 2.5 mm, and a silicate-carbonate mineralogic composition. The technical data sheet points out an optimized effective water (w_{eff})-to-mortar ratio of 0.204, and a fresh mortar flow diameter of 180 mm (UNI EN 459-2:2002). Moreover, it certifies the mortar as belonging to the M15 strength class (UNI EN 998-2).

Increasing cork content was added from 1 wt.% to 4 wt.% of mortar, which in terms of volume corresponds to much higher percentages, 16 vol.% and 65 vol.%, respectively.

The mix design of the four lime-based mortars containing cork waste is reported in Table 1 compared to the reference commercial one. As displayed in Table 1, a contribution of effective water (w_{eff}) was set to reproduce an effective water-to-mortar ratio equal to 0.204. At the same time, extra water (w_{extra}) was also considered to compensate for the amount of water absorbed by the cork, as assessed by the WA test on cork waste.

Table 1. Mix design of mortars containing increasing content of cork waste (from 0 wt.% to 4 wt.%).

Cork (wt.%)	Cork (vol.%)	Cork (g)	Mortar [1] (g)	Eff. water [2] (g)	Extra water [3] (g)	Superplast. (g)
0	0.00	0.00	8041.04	1604.40	0.00	0.00
1	16.15	69.31	6931.04	1413.93	122.88	29.6
3	48.49	162.04	5431.49	1108.02	288.88	49.84
4	64.66	196.05	4901.29	999.86	347.58	44.96

[1] NHL3.5 + Portland cement + natural aggregate, commercial powder mix.
[2] water available for the binder hydration.
[3] water added to compensate for water absorption by the cork.

The workability of the reference mortar (flow diameter of 180 mm) was set as the target value to be also maintained for mixes containing cork. Thereby, the flow table test (UNI EN 459-2:2002, performed through Flow Table 64, ControlsGroup, Milan, Italy) was preliminary involved to evaluate the effect of filler addition on workability. In order to improve the workability of the fresh mortars containing cork waste, a commercial superplasticizer was considered following its datasheet prescriptions and as reported in Table 1. Cork contents higher than 4 wt.% were not considered due to workability issues.

First, water and mortar were mixed at low speed (300 rpm) for 30 s through a high-speed laboratory mixer (RW20 DZM, IKA-Werke GmbH & Co. KG, Staufen, Germany), then the cork was added, continuing mixing for other 30 s. Subsequently, the mixing phase continued for 1:30 min at high speed (500 rpm), following the prescriptions of UNI EN 459-2:2002.

The mixes were cast into 40 × 40 × 160 mm^3 and 300 × 300 × 30 mm^3 formworks to produce samples for the three-point bending and thermal conductivity tests, respectively. Four samples for mechanical tests and three for thermal conductivity were produced for each mortar type.

According to UNI EN 196-1, samples were cured for 28 days in a climatic chamber with RH 90% ± 5% and a temperature of 20 °C ± 2 °C. Moreover, additional 7 days of cure at laboratory conditions

(RH 60% ± 5% and temperature of 25 °C ± 2 °C) were considered to have complete evaporation of the water potentially still present in cork particles.

Four 40 × 40 × 160 mm^3 samples for each designed mix were mechanically tested through three-point bending, while a compressive strength test was carried out on four 40x40x40 mm^3 residual samples from the three-point bending test. The tests were performed following the UNI EN 196-1:2005 and using a universal testing machine (UTM, INSTRON 5567) equipped with a load cell of 30 kN. The three-point bending test was performed at a nominal rate of 1mm/min under displacement control mode, and a distance of 10 cm was set between the two steel supports. The compressive strength test was also carried out with the same testing parameters and using two circular steel plates.

Apparent density was geometrically evaluated as the ratio between the measured mass and the known volume (40 × 40 × 160 mm^3). The mean apparent density of each hardened mortar type was computed as the average over three measurements.

Optical microscopy (LEICA EZ4D, Leica Microsystems) allowed the description of the cork distribution within the mortar, whereas the colorimetry (CIELab method through PCE-CSM6 colorimeter, PCE Instruments) to see the color change of mortar samples at increasing cork content.

The thermal conductivity of mortars was measured through a heat flow meter (HFM Lambda, Netzsch-Gerätebau GmbH, Selb, Germany) after drying the samples for 12 h at 50 °C; the mean thermal conductivity was derived as the average over three measurements.

5.3. Results and Discussion

Characterization of Cork Waste

The FTIR and the STA analyses confirmed the chemical composition of the cork waste resulting in cork, polyurethane glue, and paraffin (Figure 1). Precisely, in the FTIR spectrum of Figure 1a, the characteristic peaks of cork can be identified at 3400 cm^{-1} (-OH bond), 2920, 2850 cm^{-1} (stretching) and 1737 cm^{-1} (bending) [19]. Paraffin can be detected at 1459 cm^{-1} (bending) [20], and polyurethane glues at 1235, 1156, 1094 (bending) and 721 cm^{-1} (bending-rocking) [21].

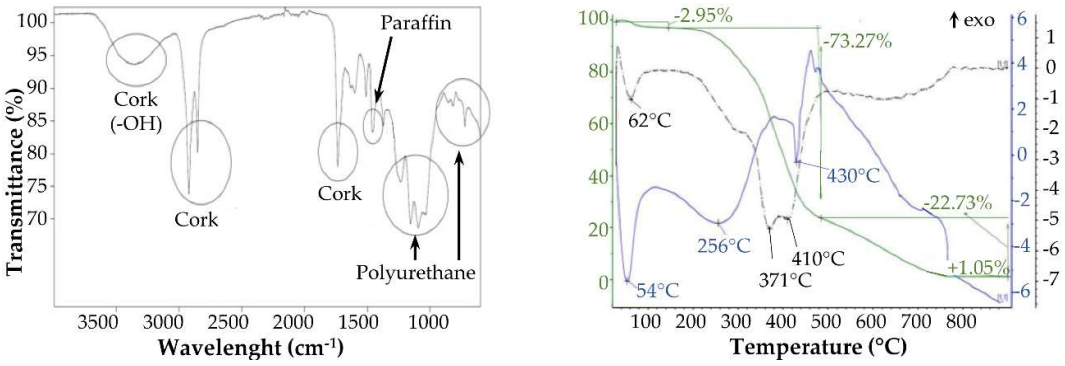

Figure 1. Composition of cork waste through ATR FT-IR analysis (a) and STA analysis (b). In Figure 1b are displayed the following curves: TGA (green line), first derivative of TGA (DTGA, black dashed line) and DSC (blue line).

On the other hand, the presence of cork, paraffin, and polyurethane glue was confirmed by thermal analysis. Considering DTGA (Figure 1b, black dashed line), the complete degradation of cork can be observed at around 371 °C and 410 °C [19]. The other exothermic peaks (between 600 °C and 800 °C) can be attributed to the degradation of paraffin [22] and polyurethane glue [21]. Moreover,

the TGA curve (continuous green line) showed a mass loss of around 76.22% related to cork degradation [23] and a mass loss of 22.73% attributable to the degradation of paraffin and polyurethane glue [21,24]. Contrary to expectations, a greater content of glue and paraffin (>21 wt.%) was observed. This is attributable to the fact that, during the production of agglomerated cork caps, the glue and paraffin tend to concentrate on the cap surface, which is the part subject to smoothing and from which the cork waste is generated. So, the cork waste under investigation displayed a slight difference in composition compared to the original agglomerated cork cap.

As reported in Figure 2, the cork waste displayed a bimodal particle size distribution with main peaks at 150 μm and 600 μm. A fine particle size of cork waste can also be observed (0.063 mm < d < 1mm).

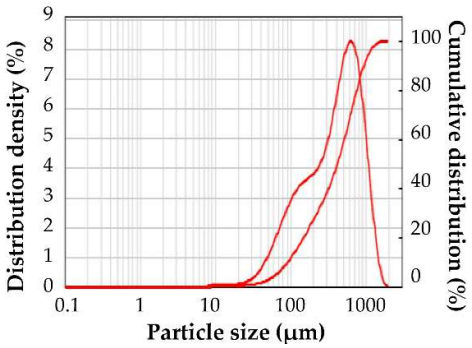

Figure 2. Particle size distribution of cork waste.

Figure 3 shows the morphology of cork waste at different magnifications, namely 8× and 35× magnification. The powder particles own the peculiar cork color, have an angular shape, and are different in size. Particle agglomerations and a high porosity rate between them can be observed.

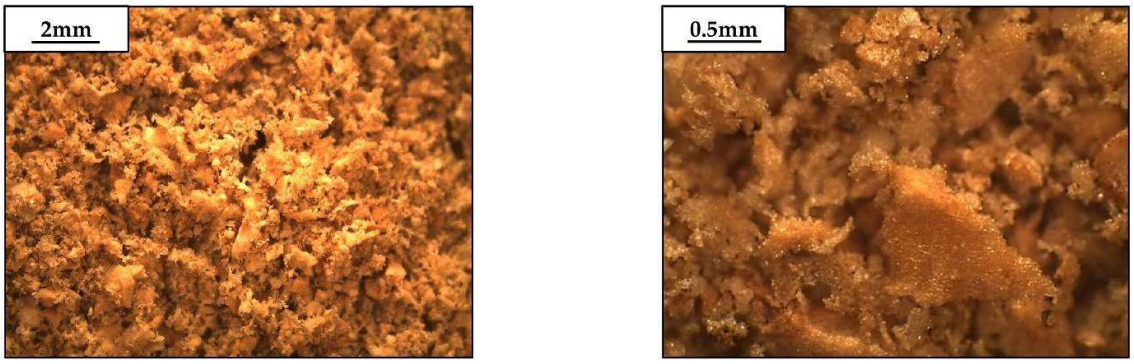

(**a**) (**b**)

Figure 3. Optical microscopy images of cork waste: (a) 8× magnification, (b) 35× magnification.

Remarkably, a water absorption of 177% was detected for cork waste, which is a consistent value considering the low particle size of the cork powder [22,25]. Moreover, an apparent density of 340 kg/m^3 and a real density of 1110 kg/m^3 were registered. These values are slightly higher than those about virgin cork from the literature [22] but are consistent considering the presence of polyurethane glue and paraffin.

Characterization of Mortars Containing Cork Waste

A good and homogeneous distribution of cork within mortars was detected for all the design mortar mixes through optical microscopy. A comparison between the reference mortar without cork (Figure 4a) and mortar with 4 wt.% (Figure 4b) is reported as a representative comparison for the other

mixes in Figure 4. In Figure 4b, the cork particles, recognizable by their characteristic color, are well distributed within the matrix and have both fine and coarse particles. Moreover, it can be observed that the maximum size of cork particles is smaller than that of natural aggregate (gray grains).

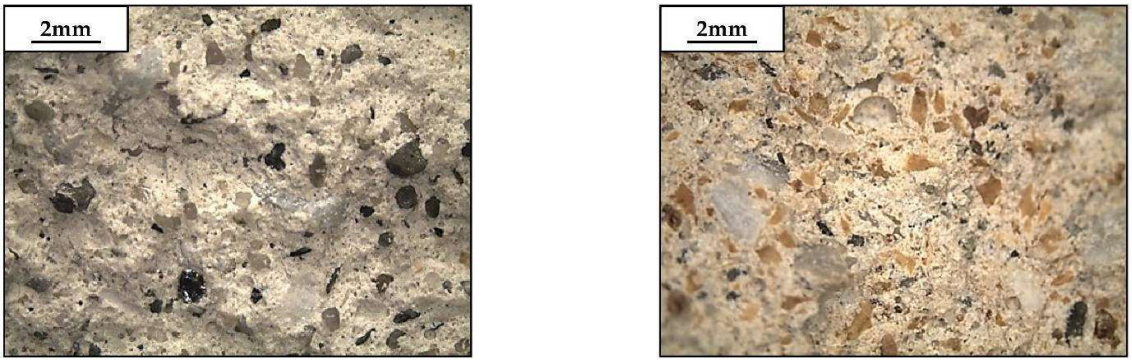

(**a**) (**b**)

Figure 4. Optical microscopy images at 8× magnification of mortars containing 0 wt.% (a) and 4 wt.% (b) of cork waste.

The introduction of increasing cork content involved a color variation in mortars. This phenomenon was visually and macroscopically observed (Figure 5a) and also confirmed through the colorimeter test (Figure 5b and Table 3).

Table 3 shows the results obtained by the colorimetry test in terms of a*, b*, L* values, where:

- a* > 0 predominance of red; a* < 0 predominance of green,
- b* > 0 predominance of yellow; b* < 0 predominance of blue,
- L*: 0 = dark, 100 = bright [26].

It can be observed that at increasing content of cork, mortars increase in yellow component (increasing positive a* values), in red one (increasing positive b* values) and become darker (decreasing L* values). Representative color comparison between the samples containing 0 wt.% and 4 wt.% of cork is graphically reported in Figure 5b within the CIELAB color space.

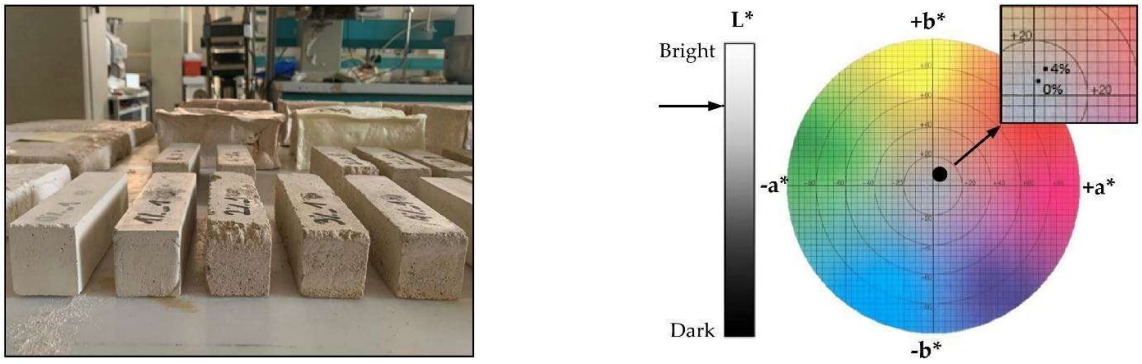

(**a**) (**b**)

Figure 5. Color variation of mortar samples induced by the addition of cork waste: visual macroscopic evidence of mortars containing increasing cork content from left to right (a) and colorimetry values of representative samples containing 0 wt.% and 4 wt.% of cork (b).

Table 2. Colorimetry test results for mortars.

Cork content (wt.%)	a*	b*	L*
0	1.86	6.79	83.22
1	2.16	6.90	82.26
3	2.87	11.17	74.52
4	3.09	11.29	74.35

The thermal conductivity test showed that, although the cork is regarded as an insulating material [19], the introduction of increasing cork content did not make the mortar an insulator. Indeed, thermal conductivity values above 0.1 W/mK, the limit not to be exceeded for the definition of thermally insulating material according to UNI EN 998-1, were recorded for all mortar mixes (Figure 6). The mortars containing up to 3 wt.% of cork displayed similar thermal conductivities to the reference mortar (0 wt.%). Interestingly, the thermal conductivity of mortars tends to increase with cork addition and increased by 12% for the mortar with 4 wt.%. This phenomenon resulted from the promotion of binder hydration by the progressive and slow release in time of the water absorbed by the cork (w_{extra}), which contributed to reducing the matrix porosity with hydration products. So, even if an insulating material was added, the mortar with more cork (4 wt.%) was more thermally conductive than the other. On the other hand, the reduction of matrix porosity stands as a highly valuable consequence of cork addition, and that could contribute to the prevention of chemical degradation at equal or enhanced lightweight conditions.

Since the cork is much lighter than mortar (−87%), as expected it was observed a gradual decrease in the apparent mortar density with the increase in cork content (Figure 6). So, even though adding higher cork content increased thermal conductivity due to the lower porosity of the lime-based matrix, the designed mortars were lighter because the cork was an extremely lightweight material. Despite this, the designed mortars can not be defined as lightweight mortars because they all exceeded the apparent density threshold value of 1100 kg/m^3 according to UNI EN 206-1.

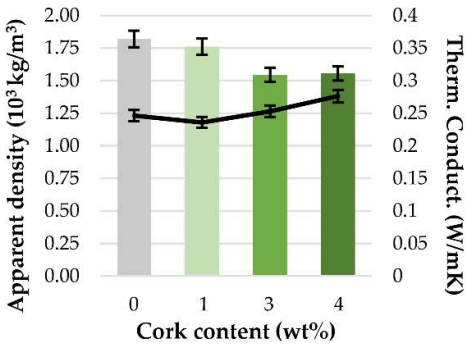

Figure 6. Correlation between apparent density (bar chart) and thermal conductivity (black line) of mortars containing increasing cork content. The error bars stand for standard deviation error.

As expected, the increase of cork percentage in mortars involved a strength decrease for both three-point bending and compressive strength tests (Figure 7). This has also been observed by literature and is mainly attributable to the poor mechanical strength and stiffness of cork [15,16]. However, the decrease in mechanical properties was not as pronounced as expected. This might result from the promotion of the binder hydration phenomenon by a slow but progressive release of the water absorbed by the cork (w_{extra}). Remarkably, this could be an interesting phenomenon for mortar

application in dry conditions; indeed, it would involve better binder hydration, contrast the water evaporation, and avoid shrinkage cracking [16,27].

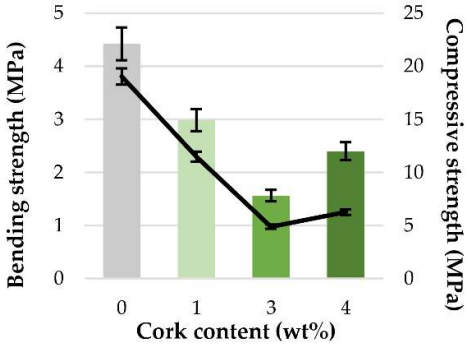

Figure 7. Mean failure strength from mechanical testing of mortars containing increasing cork content: three-point bending (bar chart), compressive strength (black line). The error bars stand for standard deviation error.

Despite the presence of high cork content (Table 1), all mortar mixes demonstrated good mechanical performance. Referring to results from the compressive strength test and prescriptions by UNI EN 998-2, different strength classes were assigned to the involved mixes. The reference mortar without cork was classified in the M15 class, to be used for structural recovery or anti-seismic reinforcement. The mortars containing 1 wt.% and 2 wt.% of cork were classified in the M10 strength class, so they were considered to have a good mechanical strength; these can be used both for seismic and insulating applications. The mortar containing 4 wt.% of cork was classified in the M5 class, so it could be primarily used for lightweight and insulating applications.

Following these promising results, future works will investigate the effect of cork waste addition on the durability, temperature-dependent mechanical properties, and flame resistance of mortar.

5.4. Conclusions

The continuous growth of the world population is the main cause of generating a large volume of waste from industrial processes. Among these, cork waste from the manufacturing of bottle caps has not found any valorization application and is currently delivered to waste-to-energy plants. In order to face this problem, this work proposes its valorization as filler within lime-based mortars, with the double objective of valorizing the waste and providing sustainability to traditional building materials.

The cork waste under investigation was characterized through FTIR and STA and resulted in a mixed composition of cork (about 76%), paraffin and polyurethane glue (about 24%). The cork displayed a particle size distribution of 0.063 mm < d < 1 mm and a low apparent density of 340 kg/m^3. High water absorption (about 180%) was observed and considered for cork application within mortar.

The addition of increasing contents of cork in mortars, i.e., from 1 wt.% to 4 wt.% (16 vol.% to 65 vol.%), gradually decreased the three-point bending and compressive strength of the reference mortar (0 wt.%). However, the decrease in mechanical performance was less than expected, thanks to a continuous hydration promotion. In fact, the water absorbed by the cork during the mixing phase was later released over time and promoted better hydration of the binder. Therefore, better mechanical properties and less porosity of the final product were observed than expected. The apparent density of mortar mainly decreased with higher cork content, i.e., from 1820 kg/m^3 (0 wt.%) to 1560 kg/m^3 (4 wt.%). In conclusion, green mortars possibly suitable for masonry restoration were obtained, with a reduced density by 15%. Lightness is a major property of restoration materials because it allows reduced loads applied to the pre-existing structure.

The peculiar hygroscopic property of cork could be exploited for applications in dry environments, where too fast water evaporation, which could lead to the creation of cracks and early degradation, could be avoided by the release of water over time by cork.

The addition of cork waste in mortar also caused a color shift toward red-yellow color, which could be regarded as a positive aesthetic factor.

In conclusion, this preliminary investigation allowed to identify possible alternative solutions to waste-to-energy of cork waste, thus making a so-far-linear economy circular and moving towards a more sustainable industry. The encouraging results displayed that it is feasible to valorize manufacturing cork waste as a secondary raw material for construction materials and involve desired properties such as sustainability, lightness, coloring, etc., without affecting mechanical and thermal insulating performances. The companies involved in cork waste management issues can take advantage of these sustainable practices and valorize their manufacturing waste from an economic and sustainability point of view. Even though policies generally do not encourage the effective use of secondary raw materials in construction materials by strongly limiting their content or application use, this work points out positive performance that could be considered for real applications. Moreover, this study displays for the first time the properties of cork waste from the manufacturing of cork bottle caps and the influence of cork waste use in traditional construction materials such as mortars. Therefore, it seeks to fill the research gap on cork waste recycling and contribute to the first valorization solutions.

References

[1] Laurent, A.; Bakas, I.; Clavreul, J.; Bernstad, A.; Niero, M.; Gentil, E.; Hauschild, M.Z.; Christensen, T.H. Review of LCA studies of solid waste management systems–Part I: Lessons learned and perspectives. Waste Manag. 2014, 34, 573–588.

[2] Ahmad,W.; Ahmad, A.; Ostrowski, K.A.; Aslam, F.; Joyklad, P. A scientometric review of waste material utilization in concrete for sustainable construction. Case Stud. Constr. Mater. 2021, 15, e00683.

[3] Gomes, S.D.C.; Zhou, J.L.; Li, W.; Long, G. Progress in manufacture and properties of construction materials incorporating water treatment sludge: A review. Resour. Conserv. Recycl. 2019, 145, 148–159.

[4] Li, X.; Qin, D.; Hu, Y.; Ahmad, W.; Ahmad, A.; Aslam, F.; Joyklad, P. A systematic review of waste materials in cement-based composites for construction applications. J. Build. Eng. 2021, 45, 103447.

[5] Guo, P.; Meng, W.; Nassif, H.; Gou, H.; Bao, Y. New perspectives on recycling waste glass in manufacturing concrete for sustainable civil infrastructure. Constr. Build. Mater. 2020, 257, 119579.

[6] Mohan, H.T.; Jayanarayanan, K.; Mini, K. Recent trends in utilization of plastics waste composites as construction materials. Constr. Build. Mater. 2021, 271, 121520.

[7] Asim, M.; Uddin, G.M.; Jamshaid, H.; Raza, A.; Tahir, Z.U.R.; Hussain, U.; Satti, A.N.; Hayat, N.; Arafat, S.M. Comparative experimental investigation of natural fibers reinforced light weight concrete as thermally efficient building materials. J. Build. Eng. 2020, 31, 101411.

[8] Belakroum, R.; Gherfi, A.; Kadja, M.; Maalouf, C.; Lachi, M.; El Wakil, N.; Mai, T. Design and properties of a new sustainable construction material based on date palm fibers and lime. Constr. Build. Mater. 2018, 184, 330–343.

[9] Kang, S.; Zhao, Y.; Wang, W.; Zhang, T.; Chen, T.; Yi, H.; Rao, F.; Song, S. Removal of methylene blue from water with montmorillonite nanosheets/chitosan hydrogels as adsorbent. Appl. Surf. Sci. 2018, 448, 203–211.

[10] Dawood, A.O.; Al-Khazraji, H.; Falih, R.S. Physical and mechanical properties of concrete containing PET wastes as a partial replacement for fine aggregates. Case Stud. Constr. Mater. 2021, 14, e00482.

[11] Merlo, A.; Lavagna, L.; Suarez-Riera, D.; Pavese, M. Mechanical properties of mortar containing waste plastic (PVC) as aggregate partial replacement. Case Stud. Constr. Mater. 2020, 13, e00467.

[12] Colangelo, F.; Cioffi, R.; Liguori, B.; Iucolano, F. Recycled polyolefins waste as aggregates for lightweight concrete. Compos. Part B Eng. 2016, 106, 234–241.

[13] Rashad, A.M. Recycled waste glass as fine aggregate replacement in cementitious materials based on Portland cement. Constr. Build. Mater. 2014, 72, 340–357.

[14] Awolusi, T.F.; Sojobi, A.O.; Afolayan, J.O. SDA and laterite applications in concrete: Prospects and effects of elevated temperature. Cogent Eng. 2017, 4, 1387954.

[15] Jerónimo, A.; Soares, C.; Aguiar, B.; Lima, N. Hydraulic lime mortars incorporating micro cork granules with antifungal properties. Constr. Build. Mater. 2020, 255, 119368.

[16] Merabti, S.; Kenai, S.; Belarbi, R.; Khatib, J. Thermo-mechanical and physical properties of waste granular cork composite with slag cement. Constr. Build. Mater. 2021, 272, 121923.

[17] El Wardi, F.Z.; Cherki, A.-B.; Mounir, S.; Khabbazi, A.; Maaloufa, Y. Thermal characterization of a new multilayer building material based on clay, cork and cement mortar. Energy Procedia 2019, 157, 480–491.

[18] Bruno, S. Manuale di Bioarchitettura—Bioedilizia e Fonti Alternative di Energia Rinnovabile; Dario Flaccovio Editore: Palermo, Italy, 2009.

[19] Riboulet, J.-M.; Alegoet, C. Aspetti Tecnici Della Tappatura Dei Vini; Oenoplurimedia: Chaintre, France, 1986.

[20] Kalidasan, B.; Pandey, A.; Shahabuddin, S.; George, M.; Sharma, K.; Samykano, M.; Tyagi, V.; Saidur, R. Synthesis and characterization of conducting Polyaniline@cobalt-Paraffin wax nanocomposite as nano-phase change material: Enhanced thermophysical properties. Renew. Energy 2021, 173, 1057–1069.

[21] Van Oosten, T. PUR Facts: Conservation of Polyurethane Foam in Art and Design; Amsterdam University Press: Amsterdam,The Netherlands, 2011.

[22] Da Silva, S.M.; Oliveira, J. Cork powders wettability by theWashburn capillary rise method. Powder Technol. 2021, 387, 16–21.

[23] Fernandes, E.M.; Aroso, I.M.; Mano, J.F.; Covas, J.A.; Reis, R.L. Functionalized cork-polymer composites (CPC) by reactive extrusion using suberin and lignin from cork as coupling agents. Compos. Part B Eng. 2014, 67, 371–380.

[24] Liu, Z.; Zang, C.; Ju, Z.; Hu, D.; Zhang, Y.; Jiang, J.; Liu, C. Consistent preparation, chemical stability and thermal properties of a shape-stabilized porous carbon/paraffin phase change materials. J. Clean. Prod. 2020, 247, 119565.

[25] Vilela, C.; Sousa, A.F.; Freire, C.S.; Silvestre, A.J.; Neto, C.P. Novel sustainable composites prepared from cork residues and biopolymers. Biomass Bioenergy 2013, 55, 148–155.

[26] Sato, T.; Ishida, F.; Tanioka, S.; Miura, Y.; Tanaka, K.; Suzuki, H. Colorimetry forWall Appearance Study of Cerebral Aneurysms. Brain Hemorrhages, 2021; in press.

[27] Jiang, C.; Jin, C.; Wang, Y.; Yan, S.; Chen, D. Effect of heat curing treatment on the drying shrinkage behavior and microstructure characteristics of mortar incorporating different content ground granulated blast-furnace slag. Constr. Build. Mater. 2018, 186, 379–387.

6. Recycling of textile microfibers waste as fiber reinforcement in cementitious materials

Note: This chapter is based on a research paper published in a peer reviewed journal.

Submission title-Conference paper: A Practical Valorization Approach for Mitigating Textile Fibrous Microplastics in the Environment: Collection of Textile-Processing Waste Microfibers and Direct Reuse in Green Thermal-Insulating and Mechanical-Performing Composite Construction Materials

B. Malchiodi, E.I. Cedillo-González, C. Siligardi, P. Pozzi

Published in Microplastics, MDPI

DOI: https://doi.org/10.3390/microplastics1030029

Contribution of the candidate: experimental design, conduction of the experiments, writing and reviewing, corresponding author.

Microplastic (MP) contamination is an urgent environmental issue to address. Fibrous microplastics (FMPs) are the principal MP type in the air and have already been found in human stool and lung tissues. FMPs are generated from the lifecycle of synthetic and blended textiles and are expected to increase due to fast fashion. Among textile processes, the finishing of fabrics is estimated to generate 5000 t/year of textile waste fibers in Italy, including FMPs. To limit FMPs spread, this paper suggests, for the first time, the direct collection of blended finishing textile waste microfibers and reuse in designing thermal-insulating and mechanical-performing fiber-reinforced cementitious composites (FRCs). The microfibers were thoroughly characterized (size, morphology, composition, and density), and their use in FRCs was additionally evaluated by considering water absorption and release capacity. Untreated, water-saturated, and NaOH-treated microfibers were considered in RCs up to 4 wt.%. Up to a +320% maximum bending load, +715% toughness, -80% linear shrinkage, and double-insulating power of Portland cement were observed by increasing microfiber contents. NaOH-treated and water-saturated microfibers better enhanced toughness and linear shrinkage reduction. Therefore, green and performant composite construction materials were obtained, allowing for the mitigation of more than 4 kg FMPs per ton of cement paste. This is a great result considering the FMP contamination (i.e., 2–8 kg/day fallout in Paris), and that FRCs are promising and shortly-widely used construction materials.

6.1. Introduction

In the last few years, microplastic (MP) pollution has become an environmental issue of global concern. MPs are plastic debris with sizes between 0.3 µm and 5 mm [1]. They are composed of synthetic polymers such as polyethylene (PE), polystyrene (PS), polyethylene terephthalate (PET), polyester (PL), nylon (PA6), etc. MPs can be found in several shapes, such as beads, foams, films, fragments, and fibers. Like other chemical pollutants, MPs are already distributed among the four major environmental compartments: air, water, soil, and biota. Such compartments not only behave as MP reservoirs but grant the transport of MPs within them [2], allowing MPs to behave similarly to global biogeochemical cycles and spiral around the globe with different atmospheric, oceanic, cryospheric, and terrestrial residence times [3].

Several removal technologies based on physical, chemical, and biological processes have been proposed to restore the environment from MP pollution. Since the presence of MPs was first reported in water in 2004 [4], a broad spectrum of MP removal technologies from the aqueous medium, such as adsorption, sedimentation, ultrafiltration, photocatalysis, magnetic removal, microbubbles, and activated sludges, has been investigated [5–11]. When MPs were found in the terrestrial environment, biodegradation became the primary investigated strategy for soil remediation [12].

The presence of MPs in atmospheric fallout was reported in 2015, and fibrous microplastics (FMPs) represented the primary type of MP present in the air [13,14]. According to the European Chemical Agency (ECHA), fibrous microplastics are defined as MPs with lengths between 0.3 µm and 15 mm, and a length-to-diameter ratio of greater than three [1]. FMPs released into the atmosphere during the lifetime of synthetic and blended textiles (production, use, and disposal) significantly contribute to the overall issue of MP pollution. For instance, airborne FMPs can reach terrestrial and aquatic environments through wind transport, deposition on the surface of cities or agrosystems, and runoff [13,14]. In 2017, the International Union for Conservation of Nature (IUCN) estimated that FMPs released from textiles during industrial and household laundry accounted for 35% of the annual MP emission sources into the oceans [15]. Once entered into aquatic and terrestrial environments, FMPs impact their physicochemical characteristics [16] and interact in several ways with the biota, inducing health issues such as neurotoxicity, oxidative stress, oxidative damage, and even death [2,16,17]. Additionally, the transfer of FMPs from the atmosphere to aquatic and terrestrial environments represents a probable pathway to humans [17], and FMPs have already been found in human stool [18] and human lung tissues [19]. For this reason, developing innovative strategies to decrease the quantities of FMPs released into the atmosphere is a key aspect of the overall framework for reducing MP pollution.

The emissions of textile-derived FMPs are expected to increase due to the growing demand for synthetic or blended textiles and fibers [20]. This phenomenon is mainly attributable to fast fashion, which promotes mass consumption and a linear economic model. As a result, a large amount of textile waste is generated both from the industry (special waste) and consumers (urban waste). The former includes unsold clothes and industrial process waste, whereas the latter old-fashioned or end-of-life products. In Italy, textile waste production is significant and amounts to 490,000 tons/year of special waste and 146,000 tons/year of urban waste [21].

A portion of textile waste is currently recycled. Clothes waste, both from pre- and post-consumer use, is reused as clothing in the second-hand market or donated to charity. Fabrics and scraps are sorted according to color and material and recycled to create new yarns and fabrics, thermal-insulating panels, and upholstery for home and transport furniture. However, waste fibers from processing and other non-recyclable/reusable textile wastes are currently delivered to landfills.

Among these, waste microfibers from the raising and shearing of fabrics display a high risk of diffusion into the air and soil because of their volatility. Raising and shearing are mechanical finishing processes used to create heat-insulating and aesthetic fabrics. First, fibers are pulled out from the fabric to form a heat-insulating fluff; then, the fluff is cut at a defined and adjustable height for aesthetic purposes. During this finishing process, a suspension of waste microfibers is generated in the air, which is then collected by air-filtering systems, compacted, and delivered to landfills. In Italy, 5000 tons/year of these textile-waste-processing microfibers is currently disposed to landfills. This involves discharge costs for the producer and the risk of spreading textile waste from landfills into the environment. Particularly, the synthetic ones can be considered FMPs due to their size and composition, and can worsen the FMP issue in the environment.

To solve this environmental issue, this paper proposes the reuse of blended textile waste microfibers from the raising and shearing of fabrics, addressing the need to implement new strategies against the release of microfibers, particularly FMPs, into the environment. The decision to consider blended textile waste microfibers and not just synthetic ones arise from the desire to propose a mitigation

solution for FMPs that is close to reality, thus proposing a practical solution to a real issue. For the first time, we propose the reuse of FMPs as a mechanical reinforcement for fiber-reinforced cementitious composites (FRCs), which are innovative composite construction materials. In FRCs, fibers increase the ductility of the cement matrix by reducing cracking during shrinkage and loading, thus increasing the material durability compared with plain cement. Steel, carbon, glass, and polypropylene fibers are usually employed [22,23] for these purposes; however, using textile waste microfibers would additionally allow for green FRCs with better thermal insulation properties. Furthermore, the proposed solution aims to reduce the amount of textile waste disposed in landfills and waste management costs for the textile industry. Apart from the outlined benefits, recycling this kind of microfiber allows to directly collect FMPs before reaching and spreading into the atmosphere and to control their properties (i.e., size, composition, etc.).

In this study, blended textile waste microfibers from the raising and shearing of fabrics were chemically and physically characterized. Their use in FRCs was preceded by water absorption, water release, and real density measurements to enable proper mix design (water, cement, and fiber content). Untreated, water-saturated, and mercerized textile waste microfibers were added to the cementitious mix up to 4 wt.% (40 vol.%). Finally, the influence of fiber surface treatment and content on the FRC was detected in terms of linear shrinkage, three-point bending test, and thermal conductivity. It was found that at least 4 kg of FMPs per ton of cement mix could be used in creating green FRCs with increased thermal-insulating properties, mechanical strength, toughness, and reduced shrinkage compared with the reference Portland cement. Considering that 3–10 t of microfibers are deposited by atmospheric fallout every year in Paris, 29% of which is constituted by FMPs (i.e., 2.38–7.95 kg of FMPs/day) [2,14], the present approach significantly allows the same amount of FMPs falling in Paris per day to be recovered before reaching and polluting the environment.

6.2. Materials and Methods

Textile Waste Microfibers

The textile waste microfibers involved in this study were generated by a textile finishing plant located in Carpi (Modena, Italy). The company performs finishing to impart thermal insulation and aesthetic properties to the surface of different fabrics, including cotton, cotton blends, and synthetics. The process includes raising and shearing phases for heat-insulating and aesthetic purposes. The involved textile microfibers were generated during the shearing phase and collected by air-pumping and air-filtering systems (Figure 1).

The type and coloring of fabrics change periodically according to market demand and imply a heterogeneity (in composition, diameter, and color) of the textile waste microfibers produced. In addition, the length of the waste microfibers differs due to the raising and shearing phases shown in Figure 1. Six samples were collected between the months of November and December to comprise a representative batch of blended microfibers. From the company's data on fabrics subjected to finishing processes in that period, it was found that the surveyed microfibers were composed of 61% pure cotton, 29% cotton blend (cotton and PA), and 10% synthetics (PA, PC, PL, and NY).

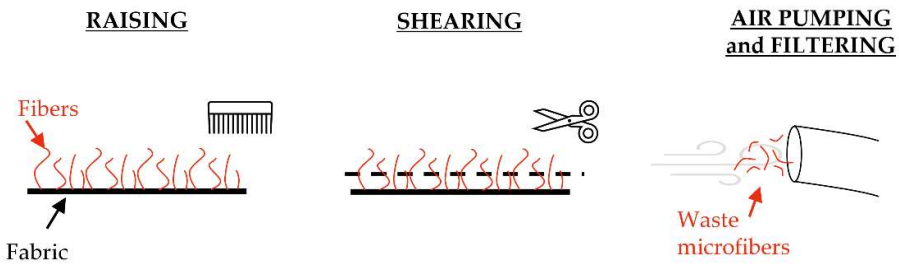

Figure 1. Generation of textile waste microfibers from the finishing of fabric for heat-insulating and aesthetic properties.

The different composition of textile waste microfibers (natural or synthetic) was detected by ATR-FTIR spectroscopy (FTIR VERTEX 70, Bruker Optics, Ettlingen, Germany). The spectra were acquired after 32 scans between a 600–4000 cm^{-1} transmittance range and with a 4 cm^{-1} resolution. Additionally, OPUS software (OPUS 6.5, Bruker Optics GmbH, Selb, Germany) was involved in the spectrum analysis. The data composition was then compared and confirmed with that from the manufacturer's waste datasheet.

An environmental scanning electron microscope in high vacuum mode (ESEM, ESEM-Quanta 200 Fei Company, Oxford Instruments, Abingdon, UK) was involved in distinguishing FMPs from natural fibers based on their different morphologies.

In addition, the fibers were characterized by optical microscopy mainly to assess the average size of the synthetic ones to determine whether they could be defined as FMPs. A Leica EZ4D (Leica Microsystems) stereo microscope was used at different magnifications, and the average size of synthetic microfibers was computed through ImageJ software (1.53k Version), with over 30 measurements for length and 50 for diameter. The Set measurements function of ImageJ (Analyze section) was used to set the measuring reference scale based on the known reference bar length of the optical images. Then the Measurements function (Analyze section) was applied to measure the length and diameter of the synthetic fibers with respect to the set reference scale.

The real density of the textile waste microfibers was achieved through a Micromeritics Accupyc 1330 helium pycnometer by Micromeritics Instruments. This value, as well as that for the water absorption and release over time by microfibers, was needed to pursue a subsequent mix design of FRCs.

The water absorption (WA) of microfibers was computed after 24 h of immersion in water at laboratory conditions (25 ± 2°C, 60 ± 5% RH) as $[(M_{wet}-M_{dry})/M_{dry}] \cdot 100$, where M_{wet} is the fiber mass after 24 h of immersion and M_{dry} is the fiber mass before immersion.

The test of water release over time was performed to quantify the amount of water released by the saturated microfibers in the FRC mix. This phenomenon would promote deferred cement hydration over time and is important in determining the water/cement ratio for the mix design of FRCs. For this purpose, 10 g of microfibers was saturated in water for 24 h at laboratory conditions, then drained and placed in a glass vessel. The container was placed on a scientific balance in a climate chamber set at 25°C and 50% RH. The weight loss of the microfibers was continuously recorded for 24 h and defined as the amount of water released over time.

Treatments of the Textile Waste Microfibers

The textile waste microfibers were considered in three different conditions within the cementitious matrix: untreated, water-saturated, and mercerized (NaOH-treated). The influence of each state was observed and derived from the characterization of FRCs.

The untreated reference condition referred to dry textile microfibers as supplied by the manufacturer.

The water-saturated condition was involved to better control the microfiber water absorption and release over time and the eventual promotion of cement hydration over time.

The mercerization treatment (hereafter named NaOH treatment) was involved to possibly increase the mechanical properties of the investigated textile microfibers, and thus those of the FRCs. This treatment, generally used for cotton fiber and other cellulose fibers, confers improved physical and mechanical properties to the textile fibers. On the one hand, it results in the breakdown and fibrillation of fibers into smaller and thinner fibers, leading to an increase in aspect ratio. On the other hand, the surface becomes rougher and more reactive, allowing for better adhesion and wettability of the fibers

with the matrix, respectively. The polymerization degree and molecular orientation of cellulose crystals change due to the cementation of hemicellulose and lignin, which are removed during the process. These changes enhance the mechanical properties and tensile strength [24,25]. First, the microfibers were dried at 80°C until reaching a mass change between two measurements lower than 0.1%. Then, they were soaked for 30 min in a 5% NaOH solution of demineralized water. Subsequently, the microfibers were bathed while being stirred in demineralized water for 15 min; this process was repeated until reaching a neutral pH. In the end, the microfibers were dried again at 80°C until obtaining a mass change between two measurements lower than 0.1%.

Water-saturated and NaOH-treated conditions improve FRC properties primarily through the optimization of natural microfiber properties. Although these treatments are not specific to synthetic microfibers, an optimization of the blended microfiber properties promotes the enhancement of all textile waste microfibers, including synthetics, and thus the mitigation of FMPs from the environment.

Cement-Based Composites Reinforced by Textile Waste Microfibers (FRCs)

CEM-I 42.5R Portland cement (Cemento Grigio 425, Knauf, Iphofen, Germany) was used to manufacture FRCs. The mix design of the FRCs considered a constant effective water-to-cement ratio (w_{eff}/c) equal to 0.42 and microfiber contents of 0 wt.%, 1 wt.%, 2 wt.%, 3 wt.%, and 4 wt.%. Microfiber contents above 4 wt.% were not investigated because of the workability loss of the FRCs in the fresh state. For the FRCs containing water-saturated microfibers, the amount of water absorbed and then released over time ($w_{released}$) was considered as part of the effective water (w_{eff}) intended for cement hydration. Thus, for FRC mixes with water-saturated microfibers, the amount of water added during the mixing phase (w) was computed as the difference between the effective water and the water released over time ($w = w_{eff} - w_{released}$). The cement was slowly added to water in an electronic mixer. The paste was mixed at a slow speed (220 rpm) for 1 min and at a high speed (440 rpm) for 4 min. Then, the selected content of microfibers (untreated, water-saturated, or NaOH-treated) was added to the paste and manually mixed with a trowel. The mix was cast into 50 × 35 × 300 mm^3 and 30 × 300 × 300 mm^3 assembled wooden formworks and was vibrated for 1 min on a vibrating plate (55-C0157/B Controls Group). Then, it was covered with a plastic cloth and cured for 28 days in a climatic chamber at 25 ± 2°C, 95 ± 5% RH. Four samples for each mix were manufactured for the linear shrinkage and three-point bending tests (50 × 35 × 300 mm^3 beams), and the thermal conductivity measurement (30 × 300 × 300 mm^3 slabs). The three-point bending test was performed by using a UTM INSTRON 5567 under displacement mode (1 mm/min), considering a 30 kN load cell and 10 cm mid-span. A heat flow meter HFM Lambda (Netzsch-Gerätebau GmbH, Selb, Germany) was used to measure the thermal conductivity of the FRC samples reinforced with untreated microfibers. For all tests on FRCs, the desired mean features were averaged over four measurements, and the standard deviation was computed.

6.3. Results and Discussion

Characterization of Textile Waste Microfibers

The composition of the microfibers under investigation was already known (61% cotton, 29% cotton blend, and 10% synthetics) from the composition data supplied by the producer (see Section 2.1). In addition to the 10% pure synthetic fibers, additional synthetic microfibers were present in the 29% cotton blend fraction, mainly PA.

The microfiber composition was experimentally validated through a comparison between the ATR-FTIR spectrum of the textile waste microfibers and that of the one-component textile fibers (i.e., pure cotton, nylon, polyester, etc.). For conciseness, Figure 2 reports the spectrum of the textile waste microfibers in which the characteristic peaks of cotton (green) and synthetics (red) are highlighted. The identification of the characteristic peaks is confirmed by the literature [26–28].

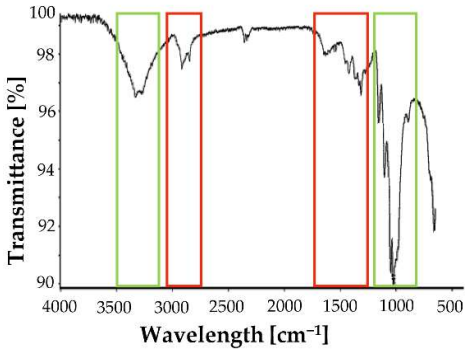

Figure 2. ATR-FTIR spectroscopy of textile waste microfibers. Characteristic peaks related to synthetic microfibers are highlighted in red, while those of cotton in green.

ESEM microscopy (Figure 3) confirmed this evidence by detecting cotton and synthetic fibers with a predominance of cotton. In particular, cotton fibers can be distinguished from synthetic ones since they are flattened and rolled up [27–29]. By contrast, synthetic fibers display a cylindrical cross-section with a rough surface and grooves (Figure 3) [27,28].

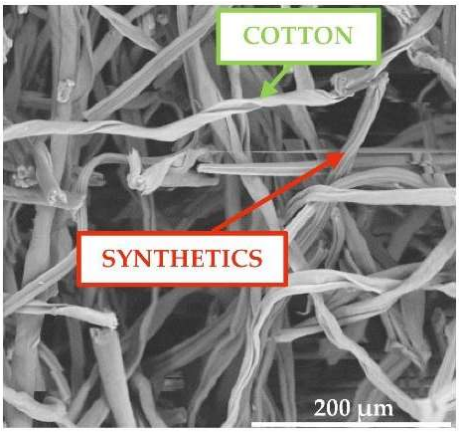

Figure 3. ESEM micrograph of textile waste microfibers at 600× magnitude.

Focusing on synthetic microfibers (at least 10% of the textile microfibers under investigation), a length of 3.65 ± 2.57 mm and a diameter of 17.28 ± 1.68 µm were determined with ImageJ software from optical images (Figure 4). Since synthetic microfibers displayed a 0.3 µm–15 mm length and a length-to-diameter ratio of greater than three, then they can be considered a source of FMPs according to the ECHA definition.

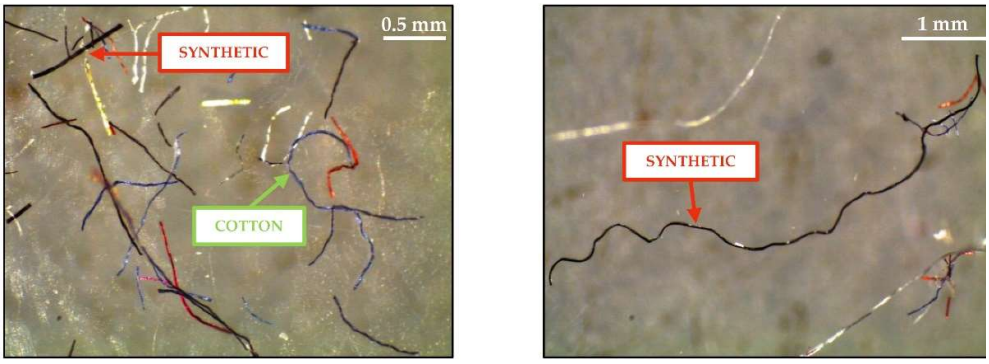

(**a**) (**b**)

Figure 4. Optical images of textile waste microfibers at (a) 30x and (b) 20x magnitude.

The mean real density of microfibers was evaluated at 1.15 g/cm^3. It was found that the microfibers were dry while displaying a water absorption of 340%. However, this amount of water was entirely released over time ($w_{released}$), and 95% of the water was released after 24 h. During the first few hours (from 0 to 3:45 h, Figure 5a), the water release was slower, but then it followed a faster and linear trend over time (from 3:45 to 7:30 h, Figure 5b).

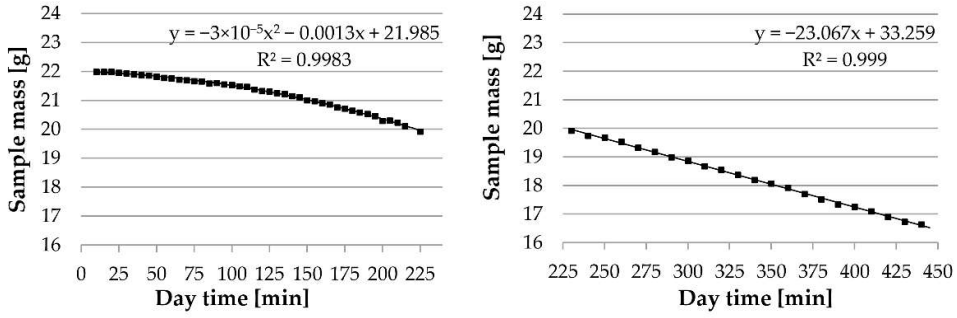

(**a**) (**b**)

Figure 5. Water release over time by textile waste microfibers at early stage: (a) up to 225 min (3:45 hours); (b) from 225 to 450 min (between 3:45 and 7:30 h).

Characterization of Composite Construction Materials Containing Textile Waste Microfibers

The three-point bending test displayed that the mechanical performance of FRCs, such as the maximum bending load (Figure 6a) and toughness (Figure 6b), gradually improved with increasing fiber content.

Compared to the reference value of Portland cement (0 wt.% microfibers), an improvement of up to 320% in the maximum bending load was observed for FRCs containing 4 wt.% microfibers. However, a more significant influence on maximum bending load enhancement was observed for fiber content, rather than for fiber treatment (Figure 6a).

By contrast, toughness was affected by both fiber content and treatment (Figure 6b). The toughness enhancement was magnified with increasing fiber contents [30,31], and NaOH treatment resulted in more efficiency for contents ≥ 3 wt.%. Remarkably, a 715% enhancement in toughness was displayed by the FRC containing 4 wt.% of NaOH-treated microfibers, compared with that of the reference sample with 0 wt.% microfibers. The better performance of NaOH-treated microfibers was attributable to the effect of mercerization treatment, which promoted a rougher and more functionalized fiber surface [24,25,32]. Therefore, NaOH treatment resulted in increased mechanical and chemical adhesion between the constituent phases of the composite material (cementitious matrix and textile microfiber), which is known and generally sought to improve the overall mechanical behavior of FRCs [32,33]. The water-saturated microfibers behaved better than the untreated ones, likely due to a greater $w_{released}$ over time, which promoted a differed hydration of the cementitious binder, and thus better mechanical properties. Supporting this hypothesis, the difference in performance was detected for 3 and 4 wt.%, which had a higher amount of water released compared to that of 1 and 2 wt.%.

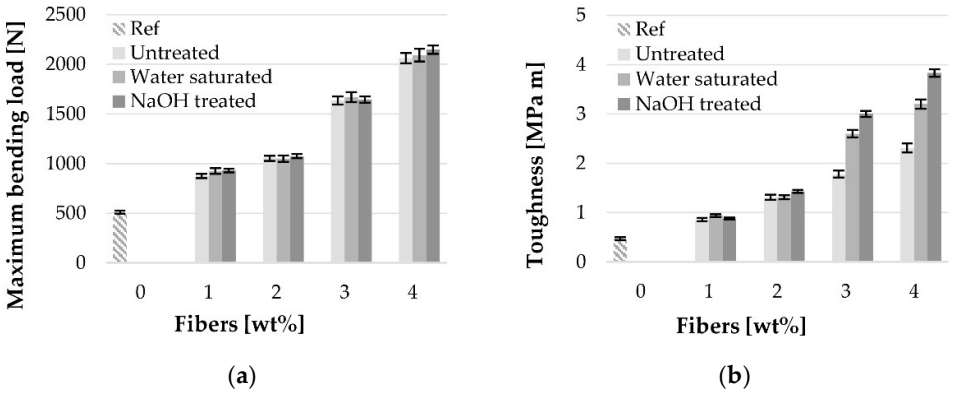

Figure 6. Improvement in three-point bending performance of FRCs when increasing microfiber content: (a) maximum bending load; (b) toughness. The error bars stand for standard deviation.

These mechanical improvements were attributable to the good fiber distribution, fiber mechanical reinforcement, and crack-bridging effect [30,34,35]. Although microfibers are generally regarded as affecting the FRC strength prior to the maximum bending load (first cracking load), they can also influence the post-peak behavior, especially if they are embedded into cementitious matrices with low-grade aggregates or cement paste [34]. As reported in Figure 7f, the microfibers acted as anchors between the two matrix edges at the fracture section. This action, called crack-bridging, limits crack formation and propagation during both shrinkage (especially for microfibers) and mechanical loading [30,34,35]. During loadings, the tensile stresses are transferred from the cementitious matrix to the fiber reinforcement, which, being more ductile than the matrix, allows the FRC to have greater overall ductility and energy absorption [34]. Since the crack-bridging effect was stronger as the fibers acted in a direction perpendicular to the cross-sectional area, the microfibers exploited their maximum crack-bridging effect during the three-point bending test of the FRCs (Figure 7f) [30].

Moreover, a high specific surface area of reinforcing fibers is a main factor in enhancing the energy absorption capacity and toughness of FRCs [36]. This property allows for a better fiber-to-matrix adhesion, and thus a better mechanical behavior of the FRC. A high surface-to-volume ratio is a characteristic property of MPs. According to Zhang et al. [2], the same property is considerably higher for FMPs than, for example, spherical MPs. When present in polluted environments, the high surface-to-volume ratio leads to the absorption of persistent organic pollutants (POPs) on the MP surface. The absorption of such pollutants may increase the hazardous nature of both MPs and FMPs [2]. If consumed by biota, they may act as POP vectors, leading to bioaccumulation in such organisms. Although there is still a debate questioning whether MPs constitute significant sinks and vectors of POPs [37,38], predictions estimate that large quantities of MPs will be released into the sea in the next 30 years [39], increasing the likelihood of POP transfer from MPs to biota. The approach used in this study took advantage of the high surface-to-volume ratio of FMPs. Thus, although this property represents an increased capacity for absorbing hazardous organic chemicals if FMPs are released into the environment, in this study, their intrinsically high specific surface area-to-volume ratio was expected to promote FRC properties, accordingly. Given the evidence from Figure 6 and Figure 7f, a decrease in crack width and crack propagation was observed as the microfiber content in FRCs increased (Figure 7). The limitation of crack opening allows the prevention of the early degradation of the material due to environmental chemical attacks, thus extending the service life of the structure in which the material is employed.

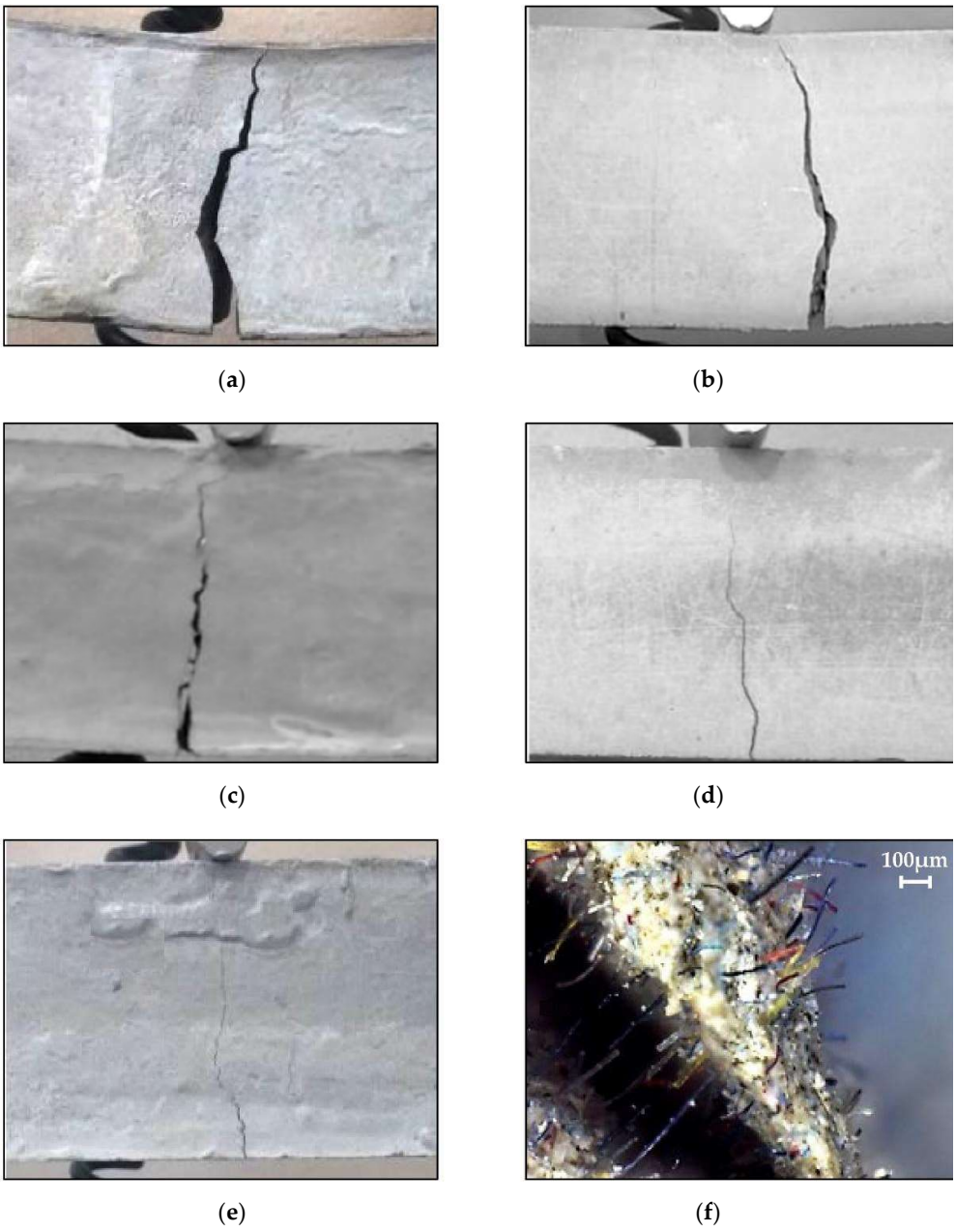

Figure 7. Reduction of crack opening during three-point bending test due to the crack-bridging effect of higher microfiber content: (a) reference unreinforced sample (0 wt.% microfibers); (b) 1 wt.% microfibers; (c) 2 wt.% microfibers; (d) 3 wt.% microfibers; (e) 4 wt.% microfibers; (f) detail of the crack-bridging effect. The pictures are related to untreated microfibers, but the same results were obtained for water-saturated and NaOH-treated microfibers.

Figure 8 displays the influence of the crack-bridging effect on the linear shrinkage measurement. The use of microfibers, particularly synthetic ones, has been highlighted as the best solution to reduce hydraulic shrinkage by the standard prescriptions [30]. In this study, it was observed that the linear shrinkage of the unreinforced reference sample was positively reduced by both increasing the microfiber content and treatment type. NaOH treatment resulted in more efficiency for reduced microfiber contents (−60% at 1 wt.%). However, 1 wt.% water-saturated and untreated microfibers reduced it by 40% and 20%, respectively. The influence of microfiber treatment was reduced by increasing the microfiber content until becoming negligible at 4 wt.%. Up to 80% linear shrinkage

reduction was observed for all FRCs with 4 wt.% microfibers compared with that of the reference Portland cement (0 wt.%).

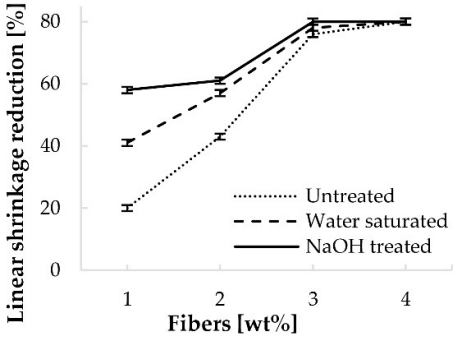

Figure 8. Reduction in linear shrinkage of FRCs compared with that of Portland cement when increasing the microfiber content of untreated, water-saturated, and NaOH-treated textile waste microfibers.

The increase in microfiber content also contributed to reducing the thermal conductivity, thereby increasing the thermal-insulating power of the final FRC (Figure 9). Indeed, textile fibers are known for their thermal insulation properties, which is the main reason they are used to manufacture clothing [40]. In particular, the addition of 4 wt.% of untreated microfibers reduced the thermal conductivity of the reference unreinforced sample by 42%, almost doubling the insulating power of solely Portland cement.

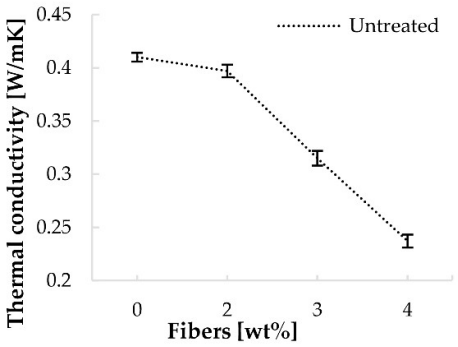

Figure 9. Improvement in power insulation of FRCs when increasing untreated textile waste microfiber content.

6.4. Conclusions

In recent years, the presence of microplastics (MPs) within all environmental compartments (air, water, soil, and biota) has become an emerging global issue, both for the concerning number of MPs and induced health issues in biota. The most prevalent MPs in the air are fibrous microplastics (FMPs), which can spread rapidly from one compartment to another (35% of MPs are in oceans) and have already been found within human tissues and stool. FMPs arise from the lifecycle of synthetic and blended textiles (production, use, and disposal), and their impact on the environment is expected to worsen because of the fast-fashion concept that favors mass production to a circular economic system. Among textile waste (490,000 t/year of special waste and 146,000 t/year of urban waste in Italy), processing waste fibers, including FMPs, are currently not recycled. In particular, waste microfibers from the finishing of fabrics (5000 t/year in Italy) are volatile and are therefore easily released into the environment.

For the first time, this paper proposes a viable solution to the problem of FMPs from processing textile waste microfibers by arranging for their collection directly at the process stage, before spreading into the air or soil. Their collection can occur during the finishing of fabrics using an air-filtering system, and their reuse is hypothesized as reinforcing microfibers into construction materials. Therefore, at the same time, a new mitigation technique for FMPs and the manufacturing of green fiber-reinforced cementitious composite materials (FRC) are proposed. Moreover, by considering blended textile waste microfibers and not only synthetics, this study addresses the issue of FMPs from textile waste by considering a real-like condition.

A composition of 61% pure cotton, 29% cotton blend (cotton and synthetics), and 10% synthetics resulted from the characterization of the blended textile waste microfibers. From size measurements, the synthetic microfibers (accounting for at least 10% of the textile waste microfibers involved) were classified as FMPs, following the ECHA definition.

Portland cement-based FRCs were designed, including up to 4 wt.% of blended textile waste microfibers both in untreated, water-saturated, and NaOH-treated conditions. As expected, the maximum bending load and toughness linearly improved with increased microfiber contents due to the crack-bridging effect enacted by the microfibers. Additionally, the propagation of crack width appeared to be reduced. Remarkably, adding 4 wt.% microfibers enhanced the maximum bending load and toughness of the reference Portland cement by 320% and 715%, respectively. Linear shrinkage and thermal conductivity also appeared to be dependent upon microfiber content. A reduction of up to 80% in linear shrinkage was displayed by FRCs with 4 wt.% microfibers, compared with that of Portland cement, thus strongly preventing the crack formation from shrinkage and lengthening the nominal life of the material. Moreover, the 4 wt.% microfibers also allowed a doubling of the thermal-insulating power. This enhancement stands as a significant achievement for the thermal–energetic performance of buildings and is a direct result of using intrinsically thermal-insulating textile microfibers. Concerning the microfiber treatments, NaOH-treated microfibers displayed the best performance in toughness (above 3 wt.%) and linear shrinkage (below 4 wt.%) due to improved chemical and mechanical adhesion with the cementitious matrix. For microfiber content lower than 3 wt.%, no difference in toughness was detected between different surface conditions, and the same was for 4 wt.% microfiber content in shrinkage. The water-saturation condition was the second most performant treatment in promoting a cement hydration process more controlled and differed over time. Water saturation and NaOH treatment, which are generally intended to improve natural fiber properties, optimized the FRC behavior, thus promoting the use of the overall blended textile microfiber waste, including FMPs.

The viability of producing green FRCs by reusing hitherto-unrecycled-textile waste microfibers was demonstrated. The inclusion of textile waste microfibers additionally brought improved thermal-insulating and mechanical properties to Portland cement. Remarkably, considering the composition of the microfibers, the suggested solution promotes the removal of at least 4 kg of FMPs (almost the same number of FMPs falling in a day in Paris) per ton of cement paste. Hence, a mitigation of MPs from the environment and the production of green and optimized FRCs were validated.

References

[1] Committee for Risk Assessment (RAC); Committee for Socio-economic Analysis (SEAC). *Background Document to the Opinion on the Annex XV Report Proposing Restrictions on Intentionally Added Microplastics*; European Chemicals Agency (ECHA): Helsinki, Finland, 2000.

[2] Zhang, Y.-Q.; Lykaki, M.; Markiewicz, M.; Alrajoula, M.T.; Kraas, C.; Stolte, S. Environmental Contamination by Microplastics Originating from Textiles: Emission, Transport, Fate and Toxicity. *J. Hazard. Mater.* **2022**, *430*, 128453. https://doi.org/10.1016/j.jhazmat.2022.128453.

[3] Brahney, J.; Mahowald, N.; Prank, M.; Cornwell, G.; Klimont, Z.; Matsui, H.; Prather, K.A. Constraining the Atmospheric Limb of the Plastic Cycle. *Proc. Natl. Acad. Sci. USA* **2021**, *118*, e2020719118. https://doi.org/10.1073/pnas.2020719118.

[4] Thompson, R.C.; Olsen, Y.; Mitchell, R.P.; Davis, A.; Rowland, S.J.; John, A.W.G.; McGonigle, D.; Russell, A.E. Lost at Sea: Where Is All the Plastic? *Science* **2004**, *304*, 838–838. https://doi.org/10.1126/science.1094559.

[5] Tadsuwan, K.; Babel, S. Microplastic Abundance and Removal via an Ultrafiltration System Coupled to a Conventional Municipal Wastewater Treatment Plant in Thailand. *J. Environ. Chem. Eng.* **2022**, *10*, 107142. https://doi.org/10.1016/j.jece.2022.107142.

[6] Ahmed, R.; Hamid, A.K.; Krebsbach, S.A.; He, J.; Wang, D. Critical Review of Microplastics Removal from the Environment. *Chemosphere* **2022**, *293*, 133557. https://doi.org/10.1016/j.chemosphere.2022.133557.

[7] Vital-Grappin, A.D.; Ariza-Tarazona, M.C.; Luna-Hernández, V.M.; Villarreal-Chiu, J.F.; Hernández-López, J.M.; Siligardi, C.; Cedillo-González, E.I. The Role of the Reactive Species Involved in the Photocatalytic Degradation of HDPE Microplastics Using C,N-TiO2 Powders. *Polymers* **2021**, *13*, 999. https://doi.org/10.3390/polym13070999.

[8] Domínguez-Jaimes, L.P.; Cedillo-González, E.I.; Luévano-Hipólito, E.; Acuña-Bedoya, J.D.; Hernández-López, J.M. Degradation of Primary Nanoplastics by Photocatalysis Using Different Anodized TiO2 Structures. *J. Hazard. Mater.* **2021**, *413*, 125452. https://doi.org/10.1016/j.jhazmat.2021.125452.

[9] Acuña-Bedoya, J.D.; Luévano-Hipólito, E.; Cedillo-González, E.I.; Domínguez-Jaimes, L.P.; Hurtado, A.M.; Hernández-López, J.M. Boosting Visible-Light Photocatalytic Degradation of Polystyrene Nanoplastics with Immobilized CuxO Obtained by Anodization. *J. Environ. Chem. Eng.* **2021**, *9*, 106208. https://doi.org/10.1016/j.jece.2021.106208.

[10] Tang, Y.; Zhang, S.; Su, Y.; Wu, D.; Zhao, Y.; Xie, B. Removal of Microplastics from Aqueous Solutions by Magnetic Carbon Nanotubes. *Chem. Eng. J.* **2021**, *406*, 126804. https://doi.org/10.1016/j.cej.2020.126804.

[11] Zhang, M.; Yang, J.; Kang, Z.; Wu, X.; Tang, L.; Qiang, Z.; Zhang, D.; Pan, X. Removal of Micron-Scale Microplastic Particles from Different Waters with Efficient Tool of Surface-Functionalized Microbubbles. *J. Hazard. Mater.* **2021**, *404*, 124095. https://doi.org/10.1016/j.jhazmat.2020.124095.

[12] Kumari, A.; Rajput, V.D.; Mandzhieva, S.S.; Rajput, S.; Minkina, T.; Kaur, R.; Sushkova, S.; Kumari, P.; Ranjan, A.; Kalinitchenko, V.P.; et al. Microplastic Pollution: An Emerging Threat to Terrestrial Plants and Insights into Its Remediation Strategies. *Plants* **2022**, *11*, 340. https://doi.org/10.3390/plants11030340.

[13] Dris, R.; Gasperi, J.; Rocher, V.; Saad, M.; Renault, N.; Tassin, B.; Dris, R.; Gasperi, J.; Rocher, V.; Saad, M.; et al. Microplastic Contamination in an Urban Area: A Case Study in Greater Paris. *Environ. Chem.* **2015**, *12*, 592–599. https://doi.org/10.1071/EN14167.

[14] Dris, R.; Gasperi, J.; Saad, M.; Mirande, C.; Tassin, B. Synthetic Fibers in Atmospheric Fallout: A Source of Microplastics in the Environment? *Mar. Pollut. Bull.* **2016**, *104*, 290–293. https://doi.org/10.1016/j.marpolbul.2016.01.006.

[15] Boucher, J.; Friot, D. *Primary Microplastics in the Oceans: A Global Evaluation of Spurces*; International Union for Conservation of Nature and Natural Resources (IUCN): Gland, Switzerland, 2017.

[16] Zhao, T.; Lozano, Y.M.; Rillig, M.C. Microplastics Increase Soil PH and Decrease Microbial Activities as a Function of Microplastic Shape, Polymer Type, and Exposure Time. *Front. Environ. Sci.* **2021**, *9, 675803*.

[17] Barboza, L.G.A.; Lopes, C.; Oliveira, P.; Bessa, F.; Otero, V.; Henriques, B.; Raimundo, J.; Caetano, M.; Vale, C.; Guilhermino, L. Microplastics in Wild Fish from North East Atlantic Ocean and Its Potential for

Causing Neurotoxic Effects, Lipid Oxidative Damage, and Human Health Risks Associated with Ingestion Exposure. *Sci. Total Environ.* **2020**, *717*, 134625. https://doi.org/10.1016/j.scitotenv.2019.134625.

[18] Schwabl, P.; Köppel, S.; Königshofer, P.; Bucsics, T.; Trauner, M.; Reiberger, T.; Liebmann, B. Detection of Various Microplastics in Human Stool: A Prospective Case Series. *Ann. Intern. Med.* **2019**, *171*, 453–457. https://doi.org/10.7326/M19-0618.

[19] Jenner, L.C.; Rotchell, J.M.; Bennett, R.T.; Cowen, M.; Tentzeris, V.; Sadofsky, L.R. Detection of Microplastics in Human Lung Tissue Using MFTIR Spectroscopy. *Sci. Total Environ.* **2022**, *831*, 154907. https://doi.org/10.1016/j.scitotenv.2022.154907.

[20] Grand View Research. *Synthetic Fibers Market Growth Analysis Report, 2021–2028*; 2021; p. 145; Grand View Research, San Francisco, CA, United States.

[21] Istituto Superiore per la Protezione e la Ricerca Ambientale. *Rapporto Rifiuti Speciali, Edizione 2020*; ISPRA-Istituto Superiore per la Protezione e la Ricerca Ambientale: Roma, Italy, 2020; p. 611.

[22] Brandt, A.M. Fibre Reinforced Cement-Based (FRC) Composites after over 40 Years of Development in Building and Civil Engineering. *Compos. Struct.* **2008**, *86*, 3–9. https://doi.org/10.1016/j.compstruct.2008.03.006.

[23] Signorini, C.; Sola, A.; Malchiodi, B.; Nobili, A. Highly Dissipative Fiber-Reinforced Concrete for Structural Screeds. *J. Mater. Civ. Eng.* **2022**, *34*, 04022022. https://doi.org/10.1061/(ASCE)MT.1943-5533.0004160.

[24] Verma, D.; Goh, K.L. Effect of Mercerization/Alkali Surface Treatment of Natural Fibres and Their Utilization in Polymer Composites: Mechanical and Morphological Studies. *J. Compos. Sci.* **2021**, *5*, 175. https://doi.org/10.3390/jcs5070175.

[25] Giraldo, L.J.Q.; Cruz, L.J.; García, J.A.; Alcaraz, A.; González, E.; Osorio, J.A. Incidence of Mercerization Treatment in the Mechanical Properties of Bamboo Fibre Bundles “Guadua Angustifolia Kunth” from Colombian Origin. *DYNA* **2019**, *86*, 156–163. https://doi.org/10.15446/dyna.v86n210.71782.

[26] Rizal, S.; Olaiya, F.G.; Saharudin, N.I.; Abdullah, C.K.; Olaiya, N.G.; Mohamad Haafiz, M.K.; Yahya, E.B.; Sabaruddin, F.A.; Ikramullah; Abdul Khalil, H.P.S. Isolation of Textile Waste Cellulose Nanofibrillated Fibre Reinforced in Polylactic Acid-Chitin Biodegradable Composite for Green Packaging Application. *Polymers* **2021**, *13*, 325. https://doi.org/10.3390/polym13030325.

[27] Hanoğlu, A.; Çay, A.; Yanık, J. Production of Biochars from Textile Fibres through Torrefaction and Their Characterisation. *Energy* **2019**, *166*, 664–673. https://doi.org/10.1016/j.energy.2018.10.123.

[28] Yousef, S.; Tatariants, M.; Tichonovas, M.; Kliucininkas, L.; Lukošiūtė, S.-I.; Yan, L. Sustainable Green Technology for Recovery of Cotton Fibers and Polyester from Textile Waste. *J. Clean. Prod.* **2020**, *254*, 120078. https://doi.org/10.1016/j.jclepro.2020.120078.

[29] Rafikov, A.S.; Khakimova, M.S.; qizi Fayzullayeva, D.A.; Reyimov, A.F. Microstructure, Morphology and Strength of Cotton Yarns Sized by Collagen Solution. *Cellulose* **2020**, *27*, 10369–10384. https://doi.org/10.1007/s10570-020-03450-w.

[30] National Research Council Guide for the Design and Construction of Fiber-Reinforced Concrete Structures 2007.

[31] Payrow, P.; Nokken, M.R.; Banu, D.; Feldman, D. Effect of Surface Treatment on the Post-Peak Residual Strength and Toughness of Polypropylene/Polyethylene-Blended Fiber-Reinforced Concrete. *J. Compos. Mater.* **2011**, *45*, 2047–2054. https://doi.org/10.1177/0021998311399481.

[32] Latif, R.; Wakeel, S.; Zaman Khan, N.; Noor Siddiquee, A.; Lal Verma, S.; Akhtar Khan, Z. Surface Treatments of Plant Fibers and Their Effects on Mechanical Properties of Fiber-Reinforced Composites: A Review. *J. Reinf. Plast. Compos.* **2019**, *38*, 15–30. https://doi.org/10.1177/0731684418802022.

[33] Signorini, C.; Sola, A.; Malchiodi, B.; Nobili, A.; Gatto, A. Failure Mechanism of Silica Coated Polypropylene Fibres for Fibre Reinforced Concrete (FRC). *Constr. Build. Mater.* **2020**, *236*, 117549. https://doi.org/10.1016/j.conbuildmat.2019.117549.

[34] Shafei, B.; Kazemian, M.; Dopko, M.; Najimi, M. State-of-the-Art Review of Capabilities and Limitations of Polymer and Glass Fibers Used for Fiber-Reinforced Concrete. *Materials* **2021**, *14*, 409. https://doi.org/10.3390/ma14020409.

[35] Zhong, H.; Zhang, M. Experimental Study on Engineering Properties of Concrete Reinforced with Hybrid Recycled Tyre Steel and Polypropylene Fibres. *J. Clean. Prod.* **2020**, *259*, 120914. https://doi.org/10.1016/j.jclepro.2020.120914.

[36] Rostami, R.; Zarrebini, M.; Sanginabadi, K.; Mostofinejad, D.; Abtahi, S.M.; Fashandi, H. The Effect of Specific Surface Area of Macro Fibers on Energy Absorption Capacity of Concrete. *J. Text. Inst.* **2019**, *110*, 707–714. https://doi.org/10.1080/00405000.2018.1512040.

[37] Arienzo, M.; Ferrara, L.; Trifuoggi, M. The Dual Role of Microplastics in Marine Environment: Sink and Vectors of Pollutants. *J. Mar. Sci. Eng.* **2021**, *9*, 642. https://doi.org/10.3390/jmse9060642.

[38] Rodrigues, J.P.; Duarte, A.C.; Santos-Echeandía, J.; Rocha-Santos, T. Significance of Interactions between Microplastics and POPs in the Marine Environment: A Critical Overview. *TrAC Trends Anal. Chem.* **2019**, *111*, 252–260. https://doi.org/10.1016/j.trac.2018.11.038.

[39] Luan, X.; Kou, X.; Zhang, L.; Chen, L.; Liu, W.; Cui, Z. Estimation and Prediction of Plastic Losses to the Environment in China from 1950 to 2050. *Resour. Conserv. Recycl.* **2022**, *184*, 106386. https://doi.org/10.1016/j.resconrec.2022.106386.

[40] Siddiqui, M.O.R.; Sun, D. Development of Experimental Setup for Measuring the Thermal Conductivity of Textiles. *Cloth. Text. Res. J.* **2018**, *36*, 215–230. https://doi.org/10.1177/0887302X18768041.

7. Optimized polypropylene fiber reinforced cementitious composites (PP-FRCC)

Note: This chapter is based on a research paper published in a peer reviewed journal.

Submission title-Conference paper: Three sustainable polypropylene surface treatments for the compatibility optimization of PP fibers and cement matrix in fiber-reinforced concrete.

B. Malchiodi, R. Pelaccia, P. Pozzi, C. Siligardi,

Published in Ceramic International, Elsevier

DOI: 10.1016/j.ceramint.2023.02.105

Contribution of the candidate: search for material supply, search for collaboration, experimental design, conduction of the experiments, writing and reviewing, corresponding author.

Fiber-reinforced concrete (FRC) is a cementitious composite material that is gaining interest in the construction field to limit crack propagation and increase toughness. Polypropylene (PP) fibers are promising alternatives to steel fibers, primarily used in FRC, as they reduce weight and cost and are resistant to corrosion. However, the hydrophobic surface of PP inhibits a good adhesion with the surrounding cementitious matrix and so the exploitation of optimized mechanical performance. Though several chemical treatments have been studied, this work suggests more sustainable, cost-efficient, and fast surface treatments for the first time to increase the hydrophilicity of PP: UV-LED, picosecond UV-LASER, and corona discharge treatment. The treatments mainly provided a chemical functionalization without altering the surface morphology of PP, and their effectiveness in increasing PP hydrophilicity was confirmed by ATR-FTIR spectroscopy and optical contact angle measurements. The improved adhesion with the matrix was assessed by the pullout test of treated PP specimens from lime-based and cement-based matrices and by detecting the failure mode in the interphase zone through scanning electron microscopy.

7.1. Introduction

Concrete is the most used construction material worldwide and, thanks to its unrivalled properties (i.e., cost-effectiveness, versatility, easy technology, etc.), its demand is expected to increase further to meet the growing demand for structures and infrastructures in new emergent Countries. On the other hand, the high demand for concrete is significantly responsible for CO_2 emissions, i.e., 8% of global CO_2 emissions [1]. Great efforts are spent to decarbonize the construction sector, including using secondary raw materials, more sustainable blend cement, and optimized concrete mix design and structural design [1]. Among these, the reduction of concrete demand per build-up area could be allowed by increasing concrete durability and mechanical performance. Hence, extending the service life of concrete structures and reducing the cross-section of concrete structural elements without affecting the overall strength of the structure, respectively. In recent decades Fiber Reinforced concrete (FRC), and more generally Fiber Reinforced Cementitious Composites (FRCC), have attracted interest due to their outstanding performance in improving the resistance to degradation and mechanical strength of the cementitious matrix. FRC and FRCC are composite materials mainly applied in the construction sector, which are made of a ceramic matrix (i.e., concrete, mortar) and a fiber reinforcement. As for steel-reinforced concrete, FRC can be defined as ceramic matrix composite (CMC). [2]. Apart from the mechanical properties, fiber reinforcement can modulate the property of FRC and provide additional features such as low thermal conductivity, electrical conductivity, heat resistance, fire resistance, wear resistance, corrosion resistance, etc.

[3,4]. Depending on the fiber type (i.e., steel, glass, carbon, synthetic) and content, the resulting FRC can display a reduction in cracks formation and propagation, an increase in stiffness and strength, or an increase in toughness. The first property is generally associated with microfibers, low fiber contents, and polymeric fibers. The second refers to fibers with a higher strength than the matrix, while the third relates to fibers with less stiffness than the matrix. In general terms, fibers act a crack-bridging effect allowing for the transfer of local stresses beyond cracks and their redistribution in still-resistant regions. By limiting the width of single cracks, the fibers distribute the stresses allowing for narrower and more scattered crack patterns throughout the matrix [5].

The crack-bridging effect relies on the capability of fibers to dissipate energy through friction while being pulled under direct or indirect tensile action. The phenomenon can be described assuming that the fiber is frictionally bonded to the matrix in which it is embedded and that the fiber debonding occurs through the activation of progressive interfacial frictional slip. The most common mechanical models used to describe the crack bridging effect state its dependence on interface shear stress, interface local slippage and fiber geometry. Also, they mainly correlate a higher interface shear stress to fiber surface abrasion, fragmentation of surface coatings and chemical bonding. [6]

Compared to the most used steel fibers, polypropylene (PP) fibers provide FRC toughness, lightweight, anti-spalling properties (fire resistance), chemical resistance to alkaline environments [7], and shrinkage reduction. They are also cost-efficient, easily available, and do not corrode. Nevertheless, the a-polar nature of PP inhibits the proper wettability and adhesion of PP fibers with the cementitious matrix. Several methods have been studied to improve it, either by altering the surface polarity of the fiber or increasing its roughness. The results are promising, but the most studied and effective surface treatments mainly include chemical etching and coating deposition, while the characterization techniques primarily focus on mechanical properties. [8,9]. A more sustainable approach for functionalizing PP fibers would consist of surface treatments with no added chemicals; this would also be more feasible for industrial applications. For the first time, this work suggests alternative, fast, no added chemicals and cost-efficient treatments to increase the hydrophilicity and wettability of PP, thus enhancing its adhesion with the cementitious matrix and optimizing the mechanical properties of PP-FRC. For this purpose, three surface treatments with different highlights were considered: UV-LED, picosecond LASER, and corona discharge.

The UV-LED treatment is a photo-oxidation process, i.e., a photochemical reaction in the presence of oxygen, that increases the polarity and hydrophilicity of polyolefins. It provides high-energy radiation capable of splitting the -C-C and C-H covalent bonds, thus resulting in the formation of reactive radicals and a reduction in the molecular weight of the polymeric surface. The radicals react in the presence of oxygen and generate oxidized groups responsible for an increase in surface polarity. For each polymer, there is a characteristic wavelength range that leads faster to photo-oxidation; for PP the range is between 280 nm and 370 nm.

The corona discharge treatment is an industrial process used for polyolefins films (such as PP and PE) to increase wettability before printing or gluing. The treatment is successful in it by allowing the formation of carboxyl (-COOH), carbonyl (C=O), hydroxyl (-OH), and ester (-COO-) functional groups. It is performed using a generator, a transformer, and a set of electrodes (high-voltage electrode and ground electrode). A potential difference is generated between the electrodes, and high-frequency current discharges occur. The discharge of high-frequency electrons on the desired surface breaks the surface macromolecules and creates reactive radicals. These radicals then react with the oxygen in the air and generate oxidized functional groups on the treated polyolefin surface. The corona discharge treatment does not affect the strength and appearance of the treated surface. And it is a fast, cost-efficient, and effective treatment. Nevertheless, the process ionizes the air and the functionalization effect decades over time [10-12].

The LASER treatment ablates the specimen surface with a focused LASER beam of a specific wavelength. In the context of the ultrashort LASER, the combination of proper LASER parameters

(power [W], repetition rate [KHz], scan speed [mm/s]) and the scanning strategy allow obtaining the surface texturing at the micro and nanoscales without altering the mechanical properties of the bulk material at the macroscales [13]. The main advantages of this technology are the absence of contact and consequently the contamination of the treated surface, the reduced treatment exposition, the easy automation that offers the opportunity to treat large areas, and the low environmental impact [13,14]. Notably, LASER texturing became an efficient and reliable technique to modify the wettability of different materials such as metals, ceramics, and polymers [14-16]. About the latter, some studies have investigated the effects of LASER texturing on PP wettability, taking advantage of the generation of topographical and chemical alterations [17,18].

In this context, the ultimate goal of this work is to characterize the PP surface after the three selected treatments thoroughly and to link the chemical and physical alterations to the mechanical performance of the composite material (i.e., PP-FRC). Dog-bone PP specimens instead of fibers were considered to avoid the influence of the fiber shape, thus easing the treatment and characterization of the PP surface. Contact angle, ATR-FTIR, and ESEM were involved in the surface characterization. Additionally, a 28-day pullout test was carried out for PP specimens embedded into mortars to highlight the effects of surface functionalization on the chemical and frictional adhesion of PP-FRC.

7.2. Materials and Methods

PP specimens

Polypropylene (PP) flat supports were considered instead of PP fibers to avoid the influence of fiber shape, thus simplifying the PP surface treatment and characterization. Therefore, dog-bone PP specimens (Figure 1) were manufactured by injection molding using homopolymer PP granules by INEOS Olefins & Polymers Europe with a density of 0.91 g/cm^3. As displayed by the CAD drawing in Figure 1, the PP specimens were 75 mm long, 9.9 mm wide and 2 mm thick. The manufacturing was performed using the injection molding machine Mega Tech H7/18-1 (Tecnicaduebi Srl) and considering the setting parameters from Tab. 1.

Table 1. Manufacturing parameters for the injection molding process.

Temperature [°C]		**Time [s]**	
Hopper	200	Mold Retention	9
Screw	240	Maintenance	3
Cylinder	220		
Nozzle	220		

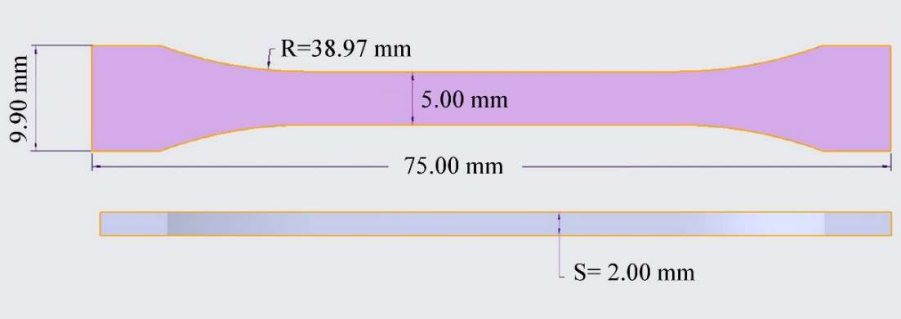

Figure 1. Geometry of the PP specimen manufactured by injection molding.

The PP specimens were then lapped with SiC papers (from P800 to P2500) and polished with colloidal diamond suspension (~3 µm size) to remove manufacturing defects and surface roughness. In the end, they were ultrasonically cleaned in acetone for 3 minutes and dried with compressed air.

Three surface treatments were considered to increase the compatibility of PP with cementitious matrices, namely UV-LED (2.1.1), picosecond LASER treatments (2.1.2), and corona discharge (2.1.3). These were expected to increase the polarity and hydrophilicity of PP through surface functionalization (oxidation and photo-oxidation) and so increase the wettability and adhesion with cementitious matrixes. All the treated PP specimens were kept in a vacuum desiccator until their characterization.

The wettability of the treated PP specimens was assessed through Optical Contact Angle (OCA) by Dataphysic and compared to that of the untreated one. The test was performed using a 3.5 µl drop of distilled water, and the contact angle image was acquired after 10 s using SCA20 software. Three measurements for each specimen were performed, and the average and standard deviation were assessed.

ATR-FTIR spectroscopy (ATR-FTIR VERTEX 70 by Bruker Optics, Ettlingen, Germany) was involved in detecting the oxidized groups characteristic of treated PP specimens compared to the untreated ones. Opus 6.5 by Bruker Optics GmbH allowed the analysis of the spectra, which were acquired after 32 scans, with a 4 cm^{-1} resolution, and in a 600 - 4000 cm^{-1} transmittance range.

Optical microscopy (CTR 4000 Leica, 100x) was involved to eventually detect morphological alteration brought by the treatments on the PP surface. Higher magnifications through optical or scanning electron microscopy were not considered because the main effects expected of the involved surface treatments were functionalizing and not morphological.

UV-LED treatment

The UV treatment was performed using a UV LED lamp by Photo Electronics with a peak wavelength of 395 nm and maximum irradiance of 12 W/cm^2. The UV lamp was fixed at 65 mm high to the specimens and set at the maximum irradiance value. A cold air source was installed at 20 cm from the specimens to reduce heat on the PP surface and limit the maximum surface temperature to 50°C. In addition, the specimens were lifted from the support by plastic clamps to encourage air circulation on the specimen surface not exposed to radiation (Fig. 2a). Different exposition times were considered for UV-LED treatment of PP, namely 6 h, 12 h, 24 h and 36 h. The setup of UV-LED treatment is shown in Fig. 2b.

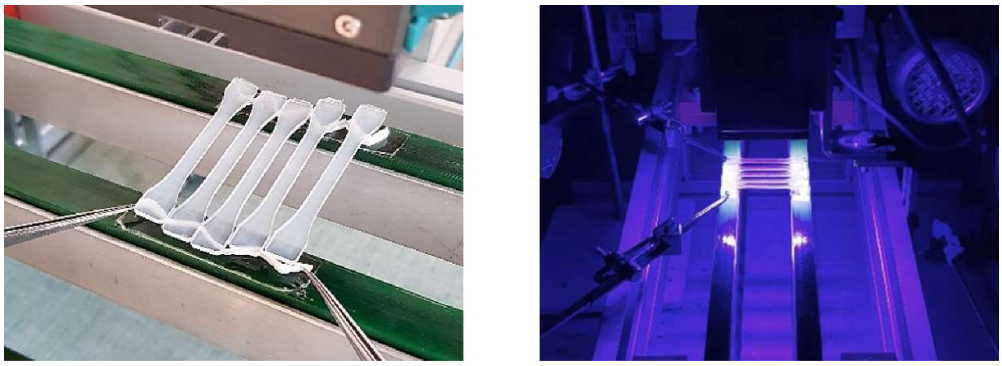

(a) (b)

Figure 2. UV-LED treatment of PP specimens: a) positioning of dog-bone PP specimens, b) treatment setup.

LASER treatment

LASER treatments were performed using a picosecond amplifier EKSPLA Atlantic 5 LASER, which allows three beamlines (1064, 532, and 355 nm) with a pulse duration of about 10 ps. In this work, the 355 nm beamline was employed to guarantee the maximum energy absorption for polymeric materials [9]. Along the optical path of each beamline, a beam expander is inserted to obtain a beam diameter of 15 mm at the entrance of the galvanometric scanner. Raylase Superscan V galvanometric scanner coupled with a 104 mm F-theta lens allowed a focused beam with a $1/e2$ spot diameter of 10 µm and a working area of 46 x 46 mm on the specimen surface. However, since the LASER system is integrated with a 3-axis (X-Y-Z) movement system, it is possible to move the worktable to increase the working area during the LASER treatment.

The LASER treatment ablated the specimen surface following overlapped parallel scanlines perpendicular to the long side of the PP specimen. Keeping the movement system fixed, it was possible to treat three specimens simultaneously (Fig.3b) in a few seconds or minutes, depending on the selected process parameters (Tab.2). The scanner strategy was chosen to generate a uniform pulse distribution and so a uniform energy deposition on the specimen surface. Notably, the combination of scanner speed (500 mm/s), pulse repetition rate (100 kHz), and distance between two consecutive scanlines (5 µm) was selected to obtain an overlapping of 50% between two successive pulses on the entire treated surface (Fig.3a). The processing time to treat three specimens at once was 80 seconds with the selected kinematic configuration.

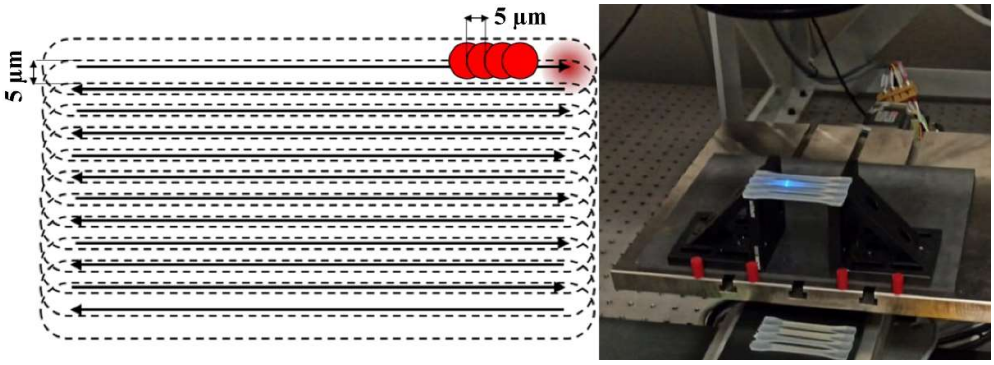

(a) (b)

Figure 3. Picosecond LASER treatment: a) schematization of the scanner pulses distribution, b) treatment of dog-bone PP specimens.

Six levels of LASER power were tested, starting from a low value (5 %) that caused no visible signs of ablation on the surface to a threshold value (40 %) that caused significant burns on the specimen (Fig.4). Tab. 2 summarizes the process parameters for all six tested conditions. The last condition (40% of LASER power) was not considered for the functionalization of the PP surface to avoid possible random results due to burning.

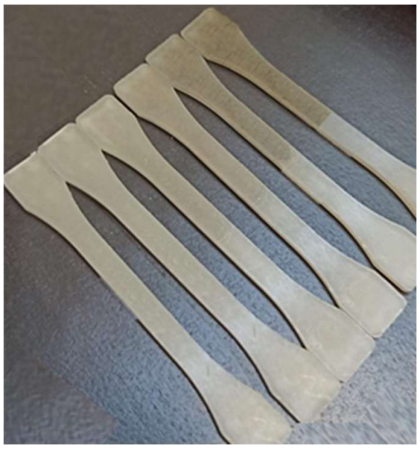

Figure 4. Macroscopic overview of LASER-treated PP specimens from 5% of laser power (left side) to 40% of laser power (right side).

Table 2. Process parameters of the six LASER treatment conditions.

Power [%]	Power [mW]	Pulse energy [µJ]	Macroscopic evidence [-]
5	1	0.01	No ablation
10	8	0.08	No ablation
15	18	0.18	Slight ablation
25	56	0.56	Ablation without burns
30	84	0.84	Ablation without burns
40	140	1.4	Significant ablation and burns

Corona discharge treatment

The corona discharge treatment was carried out using the BD-20ACV corona discharge instrument from Electro technic products, equipped with a field-effect electrode (suitable for treating both flat and curved surfaces). The device consists of a Bakelite gun containing the generator, electronic-mechanical groups, and the field effect electrode at one end. The power supply unit is separate. In addition, an aluminum plate was used as the second electrode, on which the specimens were placed individually. The experimental setup for the corona discharge treatment is displayed in Fig. 5.

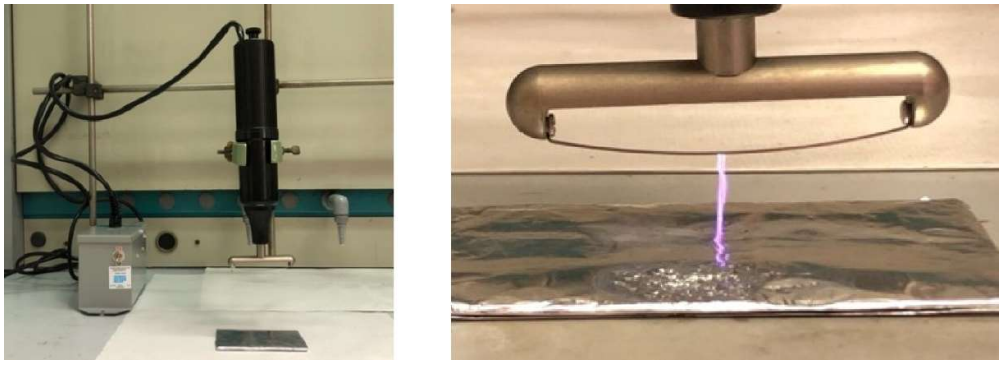

(a) (b)

Figure 5. Corona discharge treatment: a) treatment setup, b) spark discharge between the electrodes.

Based on literature evidence, the most effective discharge voltage was 35 kV [11]. Since the involved instrument could not directly set the discharge voltage value, a correlation with the spark length was found. Referring to the instrument datasheet, a discharge voltage of 35 kV was associated with a

spark length of 18 mm. Several trial setups were tested to reproduce this condition by varying the voltage knob position and the distance between the electrodes while a video recording of the discharge occurred. The variation of the spark length was evaluated through ImageJ software (1.53k Version) on different frames obtained from the video recordings. The best setups were used to treat the PP specimens and involved the voltage knob at half of a turn and 4 mm, 9 mm, and 18 mm electrode distances. Additionally, different exposition times were considered, i.e., 5 s, 10 s, 30 s, 60 s, and 120 s. The treatment was carried out under a chemical fume hood at atmospheric laboratory conditions.

The effectiveness of corona treatment is limited in time (aging) due to the reorientation of the polar molecules, which causes a decrease in the surface free energy (increase in hydrophobicity) [10,19]. For this reason, the characterization of the corona-treated PP specimens and the manufacturing of corona-treated PP composites were performed immediately after the treatment.

Composite samples for pullout test

A pullout test on the composite samples was carried out to highlight the effectiveness of surface treatments in improving PP-to-matrix adhesion. For this mechanical test, the best corona discharge treatment (18 mm electrode distance and 120 s exposure) and the best UV-LED treatment (36 hours) were considered. The pullout test of LASER-treated composite samples is part of an ongoing experimental campaign and is not discussed in this work. Two commercially available premixed mortars were used to manufacture the pullout specimens: a Natural Hydraulic Lime mortar (Geocalce G antisismico by Kerakoll S.p.A) and a cementitious mortar (Geolite by Kerakoll S.p.A). Water-to-premixed mortar ratios of 0.2 and 0.204, respectively, were considered as prescribed by the technical data sheets of the commercial products. The premixed mortars were mixed with water for 1 min at 220 rpm and 4 min at 330 rpm using an axial-flow automatic mixer (RW20 DZM, IKA-Werke GmbH & Co. KG, Staufen, Germany). The so-obtained mortars were poured into silicon cubic molds (50 x 50 x 50 mm3) and vibrated on a portable vibrating plate (Controls Group) for 3 min at maximum speed. One end of the dog-bone PP specimens was cut, and the 5 mm-constant mid-section was embedded 30 mm into the fresh mortar cubes. A metal frame consisting of vertical support brackets and horizontal bolted plates was designed and used to maintain the verticality of the PP dog-bone specimens during the composite sample preparation and curing (Fig. 6a). The composite samples were clamped to the horizontal plates for one day while covering with a plastic sheet. Then the composite samples were demolded, removed from the structure, and cured for 7 days in a climatic chamber (20 °C and RH 90%) and lately 21 days at laboratory conditions, covered with a plastic sheet. Fig. 6b shows the demolded samples after the 28-day curing.

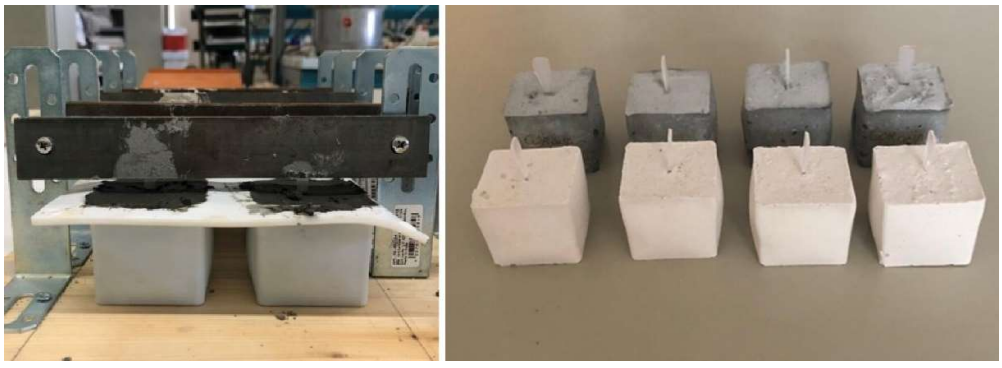

(a) (b)

Figure 6. Pullout composite samples: a) manufacturing setup for the vertical embedment of PP dog-bone specimens into the cementitious matrix and b) pullout composite samples with Geolite (dark grey) and Geomalta (white).

The pullout test was performed at 28 days using a UTM Instron 5567 equipped with a 30 kN load cell. The test was carried out at a 2 mm/min displacement rate under displacement control, and the data were collected by Bluehill software. The PP specimen was gripped with an upper pneumatic clamp (Fig. 7a). While the hardened mortar cube was constrained to a purpose-built steel hollow device with an upper hole for the passage of the PP specimen and which was fixed to a lower clamp (Fig. 7b). Four composite samples for each type of mortar and surface treatment were produced and pullout tested. The mechanical results of each composite sample were expressed in terms of load-displacement curve, maximum peak load, residual load (at 25 mm displacement), and deformation energy (until 25mm displacement). The average value and standard deviation were also evaluated. To further compare the effect of improved adhesion, scanning electron microscopy micrographs (ESEM Quanta 200, Fei Company, Oxford Instruments) detected the number of mortar particles adhering to the treated PP surfaces after pullout in comparison with the untreated ones.

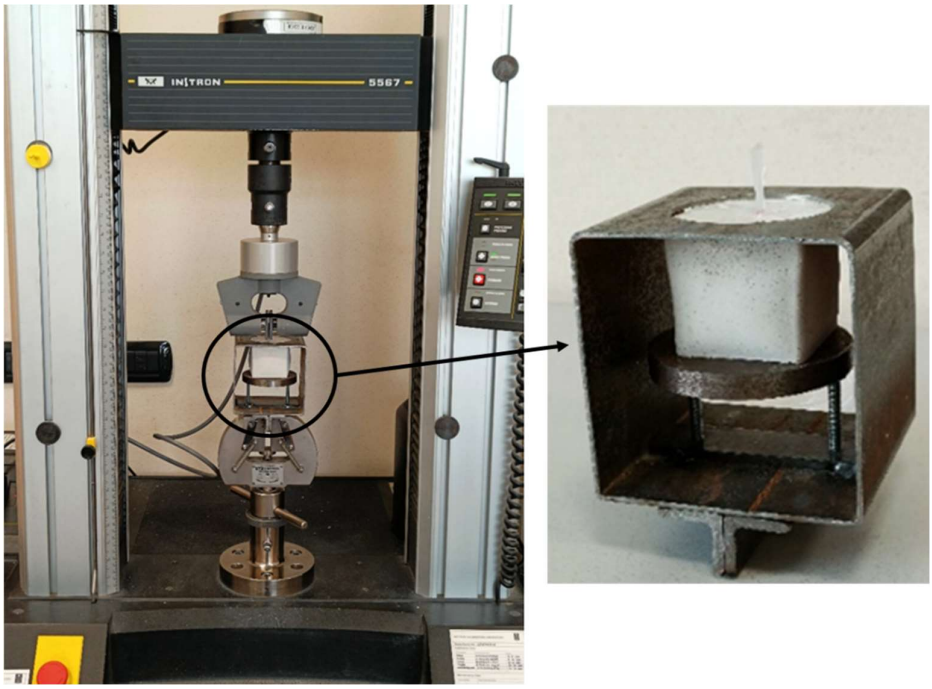

(a) (b)

Figure 7. Pullout testing setup: a) overall setup using UTM, b) retaining device for the mortar cube.

7.3. Results and discussion

The results obtained from the contact angle measurements are summarized in Fig. 8 for UV-LED (Fig. 8a), picosecond LASER (Fig. 8b) and corona discharge treatment (Fig. 8c). The graphs show the average contact angle results (bar charts) and the associated standard deviations (error bars). As can be seen in Fig. 8a, the effectiveness of UV-LED in improving the PP wettability occurred with increasing exposition time. The best contact angle reduction was around -10% compared to the reference PP specimen (around 105°deg). Although there was an actual reduction in the contact angle, the low improvement value can be related to the glossy surface of the specimens. In fact, the brightness resulting from the surface polishing phase may have partially contributed to the reflection of the UV-LED source and thus mitigated its effect.

Regarding the picosecond LASER treatment, a wettability increase was displayed as the LASER power increased (Fig. 8b). The maximum decrease in contact angle of about 20% was obtained

considering a LASER power by 30% (see Tab. 2). The reduction in contact angle was also observed by Rivero et al. [17] and Buchman et al. [18] for PP surfaces treated with ultrashort LASER.

The corona discharge treatment was more effective in reducing the contact angle of PP as the electrode distance and exposition time increased (Fig. 8c). Notably, a reduction in contact angle of up to 40% (for electrode distance of 18 mm and treatment time of 120 s) was observed. The best treatment conditions (and nomenclature assigned) resulting from the contact angle measurements are shown in Tab. 3.

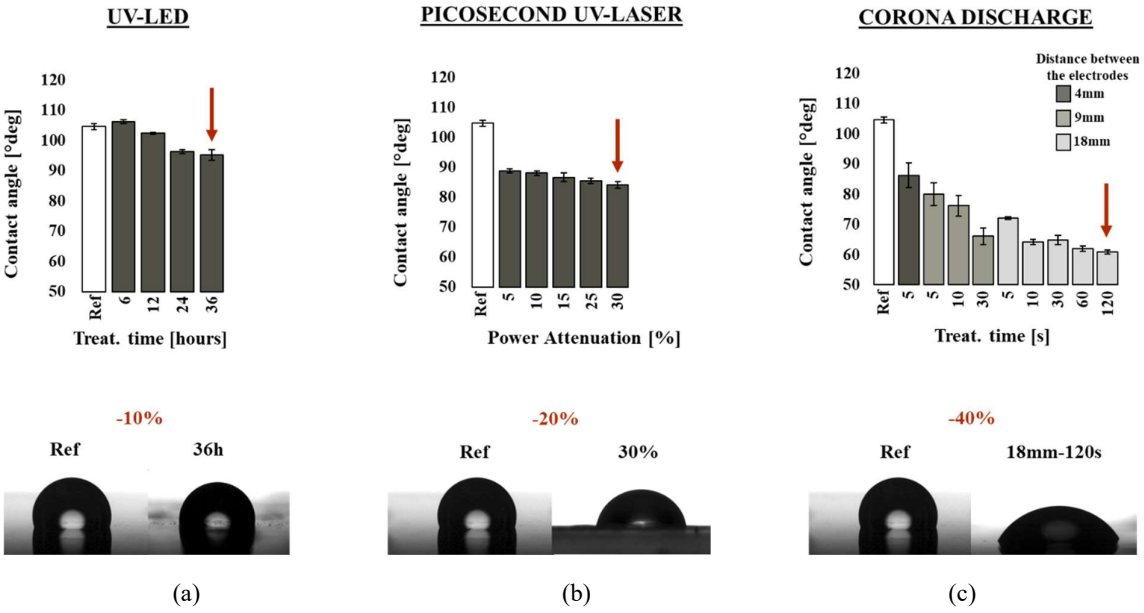

Figure 8. Contact angle results for PP specimens treated by a) UV-LED, b) picosecond LASER, and c) corona discharge. The error bars stand for standard deviation error.

Table 3. Best treatment conditions for UV-LED, picosecond LASER, and corona discharge treatments obtained from the contact angle measurements.

Treatment	**Best conditions**	**Specimen Nomenclature**
UV-LED	36 hours – exposition time	UV-LED 36
Picosecond LASER	30% - LASER power	LASER 30
Corona discharge	18 mm - electrode distance 120 s - exposition time	CORONA 18-120

The ATR-FTIR also identified the functionalization effect promoted by the PP surface treatments (Fig. 9) by detecting carboxyl (-COOH), carbonyl (C=O), hydroxyl (O-H) and ester (-COO-) groups. [11,12]. Remarkably, the infrared spectroscopy confirmed the same trend in improving the PP surface functionalization as from the contact angle measurement, and the best treatment conditions are the same of Tab. 3. The main results from the ATR-FTIR characterization of corona-treated specimens are displayed in Fig. 9 and stand as a representative overview also for UV-LED and picosecond LASER results. As the electrode distance and exposition time (and exposition time for UV-LED and LASER power for picosecond LASER treatment) increased, the intensity of the characteristic peaks related to functional groups increased, i.e., carbonyl, hydroxyl, and carboxyl ester. At the same time, those of the polypropylene structure decreased (Fig. 9a). Precisely, a peak increase is observed at 3200-3500 (-OH), 1630-1720 (C=O), 970-1250 (C-O), while a peak decrease at 2850-3000 and 1350-1470 (CH_2, CH_3, CH) and 2700-2840 (C-H) occurred. [11,12]. To better

highlight the functionalization effect, Fig. 9b compares the ATR-FTIR spectra of the untreated reference specimen (red line) and the one treated with optimal corona treatment condition (green line).

On the other hand, no morphological surface alterations resulting from the treatments were observed through optical microscopy (Fig. 10). Hence, it was concluded that the involved functionalization was mainly chemical. Fig. 10a shows the surface of untreated PP, while Fig. 10b that of a representative treated PP specimen (optimal corona discharge treatments). All the treatments involved did not cause any significant morphological alteration.

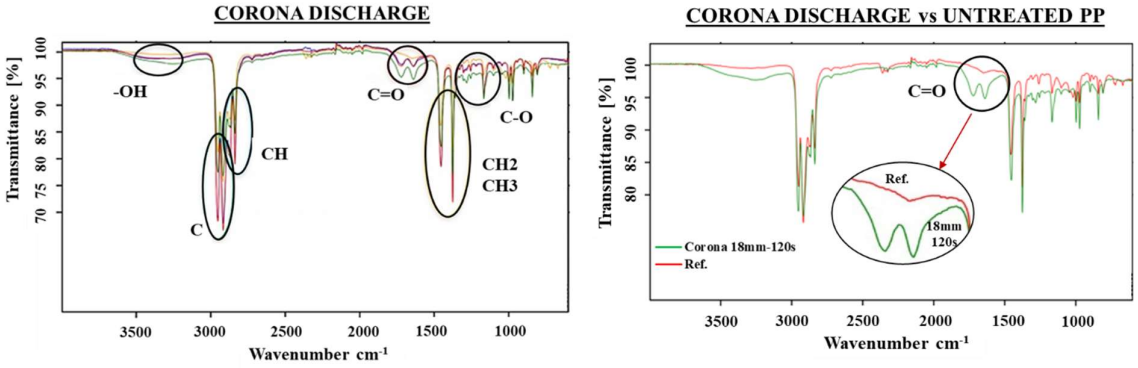

(a) (b)

Figure 9. ATR-FTIR spectra results of a) all corona discharge-treated PP specimens and b) the best corona discharge treatment compared to the reference untreated PP specimen.

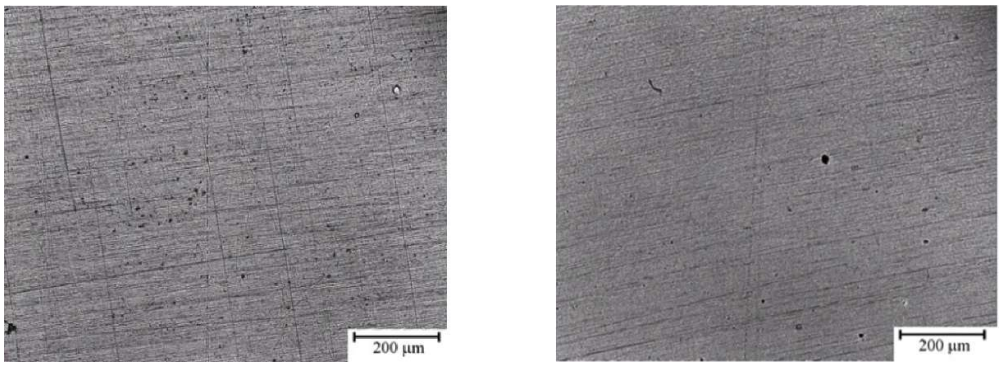

(a) (b)

Figure 10. Optical micrographs at 100x magnitude registering no surface morphological alteration a) before and b) after the surface treatments. In Fig 10b, the corona discharge-treated surface is reported as representing all other surface treatments.

The chemical functionalization of PP enhanced the mechanical performance of PP composites. Indeed, the improved chemical affinity of PP with the surrounding matrix allowed for better adhesion and, thus, the frictional interaction between the phases [6]. As a result, an overall improvement in the load-displacement curve was observed for both lime-based (Fig. 11a) and cement-based composites (Fig. 11b).

The untreated PP composite with lime-based mortar (light grey line, Fig. 11a) was less performing than that with cement-based mortar (light grey line, Fig. 11b). Remarkably, the UV-LED treatment was particularly effective in the lime-based mortar and allowed to reach maximum peak load, residual load and deformation energy comparable to that of cement-based composites (Fig. 12, Fig. 13, Fig. 14). Whereas no significant increase in maximum peak load and residual load was displayed for corona-treated PP composites in lime-based mortar.

On the other hand, the treatments slightly improved the maximum peak load for cement-based composites (Fig. 12b). As a result, treated-PP composites displayed higher resistance than untreated ones to the first tensile cracking.

Most notably, significant improvements in residual load and deformation energy were obtained for treated PP composites compared to untreated ones (Fig. 13 and Fig. 14). In detail, UV-LED improved by +134% and +66% the residual load of untreated lime-based (Fig. 13a) and cement-based composites (Fig. 13b), respectively. And corona discharge increased the residual load of cement-based composite by +45% (Fig. 13b). Deformation energy enhancements by +129% and +19% were recorded for UV-LED composites with lime-based mortar (Fig. 14a) and cement-based mortar (Fig. 14b), respectively. On the other hand, the same parameter was raised by corona discharge treatment by +46% and +22% for lime-based mortar (Fig. 14a) and cement-based mortar (Fig. 14b), respectively. Hence, the functionalization treatments promoted toughness and the capability of absorbing higher energy before failure. This is a desirable feature in composite materials like FRC; indeed, it indicates good adhesion and stress transfer from the brittle matrix to the more ductile reinforcement.

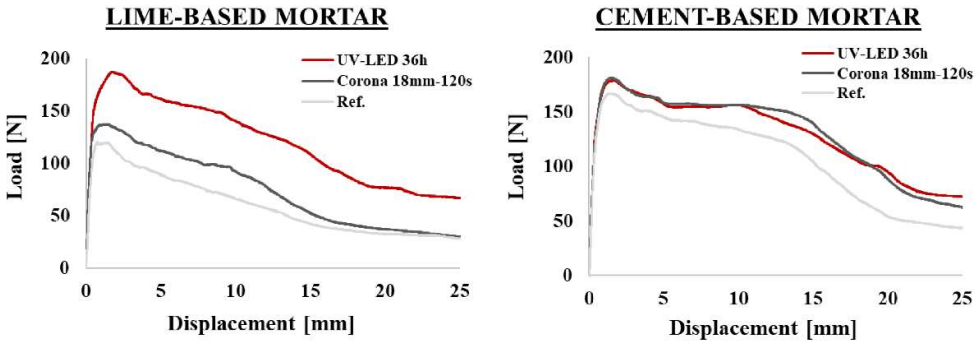

Figure 11. Load- displacement curves resulting from the pullout test of PP composite samples manufactured with a) lime-based mortar and b) cement-based mortar.

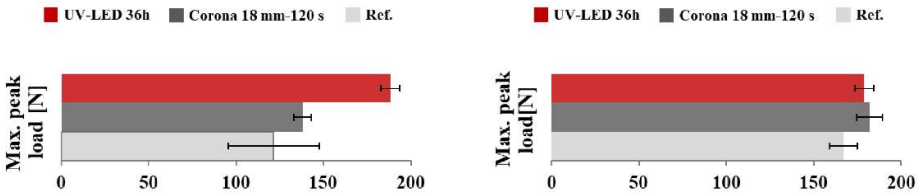

Figure 12. Maximum peak load resulting from the pullout test of PP composite samples manufactured with a) lime-based mortar and b) cement-based mortar. The error bars stand for standard deviation error.

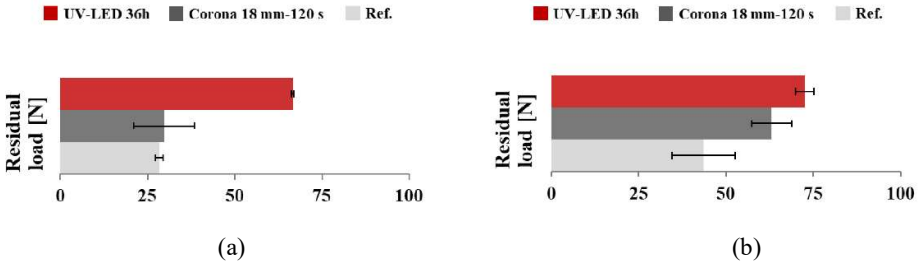

Figure 13. Residual load (at 25 mm displacement) resulting from the pullout test of PP composite samples manufactured with a) lime-based mortar and b) cement-based mortar. The error bars stand for standard deviation error.

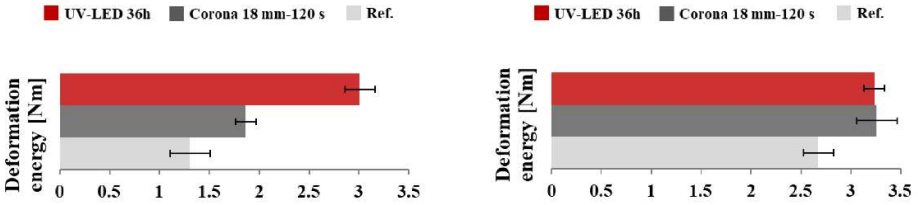

Figure 14. Deformation energy (until 25 mm displacement) resulting from the pullout test of PP composite samples manufactured with a) lime-based mortar and b) cement-based mortar. The error bars stand for standard deviation error.

The functionalized surfaces provided a chemical adhesion with the surrounding matrix, the effectiveness of which was evaluated by observing the number of mortar particles to the PP specimen after pullout from the matrix. Confirming the mechanical results and chemical functionalization evidence, the treated PP specimens (Fig. 15b) showed more mortar particles adhering to the surface after the pullout test than the untreated ones (Fig. 15a). So, the failure of the treated PP composites occurred at higher deformation energy and within the interfacial transition zone (ITZ) allowing for a better stress distribution between the bulk matrix and the reinforcement. This means that the treatments promoted stronger adhesion between the phases and a higher shear frictional strength during pullout [20]. Conversely, the failure occurred through debonding and slipping from the matrix for the untreated PP composites (no mortar particles adhering, Fig. 15a) [21]. Confirming the literature findings, the modified adhesion between the PP reinforcement and matrix influenced the deformation mechanism of the reinforcement and, consequently, the failure mode of the composite [5].

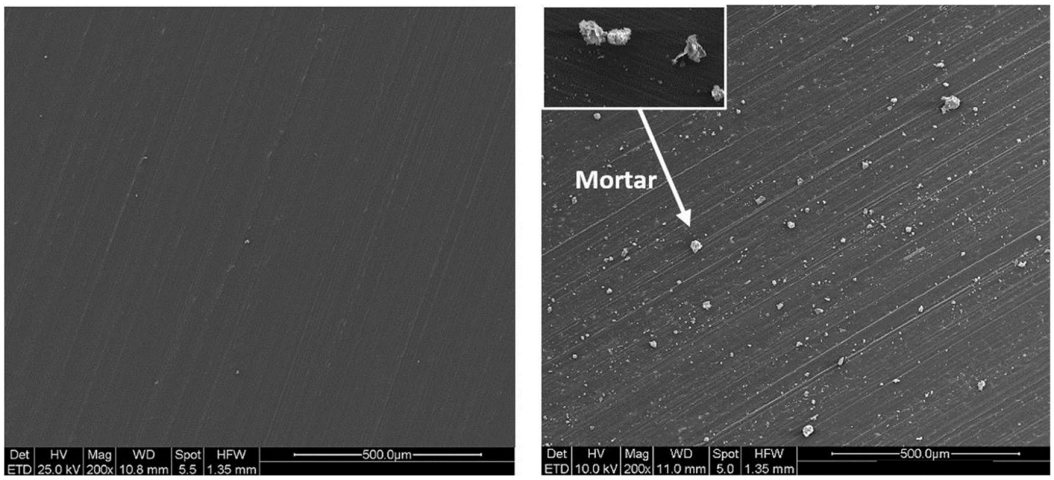

Figure 15. ESEM images at 200x showing the number of mortar particles adhering on the PP surface after the pullout test for a) untreated PP and b) treated PP.

7.4. Conclusions

Several chemical surface treatments have been studied to improve the poor adhesion of PP with cementitious matrix, thus promoting PP fibers as an alternative to steel fibers in fiber-reinforced concrete (FRC). For the first time, this work suggested more sustainable (no chemicals added), fast,

cost-efficient, and industrially scalable surface treatments (UV-LED, picosecond UV-LASER, and corona discharge) aimed at improving the adhesion between PP and cementitious matrix. Increasing exposition time from 6 h to 36 h, LASER power from 0 % to 30 %, and electrode distance from 4 mm to 18 mm with exposition time from 5 s to 120 s were considered for UV-LED, picosecond UV-LASER, and corona discharge, respectively. The most effective setups and exposition parameters were identified, and the main characterization results showed that:

- For ATR-FTIR spectroscopy, all treatments increased the PP hydrophilicity by altering the surface chemical structure (oxidation and photooxidation) and providing C=O, C=O, -OH bonds. Additionally, all treatment conditions reduced the contact angle compared to the untreated PP surface.
- The highest oxides FTIR peaks intensity and contact angle reduction set the optimized treatment conditions, namely 36 h for the UV-LED, 30% LASER power for the picosecond UV-LASER, and 18 mm electrode distance and 120 s for the corona discharge. Notably, the contact angle of PP was reduced by 10% up to 40%.
- The involved treatments resulted in the functionalization of the surface without altering its morphology. So, a chemical rather than a physical adhesion with the cementitious matrix was expected.
- The optimized treatment conditions of UV-LED and corona discharge treatments enhanced the pullout performance of PP composite samples. The residual load and deformation energy were significantly increased, and numerous mortar particles remained adhering to the treated PP surface as proof of better adhesion. Because of a better phase interaction, the failure mode changed from slipping from the matrix (untreated PP) to cracking in the interphase zone (treated PP). UV-LED and corona discharge treatments were equally effective in cement-based composites, while UV-LED was more effective than corona discharge in lime-based composites.

These promising results highlighted the feasibility of optimizing the mechanical performance of PP-FRCs by enhancing the chemical adhesion between PP and cementitious matrixes. Significant improvements, such as the change in failure mode, were observed for all the surface treatments involved. Remarkably, the possibility of considering non-chemical reactants and easy, fast, and cost-efficient setup conditions was pointed out for the first time to increase PP wettability and hydrophilicity. The present analysis is being further investigated for LASER treatment in an ongoing experimental campaign, evaluating the effects induced by surface topographical alteration at micro and nanoscales (i.e., grooves, grids, and holes) in addition to chemical functionalization.

References

[1] A Favier, C. De Wolf, et al., A sustainable future for the European Cement and Concrete Industry. Technology assessment for full decarbonisation of the industry by 2050, ETH Zurich, 2018. https://doi.org/10.3929/ethz-b-000301843.

[2] B Ralph, H.C. Yuen, W.B. Lee, The processing of metal matrix composites - an overview, J. Mater. Process. Technol. 63 (1997) 339-353. https://doi.org/10.1016/S0924-0136(96)02645-3.

[3] S. Maitra, Nanoceramic matrix composites: types, processing and applications, in: I.M. Low, Advances in Ceramic Matrix Composites, Woodhead Publishing, 2014, pp. 691-709.

[4] J. Cho, A.R. Boccaccini, M.S.P. Shaffer, Ceramic matrix composites containing carbon nanotubes, J Mater Sci 44 (2009) 1934–1951. https://doi.org/10.1007/s10853-009-3262-9.

[5] V. Zacharda, J. Němeček, P. Štemberk, 2017. Micromechanical performance of interfacial transition zone in fiber-reinforced cement matrix. IOP Conf. Ser.: Mater. Sci. Eng. 246, 012018. https://doi.org/10.1088/1757-899X/246/1/012018.

[6] Z. Lin, V. C. Li, Crack bridging in fiber reinforced cementitious composites with slip-hardening interfaces, J Mech Phys Solids 45 (5) (1997) 763-787. https://doi.org/10.1016/S0022-5096(96)00095-6.

[7] Z. Zheng, D. Feldman, Synthetic fibre-reinforced concrete, Prog. Polym. Sci. 20 (2) (1995) 185-210. https://doi.org/10.1016/0079-6700(94)00030-6.

[8] C. Signorini, A. Sola, B. Malchiodi, A. Nobili, 2022. Highly Dissipative Fiber-Reinforced Concrete for Structural Screeds. J. Mater. Civ. Eng. 34 (4), 04022022. https://doi.org/10.1061/(ASCE)MT.1943-5533.0004160.

[9] L. Akand, M. Yang, X. Wang, Effectiveness of chemical treatment on polypropylene fibers as reinforcement in pervious concrete, Constr Build Mater. 163 (2018) 32-39. https://doi.org/10.1016/j.conbuildmat.2017.12.068.

[10] J. Izdebska, Corona Treatment, in: J. Izdebska, S. Thomas, Printing on Polymers: Fundamentals and Applications, William Andrew Publishing, 2016, pp. 123-142.

[11] V. C. Louzi, J. S. de C. Campos, Corona treatment applied to synthetic polymeric monofilaments (PP, PET, and PA-6), Surf. Interfaces 14 (2019) 98–107. https://doi.org/10.1016/j.surfin.2018.12.005.

[12] N. Sellin, J. S. de C. Campos, Surface composition analysis of PP films treated by corona discharge, Mater. Res. 6 (2) (2003) 163–166. https://doi.org/10.1590/s1516-14392003000200009.

[13] L. Orazi, L. Romoli, M. Schmidt, L. Li, Ultrafast laser manufacturing: from physics to industrial applications, CIRP Ann. 70 (2) (2021) 543-566. https://doi.org/10.1016/j.cirp.2021.05.007.

[14] A. Riveiro, P. Pou, et al., Laser texturing to control the wettability of materials, Procedia CIRP 94 (2020) 879-884. https://doi.org/10.1016/j.procir.2020.09.065.

[15] A. O. Ijaola, E. A. Bamidele, et al., 2020. Wettability Transition for Laser Textured Surfaces: A Comprehensive Review. Surf. Interfaces 21, 100802. https://doi.org/10.1016/j.surfin.2020.100802.

[16] A. Riveiro, ALB Maçon, J. del Val, et al., 2018. Laser Surface Texturing of Polymers for Biomedical Applications. Front. Phys. 6, 16. https://doi.org/10.3389/fphy.2018.00016.

[17] A. Riveiro, R. Soto, et al., Texturing of polypropylene (PP) with nanosecond lasers, Appl. Surf. Sci. 374 (2016) 379-386. http://dx.doi.org/10.1016/j.apsusc.2016.01.206.

[18] A. Buchman, M. Rotel, H Dodiuk, Nd: YAG Laser Surface Treatment of Various Materials to Enhance Adhesion. in: K.L. Mittal, T. Bahners Laser Surface Modification and Adhesion, Scrivener Publishing LLC, 2014, pp. 1-53.

[19] J.E. Klemberg-Sapieha, L. Martinu, S. Sapieha, M.R. Wertheimer, Control and modification of surfaces and interfaces by corona and low pressure plasma, in: G. Akovali (Eds.), The interfacial Interactions in Polymeric Composites, Springer, Dordrecht, 1993, pp. 201–222.

[20] P. Di Maida, C. Sciancalepore, E. Radi, F. Bondioli, Effects of nano-silica treatment on the flexural post cracking behaviour of polypropylene macro-synthetic fibre reinforced concrete, Mech. Res. Commun. 88 (2018) 12-18. https://doi.org/10.1016/j.mechrescom.2018.01.004.

[21] C. Signorini, A. Sola, B. Malchiodi, A. Nobili, A. Gatto, 2020. Failure mechanism of silica coated polypropylene fibres for Fibre Reinforced Concrete (FRC). Constr Build Mater. 236, 117549. https://doi.org/10.1016/j.conbuildmat.2019.117549.

8. Limestone calcined clay cement (LC^3) as sustainable binder in structural concrete

Note: This chapter is based on a conference paper submitted for the 16th International Congress on the Chemistry of Cement 2023 (ICCC2023), September 18–22, 2023, Bangkok, Thailand. It is also based on a Magazine article for Made Mass Unit.

- Submission title - Conference paper: The use of optimized LC^3 concrete mixes to decrease the carbon footprint of a reinforced concrete building below 100 kg CO_2 eq./m^2

B. Malchiodi, H. Hafez, P. Pozzi, C. Siligardi, K. Scrivener

Contribution of the candidate: experimental design, conduction of the experiments, writing and reviewing, presenting author, corresponding author.

- Submission title - Magazine article: Limestone Calcined Clay Cement (LC^3) is leading the construction sector toward carbon neutrality

B. Malchiodi, H. Hafez, K. Scrivener

Contribution of the candidate: writing and reviewing, corresponding author.

The decarbonization of the construction industry could contribute to an 8% reduction in overall CO_2 emissions by 2050. There is a clear consensus that reducing the clinker content in cement along with reducing the cement content in concrete is the main strategy to achieve this goal. Combining both premises, this study was designed to further reduce the carbon footprint of the most promising and ready-to-use sustainable binder (limestone calcined clay cement-LC^3) and LC^3 structural concrete. The concrete mixes were designed to reduce the LC^3 binder content to 250 kg/m^3 while replacing up to 75% of the clinker content in cement.

The fresh, mechanical and durability properties of the designed concrete mixes were tested and compared to those of the correspondent Ordinary Portland cement (OPC) concrete. The results showed that lower binder content, given proper rheology maintained, does not involve a loss in performance. Nevertheless, LC^3 concrete mixes with a 40-75% reduction in clinker content showed comparable mechanical and durability performance against the control OPC concrete mixes. These performance indicators were then integrated into the functional unit of a cradle-to-gate life cycle assessment to compare the environmental impact of each LC^3 blend.

8.1. Introduction

We live in an unprecedented historical period in which the visual evidence of environmental issues caused by human activity cannot be ignored. It is a global mission to reduce CO_2 emissions as quickly and significantly as possible, and the construction sector could play a key role in this.
Indeed, it is responsible for 20% of global annual CO_2 emissions and the search for more sustainable construction technologies and materials would contribute strongly to the decarbonization targets set by 2050. This need is even more urgent given the economic growth and, consequently, urbanization demand in emergent countries such as India, Latin America and Africa. [1]

Historically, concrete was set as the most widely used construction material because of its unrivalled versatility and properties. For the same reasons, it is expected to be used to meet the growing demand for buildings and structures in emerging countries. Concrete is cheap, easily handled by

low-skilled workers, based on largely available raw materials, and with good mechanical and durability properties. In addition, it is versatile and can be used to manufacture structural elements of various geometries both on-site and precast. The ability to produce modular structural elements such as concrete bricks and blocks is particularly suitable for simple and rapid construction techniques, such as housing buildings, and where labor is a more convenient option than machinery. Although concrete is intrinsically one of the most sustainable construction materials (low kg of CO_2 embodied per kg of material), the demand for large quantities makes it a large contributor to CO_2 emissions. 90% of concrete emissions are due to just one of its components, i.e., the clinker, which contributes to 5-8% of global CO_2 emissions. [1-4]

The solution to the problem involves a multi-level approach: reducing the clinker content in cement, the cement content in concrete, and the concrete content in structures. LMC (Laboratory of Construction Materials) group of the École Polytechnique Fédérale de Lausanne is a pioneer of this approach and, since 2004 in collaboration with UCLV in Cuba, has developed the breakthrough LC^3 (limestone calcined clay cement) technology.
LC^3 is a sustainable cementitious binder that cuts up to 50% clinker (LC^3-50) by introducing calcined clays and limestones. This is the most promising and ready-to-use solution toward sustainability without penalizing the structural performance and durability of the final concrete. Other binders aim to reduce the clinker content by using waste materials such as slags, fly ash, etc., but these are in limited quantities and in depletion, so they cannot provide a long-term solution. In contrast, the major plus of LC^3 is the widespread availability of clays and limestones worldwide. Indeed, they make up most of the earth's crust and are especially abundant in the Global South areas where economic growth is occurring.
Given its low porosity, the use of LC^3 in concrete results in good resistance to weathering, such as permeability, sorptivity, chloride ions penetration and sulphate attack. Thus, it is particularly suitable for exposed marine, groundwater, and damp-proof applications. It allows an extraordinary binding capacity and plasticity, which are ideal for indoor and outdoor plaster and mortar applications. Finally, LC^3 has a highly recognizable and impactful color, typically from brick-red to pale pink, which derives from red clays. Although this could be an added architectural aesthetic property, the standard gray color of ordinary Portland cement can be obtained.
LC^3 was included in 2021 in the European cement standard EN-197-5 and efforts are currently being spent to include its use in concrete standards. [1-4]

At present, there are over 25 applications at different scales for LC^3 use. Real-scale houses have been built in Cuba and India using modular construction elements such as bricks, blocks and tiles. In India, a masonry house made with 98% LC^3 was built and allowed to save 15.5 t of CO_2 the equivalent of 10 passengers flying from Switzerland to South Africa. LC^3 precast blocks were employed to build the Swiss Embassy in Delhi. In Latin America, several applications have been built. Among those applications are an LC^3-house in Santa Clara and a pavement at UCLV in Cuba. Cement companies are embracing the change and welcoming this new sustainable cement. In fact, it not only allows the production of more sustainable and marketable products but also reduces the energy costs of the cement production process. The first clinker rotary kilns have already been converted to calciners in India and Cuba, and more and more cement companies are showing interest in the change. Remarkably, the first permanent large-scale production of LC^3 has started in Colombia and chemical companies have already developed admixtures specifically for LC^3. The benefits of using LC^3 are being disseminated worldwide at all levels, i.e., academic, industrial and social, and given the great attention this material is receiving, we hope it will soon be applied on a large scale worldwide. [2-4]

Efforts are currently being spent to push the clinker content below 50% in LC^3 and reduce the CO_2 emissions related to the final concrete structure (reduce the cement in concrete and the concrete in the structure). Large-scale tests and long-term durability tests on LC^3 structural concrete are also underway to demonstrate the feasibility of including it in the international construction codes.

To target these goals, this study aims at optimizing the mix design of LC^3 structural concrete mixes in terms of environmental impact (lower clinker in cement and lower binder in concrete) while maintaining good mechanical (elastic modulus and compressive strength) and durability (resistance to chloride penetration) performance. Previous work done on mortars at LMC showed that LC^3 25, 35, 50 and 60 can achieve (i) acceptable slump using different levels of PCE-based SP, (ii) good 7- and 28-day compressive strength, (iii) incredibly lower chloride permeability in comparison with the control OPC concrete. In this study, the clinker content was pushed below 50% in LC^3 (25% and 35%) by adding 15% and 17.5% of the calcium hydroxide to improve the binder reactivity. In this work, the same LC^3 binder compositions are involved at the concrete level as a solution to reduce the clinker content in the binder. Moreover, the binder content in the concrete was reduced below the prescribed amount of 300 kg/m^3 (250 and 275 kg/m^3) to further improve sustainability. The best LC^3 sustainable concrete mixes were identified as achieving the required performance criteria with the least environmental impact.

8.2. Materials

To lower the clinker content in the binder, four LC^3 compositions were studied, i.e., LC^3-25, LC^3-35, LC^3-50, LC^3-60 (the values represent the % of clinker in the binder mix) and compared to the control OPC. While to lower the binder content in concrete, three binder contents were considered: 250 kg/m^3, 275 kg/m^3, and 300 kg/m^3. For each binder content, trial mixes identified the minimum water-to-binder ratio (w/b) to achieve adequate slump (50 mm): w/b = 0.6 for 250 kg/m^3, w/b = 0.5 for 275 kg/m^3, w/b = 0.4 for 300 kg/m^3. The same was done to assess the optimum amount of PCE-based superplasticizer ranging between 0 and 2.5 wt.% of the cement content.

For each binder content, the binder compositions of Figure 1 were considered. In total, 15 concrete mixes were cast and tested (5 binder compositions x 3 binder contents).

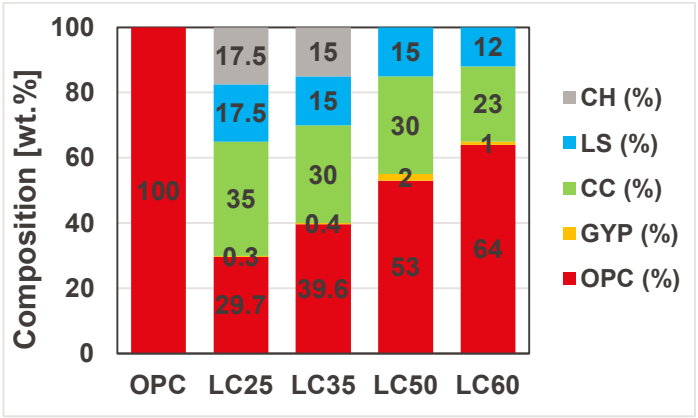

Figure 1. Binder compositions considered for the concrete mix design: OPC, $LC^3$25, $LC^3$35, $LC^3$50, $LC^3$60.

Table 1. Mix design of the concrete mixes (contents by wt.%).

	W/B	Binder (kg/m3)	% of binder by mass					
			OPC (%)	GYP (%)	CC (%)	LS (%)	CH (%)	SP (%)
OPC-0.6-250	0,6	250	100	0	0	0	0	0
LC25-0.6-250			29,7	0,3	35	17,5	17,5	1,50
LC35-0.6-250			39,6	0,4	30	15	15	1,25
LC50-0.6-250			53	2	30	15	0	0,75 1
LC60-0.6-250			64	1	23	12	0	0,75
OPC-0.5-275	0,5	275	100	0	0	0	0	0.5
LC25-0.5-275			29,7	0,3	35	17,5	17,5	1,50
LC35-0.5-275			39,6	0,4	30	15	15	1,25
LC50-0.5-275			53	2	30	15	0	1,00
LC60-0.5-275			64	1	23	12	0	1,00
OPC-0.4-300	0,4	300	100	0	0	0	0	1,00
LC25-0.4-300			29,7	0,3	35	17,5	17,5	3,50
LC35-0.4-300			39,6	0,4	30	15	15	2,50
LC50-0.4-300			53	2	30	15	0	2,23
LC60-0.4-300			64	1	23	12	0	2,00
	0.4	250	53	2	30	15	0	1.25

The following components were considered for the preparation of the concrete mixes:

- Commercial OPC-CEMI 42.5 from Holcim (Holcim Normo4),
- PCE-based SP from Sika specific for LC^3 (Sika Viscocrete – 1 LC^3, Sika Schweiz AG),
- Calcined Clay from HeidelbergCement, 50% kaolinitic content,
- Limestone from OMYA (Calcium carbonate, $CaCO_3$),
- Gypsum ≥98% from Carl Roth GmbH (Calcium sulphate dihydrate, $CaSO_4\,2H_2O$),
- Commercial pure calcium hydroxide, 95% from abcr GmbH ($Ca(OH)_2$),
- Natural crushed aggregates for concrete from Bioley (0/4 mm, 3/8 mm, 8/15 mm, 15/32 mm; Figure 2b). The aggregates were stored in silos to prevent contamination (Figure 2a).

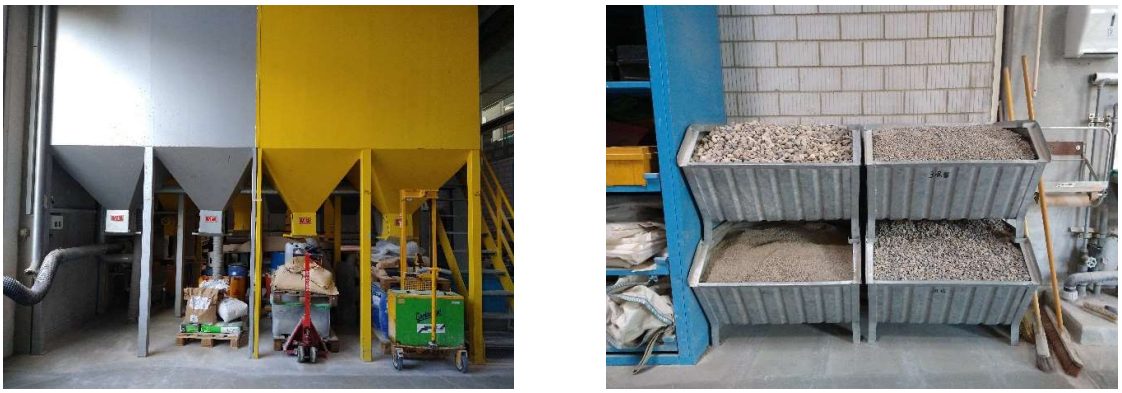

(a) (b)

Figure 2. Natural crushed aggregate for concrete: a) stored in silos, b) overview of the four fractions used: 0/4 mm, 3/8 mm, 8/15 mm, 15/32 mm.

Quality control and optimization of the aggregate particle size distribution

A high degree of control was maintained over the quality of the aggregates to prevent its influence on the results and thus reduce the dispersion of results (standard deviation). To do this, the aggregates were sieved (Figure 3a), washed (Figure 3b) and dried (Figure 3c).

The natural crushed aggregates available in the LMC laboratory (Figure 2) were sieved to obtain particle size fractions conforming to UNI EN 12620, i.e., 0/4, 4/8, 8/16 and 16/22.4mm. The aggregate size larger than 22.4 was eliminated to maintain a maximum aggregate size suitable for the 11cm diameter cylindrical molds. The sieving was carried out using a mechanical sieving machine and a stack of 45mm-diameter sieves of decreasing mesh size from top to bottom (Figure 3a). The sieving was run for 20 min with a load of 10 kg of aggregate at a time. The resulting four aggregate fractions were washed on the 0.0063 mm sieve (Figure 3b) to remove fine particles (filler containing different clays) that might affect the adhesion with the binder, the aggregate mineralogical composition, and the concrete workability. Lastly, the aggregates were dried overnight at 110°C in a ventilated oven to control their moisture content (Figure 3c).

(a) (b) (c)

Figure 3. Quality control of the aggregates: a) mechanical sieving, b) washing on a 0.063 mm sieve, c) drying.

To minimize the binder content in the concrete, the optimum relative proportion of coarse aggregates (4/8, 8/16, 16/22.4 mm) allowing for maximum packing with a prevalence of larger particles as possible was sought. Indeed, as the size of the aggregates increases, the specific surface area to be covered with binder decreases. The compliance with the ASTM C33 tolerances in Figure 4 was checked to optimize the packing of the coarse fraction, While, to select the optimized relative proportion between the aggregate fractions 4/8, 8/16, 16/22.4 mm, an excel sheet was designed comprising all possible permutations and percentage combinations of the fractions that would meet the tolerances of the ASTM C33. As a result, the best combination was 25:35:40 (%passing, 4/8mm:8/16mm:16/22.4mm). The particle size distribution of the optimized coarse aggregate fractions (≥ 4mm) is showed in Figure 4 as compared to the tolerances prescribed by the ASTM C33.

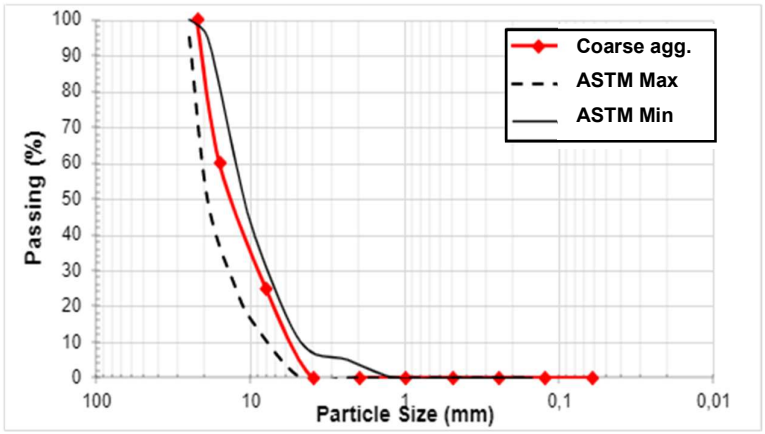

Figure 4. Optimized particle size distribution of the coarse aggregates (≥ 4mm, red line) and compliance with the ASTM C33 tolerances (black lines).

In Figure 5a, the fulfilment of the UNI 7163-72 tolerances in terms of particle size distribution was confirmed for the optimized full-graded aggregate (0/4mm and optimized ≥4mm). Significantly, Figure 5b shows the high matching of the full-graded aggregate particle size distribution with the ideal particle size distribution from Fuller. The same was observed considering the combined particle size distribution of aggregates and binder, following the ideal Bolomey's behavior. As a conclusion, the optimization of the particle size distribution of the aggregates allowed to reduce the surface area to be covered by the binder while fulfilling all the standard prescriptions and matching both the optimized particle size distribution suggested by Fuller and Bolomey.

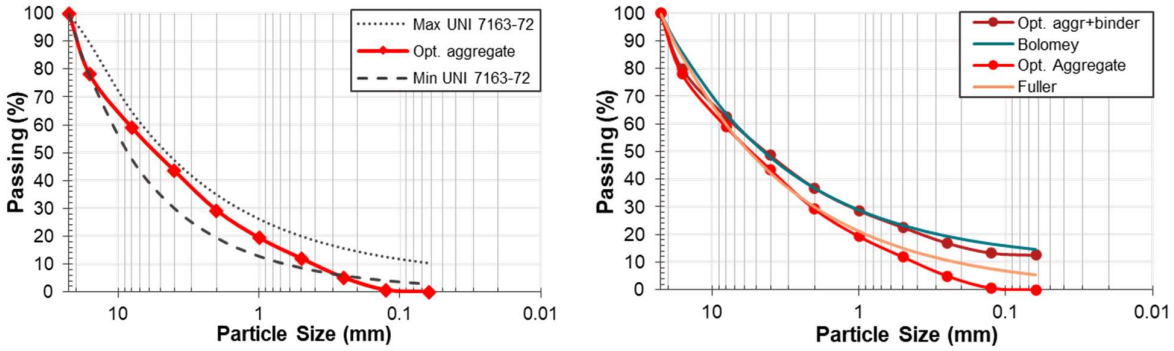

(a) (b)

Figure 5. Particle size distribution of the fully graded aggregate matching the standard prescriptions (a) and the theoretical distribution by Fuller and Bolomey (b).

Characterization of the raw materials as input for the concrete mix design

A physical characterization of the aggregates and binder components was aimed at transforming the concrete mix design from wt.% to kg/m^3 and adjusting the water content depending on the moisture content of the aggregates. The results are displayed in Table 2. The density of all components was evaluated following the ASTM C188-16 for the binder components (Figure 6) and UNI EN 1097-6 for aggregates. On the other hand, the moisture content and water absorption of aggregates were assessed following the UNI EN 1097-6 and considering a standard deviation of ±10% due to systematic error. For the aggregate characterization, a representative sampling (Figure 7b) was performed before the test using a sample splitter (Figure 7a).

Moreover, the particle size distribution of all the binder components (CEMI, calcined clay, limestone, calcium hydroxide, gypsum) was measured through a Malvern Mastersizer2000 (Malvern Instruments Ltd, Malvern UK). The results are reported in Annex B.

Table 2. Characterization of the binder components and aggregates. Density, moisture content and water absorption.

	Density		Moisture content [%]	Water absorption [%]
	Value [kg/m^3]	StD [kg/m^3]		
CEMI 42,5	3103	52		
Calcined clay	2615	16		
Limestone	2800	17		
Calcium Hydroxide	2240	13		
Gypsum	2320	14		
Sika SP	1061	6		
Sand $_{0/4}$	2338	12	0,22	1,68
Sand-Gravel $_{4/8}$	2303	12	0,24	0,81
Fine gravel $_{8/16}$	2714	14	0,20	0,65
Gravel $_{16/22.4}$	2659	13	0,09	0,79

(a) (b)

Figure 6. Density measurement of a) calcined clay, and b) cement following the standard process from ASTM C188-16.

(a) (b)

Figure 7. Representative sampling of the aggregate fractions prior to test: a) sample splitter, b) sampled fractions.

Manufacturing of the concrete specimens

For each designed concrete mix, the individual solid components, i.e., binder (Figure 8a) and aggregates (Figure 8b), were homogenized by pre-mixing in a 90L vertical mixer. The dry pre-mixing lasted 2 minutes and was operated under a plastic sheet to avoid dust pollution. Water was then added and mixed for 1 minute. Finally, the superplasticizer was added (dispersed in a part of the mixing water) and mixed for a further minute. The fresh concrete was poured in two steps into the cylindrical molds and vibrated at each step with a concrete vibrator. The molds used were disposable

cylindrical cardboard molds (11 cm diameter, 22.7 cm height) with reinforced aluminum bottom and plastic lid to prevent water evaporation (Figure 9a). The curing of the concrete samples occurred in the molds for 7 and 28 days under laboratory conditions (25 °C ± 2 °C, RH 60 % ± 5 %). For each mix of Table 1, six cylindrical concrete specimens were manufactured for a total of around 33L concrete. Four of these were tested for compressive strength and two for the rapid chloride ions penetration test.

Before the mechanical testing, the specimens were demolded and polished using an automatic polishing machine (H55-2500 Alpe, Rovereto, Italy) to rectify the samples and reduce their height to 22 cm (Figure 9a).
On the other hand, for the preparation of the specimens for the RCPT test, the cylindrical specimens were cored to a diameter of 10 cm (using a coring machine Perceuse PE-20 by Bernat Saulière Europe) and cut (using a laboratory saw to obtain slices of 5 cm thickness. The so obtained specimens (φ 10cm, h 5cm) were rinsed and dried to remove residuals, and then epoxy-coated on the side. After hardening of the epoxy resin, the specimens were polished (using a Kugel-Muller MPS-2 semi-automatic polishing machine) on the free surfaces to avoid the contamination of the epoxy resin and subsequently rinsed and dried (Figure 9b). The final specimens were vacuumed for 3 hours and then water-saturated under low-vacuum conditions for 18 ± 2 hours.

(a) (b)

Figure 8. Solid components of the concrete mix: a) LC^3 binder with CEMI in grey, calcined clay in red, limestone in white and gypsum in white-smaller quantity, b) four aggregate fractions.

(a) (b)

Figure 9. Concrete specimens for the mechanical and durability testing: a) mechanical testing specimens, from the left to the right: cylindrical specimen sealed the mold, demolded specimen, polished specimen, b) RCPT testing specimen.

8.3. Methods

The compressive strength test was carried out at 7 and 28 days with a 5000kN hydraulic press compressive strength machine by W+B (SWP-5000 by Walter + Bai ag, CH-8224 Löhningen). An adjusting-position plate was placed on the upper base of the cylinders to allow a better load distribution and correction of any surface unevenness (Figure 10a). The first of the four cylinders tested for compressive strength was used to set the maximum load value to be applied during the modulus of elasticity test. This value was evaluated as one-third of the maximum compressive strength load to ensure that the modulus of elasticity test was conducted in the material elastic range. Since the modulus of elasticity test is a non-destructive measurement, it was conducted on the second, third and fourth samples before the compressive strength test. The test was performed using a 300kN hydraulic press compressive strength machine by W+B (D-300-D by Walter + Bai ag, CH-8224 Löhningen) equipped with an adjustable top-plate to avoid unevenness and better distribute the loads. A strain-measuring equipment (Figure 10b) was placed at mid-height of the specimen and adjust to avoid pre-tensioning. After several compressive strength cycles, the software computed the elastic modulus following the ASTM C469 procedure.

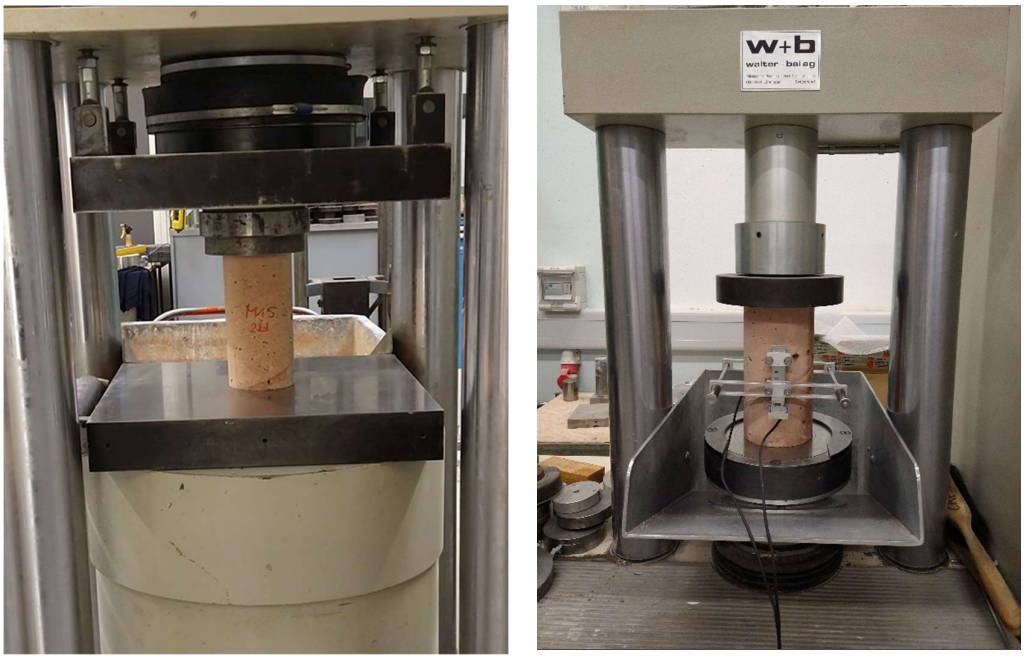

(a) (b)

Figure 10. Mechanical test on concrete specimens: a) compressive strength test, b) elastic modulus test.

A Rapid Chloride Ions Penetration test (RCPT) was carried out on 28-days concrete specimens with a two-applied voltage cell device (Figure 11) as per ASTM C1202-12. The amount of electrical current passed through the specimens over 6 hours was correlated to the concrete capability to resist to chloride ions penetration. The average and standard deviation were recorded over four measurements on different specimens.

Figure 11. Experimental set-up as per the ASTM C1202-12 for the Rapid Chloride ions Penetration Test (RCPT).

Finally, a Cradle-to-Gate scope was defined for the Life Cycle Assessment of the sustainable concrete mixes. This included all the cycle processes from the production of the concrete constituents to the delivery to the concrete batch plant until the concrete production.
The unit volume of concrete was selected as the functional unit (FU) for LCA, i.e., the LCA element responsible for quantifying the carbon footprint.
In the second stage of the LCA, an inventory database was prepared considering the Ecoinvent database and recent peer reviewed articles [5-7]. The database included the carbon footprint, or upstream impact, of each concrete element constituent (see Figure 12).
The third and final stage of the LCA estimated the environmental impact of the involved concrete mixes. This was performed by adding up the individual environmental impacts of all the associated processes.

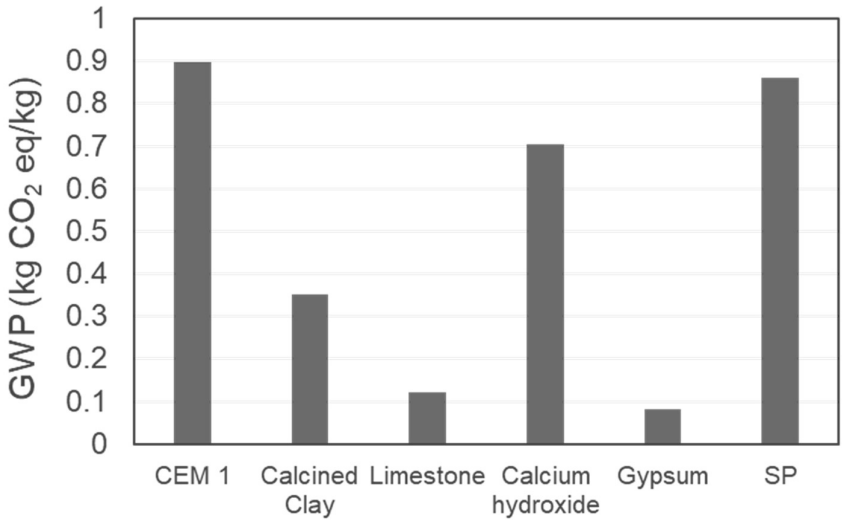

Figure 12. LCA inventory data on the environmental impact of the concrete constituents.

8.4. Results

The compressive strength values at 7- and 28-days are shown in Figure 14 ad Figure 13, respectively. As from Figure 13, all the LC^3 concrete mixes achieved good compressive strength compared to the reference OPC.

Overall, it can be observed that the concrete mixes with 250 kg/m^3 binder content achieved a compressive strength higher than 35 MPa, those with 275 kg/m^3 achieved 50 MPa and those with 300 kg/m^3 achieved 60 MPa.

For all the binder contents, the LC^3-35 and LC^3-60 mixes matched the compressive strength of the control OPC concrete. On the other hand, LC^3-50 performed comparably to OPC at 275 kg/m^3 and marginally less (max. 9%) for the other binder contents. LC^3-25 always achieved slightly lower compressive strength than the control (10-15% less). All the concrete mixes, including the LC^3-50 and LC^3-25, achieved mechanical performance suitable for structural use.

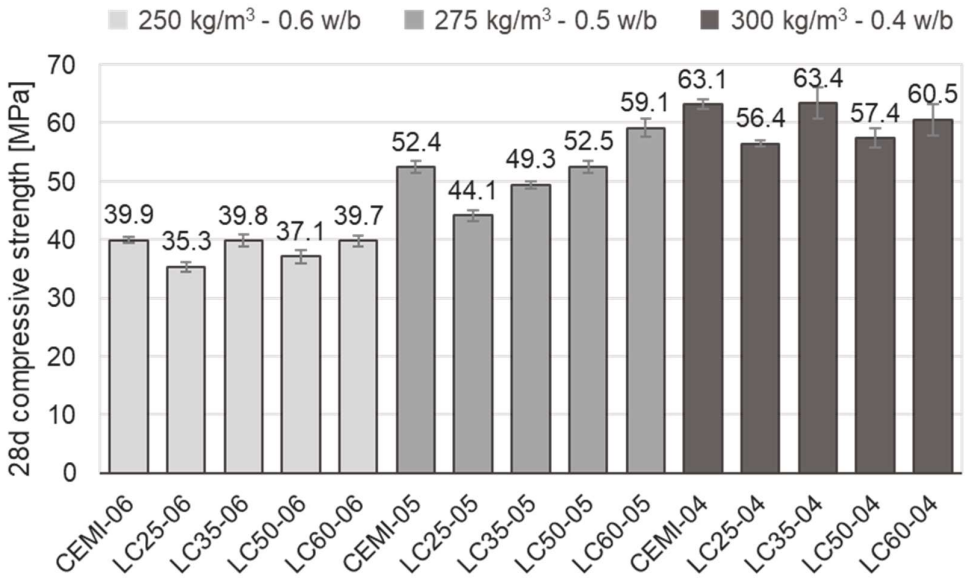

Figure 13. 28-day compressive strength.

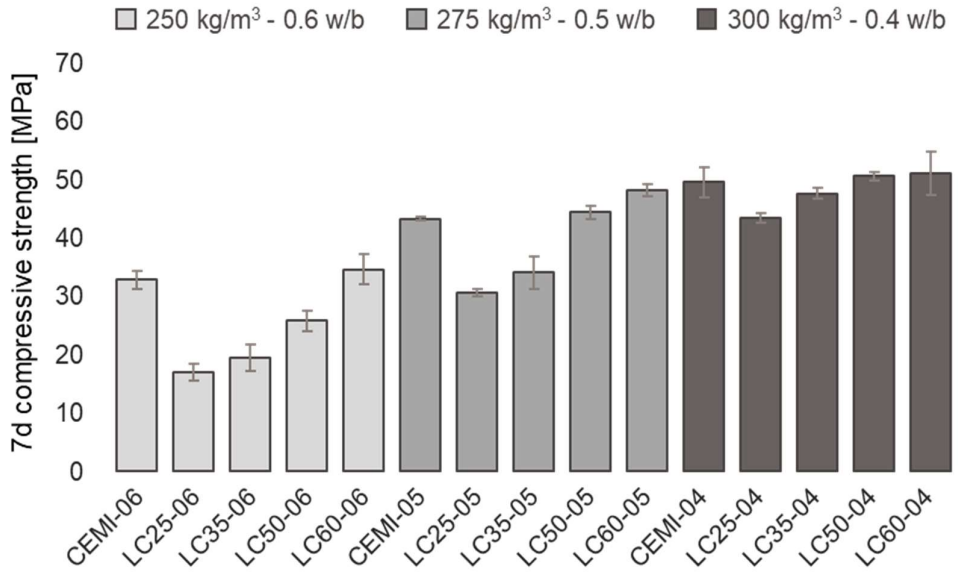

Figure 14. 7-day compressive strength.

A comparison between the compressive strengths at 7 and 28 days is shown in Figure 15 to assess the different rates of strength development over time of all concrete mixes. The higher the difference between the values at 7 and 28 days, the higher the strength development over time.
As a general trend, the LC^3 concrete mixes with lower clinker content (LC^3-25 and LC^3-35) displayed lower 7-day compressive strength compared to the control OPC and a higher strength development over time. This phenomenon is more marked at lower binder contents (250 kg/m^3 and 275 kg/m^3). On the other hand, LC^3-50 and LC^3-60 displayed early compressive strengths and strength development over time comparable to OPC concrete.

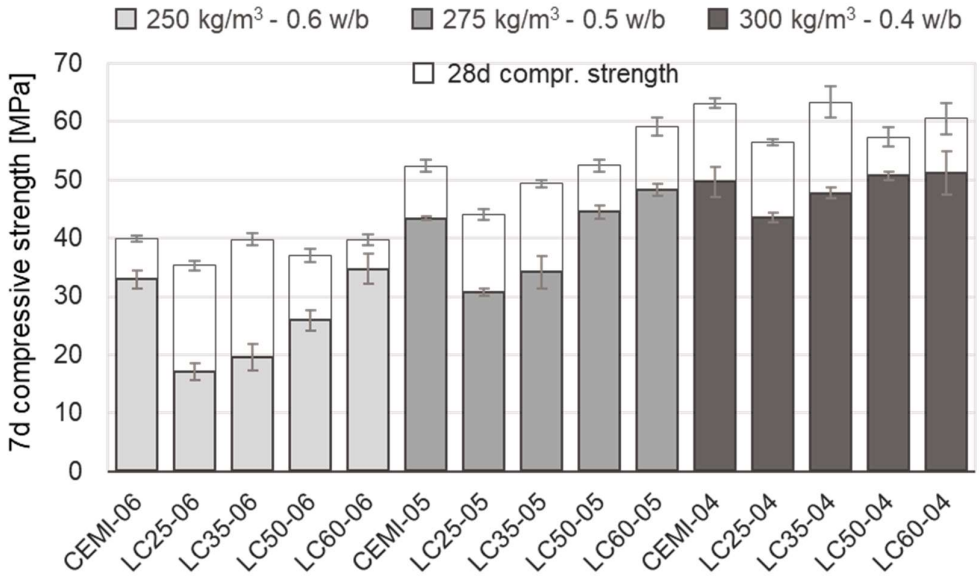

Figure 15. Development rate of compressive strength over time.

Similarly to the findings for the compressive strength, the modulus of elasticity generally increased with increasing binder content (Figure 16). However, this increase was marginal, and all the concrete mixes displayed a modulus of elasticity ranging from 30 MPa to 35 MPa. Moreover, no significant differences in the elastic modulus were registered by varying the composition of the binder, indeed OPC and all LC^3 mixes performed equally.

The results from the RCPT test are displayed in Figure 17 and compared to the limits (color ranges) given by the ASTM C1202-12, Appendix X1. As from the standard, the amount of charge passed (Coulombs) over the six hours-testing through the specimens classified the intensity of the chloride ions penetration into the concrete as:

- High: 4000 Coulombs
- Moderate: 2000-4000 Coulombs (orange area in Figure 17)
- Low: 1000-2000 Coulombs (yellow area in Figure 17)
- Very low: 1000-2000 Coulombs (green area in Figure 17)
- Negligible: <100 Coulombs

The results showed that all the LC^3 concretes had 4-5 times lower charged passed than the control OPC concrete. This matches the evidence from the literature and in mainly attributable to a refined pore structure of LC^3 compared to OPC [8]. Moreover, all the LC^3 concrete mixes were classified as having a "very low" chloride ion penetration according to the ASTM benchmark. In contrast, the OPC concrete mixes performed worse and were classified as “Moderate”. It was also observed that the LC^3-35 and LC^3-25 mixes displayed a 10-20% lower resistance to chloride penetration than LC^3-50 and LC^3-60.

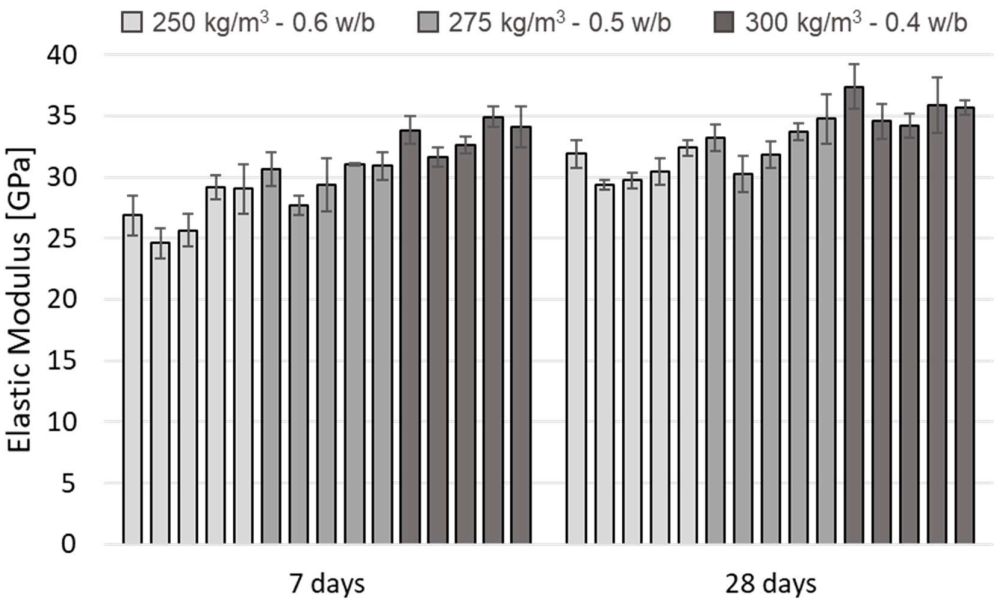

Figure 16. 7- and 28-day modulus of elasticity. For each binder content, the values in the bar chart refer, from left to right, to OPC, LC25, LC35, LC50, LC60.

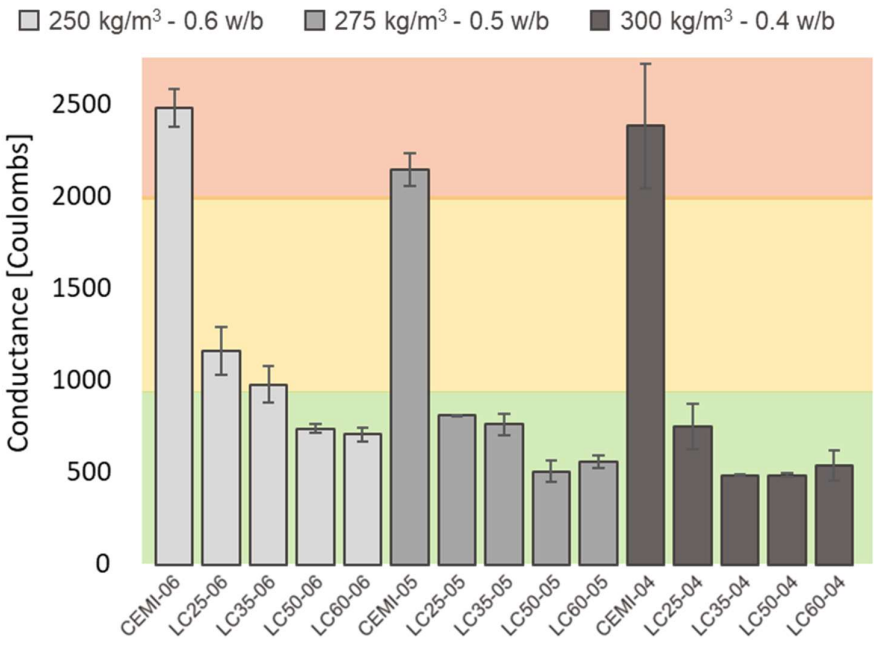

Figure 17. RCPT results against the chloride ion penetration benchmarks by ASTM C1202-12: Moderate (orange area), Low (yellow area), very low (green area).

Finally, the results obtained from the LCA analysis are shown in Figure 18. Overall, a decrease in the carbon emissions per cubic meter of concrete (GWP) was observed for decreasing binder contents. Precisely, a decrease of 8-10% in GWP was obtained for every 50 kg/m^3 decrease in the binder content.

Furthermore, considering that clinker is the concrete component with the highest carbon emissions per kg of material (Figure 12), a decrease in clinker content in the binder contributed to a decrease

in GWP. The decrease in the carbon footprint for a unit volume of concrete compared to OPC concrete was about:

- -40% in LC^3-25
- -35% in LC^3-35
- -30% in LC^3-50
- -25% in LC^3-60

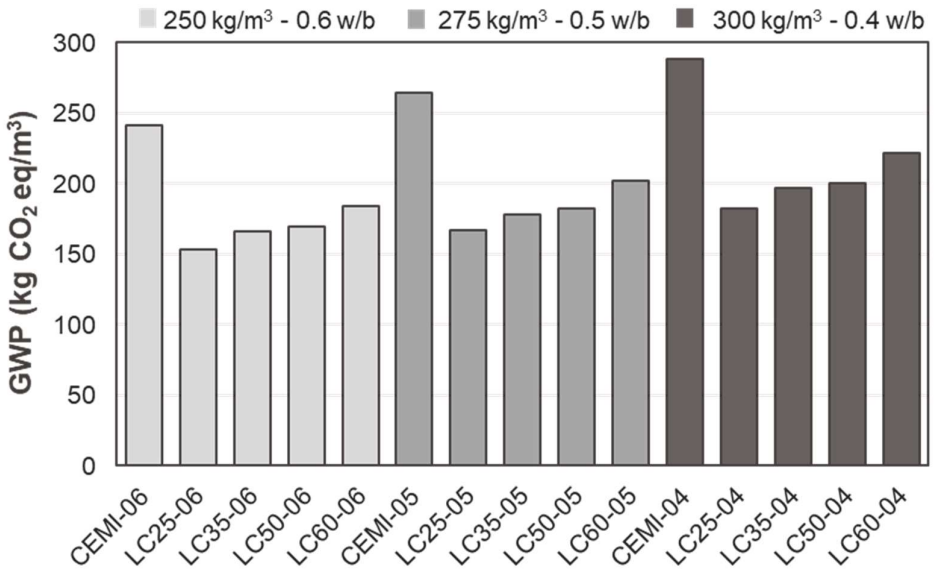

Figure 18. Carbon footprint per unit cubic meter of concrete for all the designed concrete mixes.

8.5. Conclusions

The decarbonization of the construction industry can contribute to an 8% reduction of overall CO_2 emissions by 2050 only if effective and rapid actions are adopted. There is a clear consensus that reducing the clinker content in cement along with reducing the cement content in concrete is the principal strategy to achieve this goal. Combining both premises, this study was designed to further reduce the carbon footprint of the most promising and ready-to-use sustainable LC^3 binder (Limestone Calcined Clay Cement) and of LC^3 structural concrete.

To lower the clinker content in the binder, four LC^3 compositions were studied, i.e., LC^3-25, LC^3-35, LC^3-50, LC^3-60 (the values represent the % of clinker in the binder mix) and compared to the control OPC. While to lower the binder content in concrete, three binder contents were considered: 250 kg/m^3, 275 kg/m^3, 300 kg/m^3. For the second approach, an optimization of the aggregate particle size distribution was carried out to minimize the aggregate surface area to be covered by the binder and maximize the aggregate packing. Particular attention was paid to maintaining a high degree of cleanliness and control of aggregate size.

The mechanical results displayed that structural concretes can be produced also considering lower binder content than the minimum prescribed by the standard (300 kg/m^3). Indeed, compressive strengths of 40 MPa, 50 MPa and 60MPa were achieved using 250 kg/m^3, 275 kg/m^3 and 300 kg/m^3 respectively. Among the LC^3 mixes, LC^3-35 and LC^3-60 matched the 28-day compressive strength of OPC, while LC^3-50 and LC^3-25 were marginally lower (max 10% and 15%, respectively). Despite a lower 7-day compressive strength, LC^3-25 and LC^3-35 displayed the highest strength development rate over time.

LC^3 performed very well against the penetration of chloride ions, reaching 4-5 times enhancement compared to the OPC.
For each 50 kg/m^3 reduction in binder content, a saving of 10% in carbon emission was registered. The carbon emissions were further cut up from 25 % to 40% by replacing progressively replacing clinker from 40 wt.% to 75 wt.%.
The promising results prove the feasibility of further increasing the sustainability of LC^3 structural concrete and the necessity for an update of the construction standards to enable a more sustainable design of concrete structures. Moreover, the outcome of the present work is an empirical contribution to the concrete performance testing of novel low-carbon concretes.

References

[1] Favier A., De Wolf C., Scrivener K., Habert G., A sustainable future for the European cement and concrete industry: Technology assessment for full decarbonisation of the industry by 2050, https://doi.org/10.3929/ethz-b-000301843, 2018

[2] Martirena Hernandez J.F., Alujas A., The Dissemination of the Technology “LC3” in Latin America. Challenges and Opportunities, *Calcined Clays for Sustainable Concrete, 2020,* doi:10.1007/978-981-15-2806-4_86

[3] Bishnoi S., Maity S., Limestone Calcined Clay Cement: Opportunities and Challenges, *Calcined Clays for Sustainable Concrete. Springer Singapore, 2020*

[4] Hafez. H, Zunino F., Scrivener K., LC^3 in codes and standards, International Cement Review, CemNet.com, 11 July 2022

[5] Pillai R.G., Gettu R., Santhanam M., Rengaraju S., Dhandapani Y., Rathnarajan S. and Basavaraj A.S., 2019. Service life and life cycle assessment of reinforced concrete systems with limestone calcined clay cement (LC3). *Cement and Concrete Research*, *118*, pp.111-119.

[6] Laveglia, A., Sambataro, L., Ukrainczyk, N., De Belie, N. and Koenders, E., 2022. Hydrated lime life-cycle assessment: Current and future scenarios in four EU countries. *Journal of Cleaner Production*, *369*, p.133224.

[7] Wałach, D., Dybeł, P., Sagan, J. and Gicala, M., 2019. Environmental performance of ordinary and new generation concrete structures—a comparative analysis. *Environmental Science and Pollution Research*, *26*, pp.3980-3990.

[8] Maraghechi, H., Avet, F., Wong, H. et al. Performance of Limestone Calcined Clay Cement (LC3) with various kaolinite contents with respect to chloride transport. Mater Struct 51, 125 (2018). https://doi.org/10.1617/s11527-018-1255-3

9. Conclusions

Climate change is a phenomenon that can no longer be ignored because its effects are becoming increasingly detrimental to the man-made environment and the safety of people. The primary cause of climate change is the emission of CO_2 by human activities, and the construction sector contributes more than 20%.

To achieve the goals set by the Paris Agreement of halving carbon emissions by 2030 and reaching carbon neutrality by 2050, there is a need for fast and effective solutions to drive the construction sector toward sustainability. As a general guideline, efforts should be spent in recycling waste to minimize the natural resources exploitation, optimizing the material mechanical and durability properties as well as structural design to minimize the amount of construction materials needed and developing low-embodied GHG materials. In this framework, the present thesis work showed feasible scenarios meeting the guidelines to achieve the sustainability and decarbonization of cementitious materials for the construction sector.

For the first scenario, the exploitation of natural resources was reduced by valorizing waste as secondary raw materials for cementitious material. Different waste typologies were considered: (i) Recycled Concrete Aggregate (RCA) from Construction and Demolition waste (CDW), (ii) microfiltered wastewater from the washing of concrete mixers, (iii) cork waste from the manufacturing of cork bottle caps, (iv) microfiber textile waste from the finishing of fabrics,
The following conclusions were drawn:

- The use of waste as secondary raw material requires a preliminary thorough characterization to fully understand its behavior and impact on the fresh and hardened properties of the final cementitious material.
- An optimized mix design of the cementitious material should always be performed based on the characterization results of the waste.
- The replacement of up to 90 wt.% of natural aggregate with RCA allowed producing structural concrete with common application performances i.e., XC1 exposition class, S2 consistency class and C25/30 strength class. The results proved the necessity to re-design the Italian construction codes which currently limit to 30% the maximum replacement value.
- The use of microfiltered wastewater allowed for comparable or even enhanced workability, setting time and compressive strength than the control cementitious mortar manufactured with distilled water. The results assessed the feasibility of reusing wastewater for the manufacturing of new construction materials against less sustainable practices like discharge in surface water flows and sewage.
- Cork waste can be used up to 65 vol.% in lime-based mortars to achieve desired properties such as sustainability, lightness (-15% density), coloring, etc., without affecting workability, mechanical and thermal insulating performances. The water released over time by the cork allowed for better physical performance than expected.
- Blended textile waste microfibers were used up to 4 wt.% in Portland cement-based FRCs and resulted in increasing the maximum bending load (+320%), toughness (+715%) and thermal insulating power (doubled), while reducing the linear shrinkage (-80%) and keeping good workability. The crack-bridging effect of the microfibers provided enhanced durability and performance to the FRC. On the other hand, considering the composition of the microfibers, this solution allowed the mitigation from the environment of more than 4 kg of fibrous microplastics (almost the same number of FMPs falling in a day in Paris) per ton of cement paste, thus contributing to solving the global issue of microplastic pollution.

For the second scenario, the mechanical and durability properties of polypropylene-fiber reinforced cementitious composites (PP-FRC) were optimized by considering three easy, fast, non-chemicals

added and cost-efficient surface treatments: UV-LED, picosecond UV-LASER, and corona discharge treatments. The main results are summarized as follows:

- As from ATR-FTIR spectroscopy and contact angle measurements, all the treatments were effective in increasing the PP hydrophilicity by functionalizing the PP surface. No morphological alterations were registered.
- A novel pullout test set-up allowed to detect the impact of the improved surface functionalization on the adhesion with the cementitious matrix while avoiding the shape effect of PP-fibers. A significant enhancement in residual load and deformation energy was recorded, while a better PP-to-matrix interaction allowed for the failure mode to change from slipping from the matrix (untreated PP) to cracking in the interphase zone (treated PP).
- The results showed the feasibility of optimizing the durability and mechanical properties of PP-FRC, thus promoting PP fibers over steel fibers and fast-functionalizing treatments over chemical etchings and coatings.

For the third scenario, the viability of reducing the clinker content in cement and the cement content in concrete was investigated to reduce the carbon footprint of structural concrete. The promising findings are summarized as follows:

- Current construction codes prevent a sustainable construction practice by setting the minimum binder content to 300 kg/m^3. It was observed that also 250 kg/m^3 and 275 kg/m^3 were effective in producing structural concrete with 40 MPa and 50 MPa compressive strength respectively.
- The use of low-clinker LC^3 binders provided comparable compressive strength and elastic modulus to ordinary Portland cement (OPC) and significantly improved durability against chloride ions penetration.
- A large reduction in CO_2 emission can be achieved by reducing the binder content in concrete (-10% for each -50 kg/m^3) and the clinker content in the binder (from -25 to -40%).
- The results proved the need to update the construction standards and provide evidence of ready-to-use solutions for the decarbonization of the construction sector.

All the solutions proposed by this thesis were successful in increasing the sustainability and decarbonization of cementitious construction materials.
Nevertheless, the decarbonization goals set for the construction sector can only be achieved if all the parties of the construction sector cooperate (scientists, engineers, industries, governments and regulators). In particular, there is an urgent need to update codes to ensure that more sustainable construction practices are promoted and enabled for designers. In particular, there is a need to move towards performance-based rather than prescriptive construction codes, relying on the many experimental results provided by research.

10. Annex A – Cementitious sludges

10.1. Preparation and sampling

The sludges under investigation, Milano and Trento, were supplied in already cured blocks and slurry respectively. Therefore, to characterize them, they were dried, ground and sampled. Both samples were dried in an oven at a temperature of 105 °C for 24 hours. This resulted in sludge blocks. Subsequently, these blocks were ground by hand or using a mortar to facilitate the disintegration of the very coarse pieces. The resulting powders were dried again in an oven at 105 °C for 24 hours and later homogenized using a slow jar. Finally, a quartering was carried out to obtain statistically representative samples for each characterization technique demanded.

10.2. Results

Chemical composition

The chemical composition of the Milano and Trento sludge was studied through X-ray fluorescence (XRF) analysis, with which it was possible to qualitatively and quantitatively identify the chemical compounds contained in the samples. The instrument used was the Philips PW1480 spectrometer supplied by the Department of Chemical and Geological Sciences (DSCG) of Unimore. Table 1.1 shows the results obtained. From the comparison between Milano and Trento, it can be seen that the two compositions are very similar, especially in terms of the content of Al2O3, SiO2 and CaO, oxides characteristic of the main hydrated cement compounds. This technique provides the ten major elements. Some minor elements were detected with the EDS technique.

Table 1. Chemical composition of sludges obtained by XRF analysis.

	P.F.	Na_2O	MgO	Al_2O_3	SiO_2	P_2O_5	K_2O	CaO	TiO_2	MnO	Fe_2O_3
Milano	19.13	0.31	2.99	7.39	24.13	0.01	0.70	41.44	0.39	0.10	3.41
Trento	19.50	0.27	1.90	7.07	23.71	0.00	0.65	42.91	0.33	0.07	3.59

Mineralogical composition

The test was performed as in § 4.3. This investigation was initially conducted on the samples as supplied by the manufacturer, and differences were observed in terms of mineralogical composition (Figure 2 and Figure 3). A significant difference was noted between the Milano sludge (strongly carbonated, Figure 2) and the Trento (rich in Portlandite, Figure 3). Indeed, the main mineralogical components in the Milano sludge were Dolomite and Calcite (carbonated phases, $CaCO_3$) with traces of Quartz (SiO_2). No Portlandite ($Ca(OH)_2$) was found in the Milano sludge, hence it was considered as fully carbonated. On the other hand, the Trento sludge was mainly rich in Portlandite ($Ca(OH)_2$) with traces of Quartz (SiO_2).

This difference was attributed to the different seasoning process to which the materials were subjected. In fact, given the similarity of the two samples from a chemical point of view (§ 6.2.2), it was assumed that something happened during the seasoning process: while the Milano was supplied under open-air seasoning conditions, the Trento was in slurry form. It was concluded that a true comparison from a mineralogical point of view can only be made when the same curing process is carried out, which in this case must include preliminary air-seasoning.

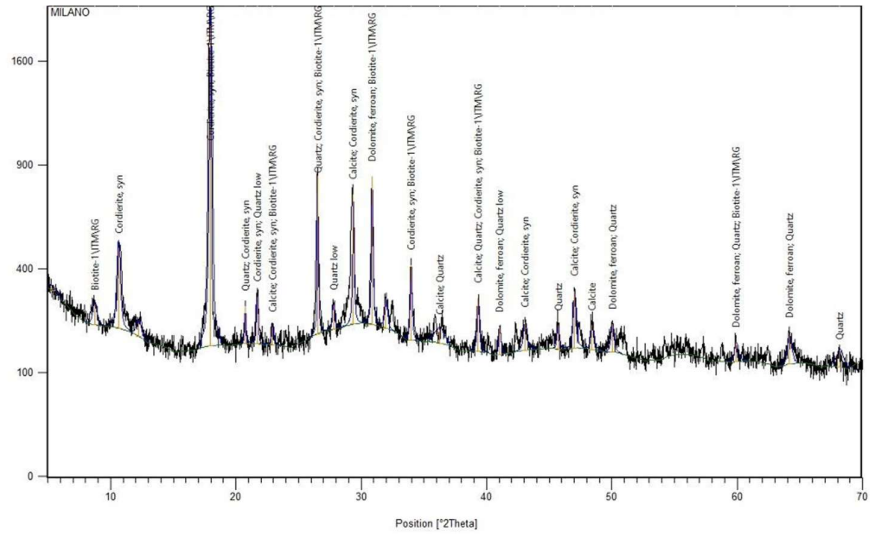

Figure 1. XRD diffractogram of Milano sludge.

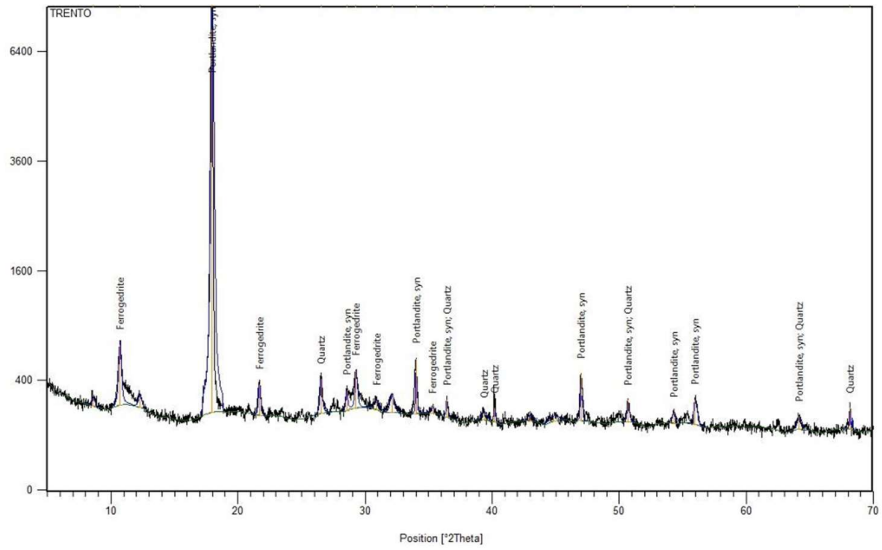

Figure 2. XRD diffractogram of Trento sludge.

The analysis of the Trento sludge was further carried out considering different air-seasoning conditions so that a later and more truthful comparison could be made with the Milano. The seasoning was carried out for two months in the open air and considering two different exposures (North and South). Therefore, XRD analyses were repeated at the end of each month. It was found that seasoning is a fundamental step as it favors the origin of carbonates crystalline phases that would otherwise not form. To better understand this aspect, please see Table 2 referring only to the Trento sample.

Table 2. Mineralogical composition of Trento sludge by varying the seasoning conditions.

Seasoning conditions	Mineralogical phases
0 months	Portlandite, $Ca(OH)_2$ Quartz, SiO_2 Clays
1 month (North)	Portlandite, $Ca(OH)_2$ Calcite, $CaCO_3$ Quartz, SiO_2 Clays
1 month (South)	Portlandite, $Ca(OH)_2$ Calcite, $CaCO_3$ Quartz, SiO_2 Clays
2 months (North)	Portlandite, $Ca(OH)_2$ Calcite, $CaCO_3$ Quartz, SiO_2 Clays
2 months (South)	Calcite, $CaCO_3$ Quartz, SiO_2 Clays

It can be observed that, compared to the as-supplied Trento sludge (0 months), air-seasoning allowed the progressive carbonation of the material.
After one month of exposure to the open air, Calcite was formed. However, since Portlandite was still present, the one-month exposition brought to just a partial carbonation. After a two-moths exposition, Portlandite was no longer detected for the sample exposed to South. This evidence shows that the North/South exposition had also an influence on the seasoning stage and carbonation of the sludge.

Scanning electron microscopy and microanalysis (ESEM-EDS)

The microstructural analysis of the sludges was carried out using scanning electron microscopy (ESEM Quanta-2000, Fei Company, Oxford Instruments) at 1600x and 3000x. The 3000x micrographs for the Milano sludge and Trento sludge are shown in Figure 4a and Figure 4b, respectively. Both samples displayed grains with a homogeneous round morphology and heterogeneous size.

In addition, a semi-quantitative chemical composition was obtained through the EDS microanalysis on three different sites of interest (Table 3 for Milano sludge and Table 4 for Trento sludge). The elements identified in the Milano sludge sample were Na, Mg, Al, Si, S, K, Ca and Fe, which, overall, are present in quantities in agreement with those obtained in the XRF chemical analysis (Table 1, § 6.2.2). Compared to XRF results, sodium oxide is not detected through EDS for the Trento sample because its content is probably below the instrumental detection limit in the selected site of interest (Table 4). The high content of Calcium, Silicon and Aluminium confirms the presence of hydrated compounds CSH and CAH, while Sulphur (S) is due to $CaSO_4$, a classic additive in Portland cement.

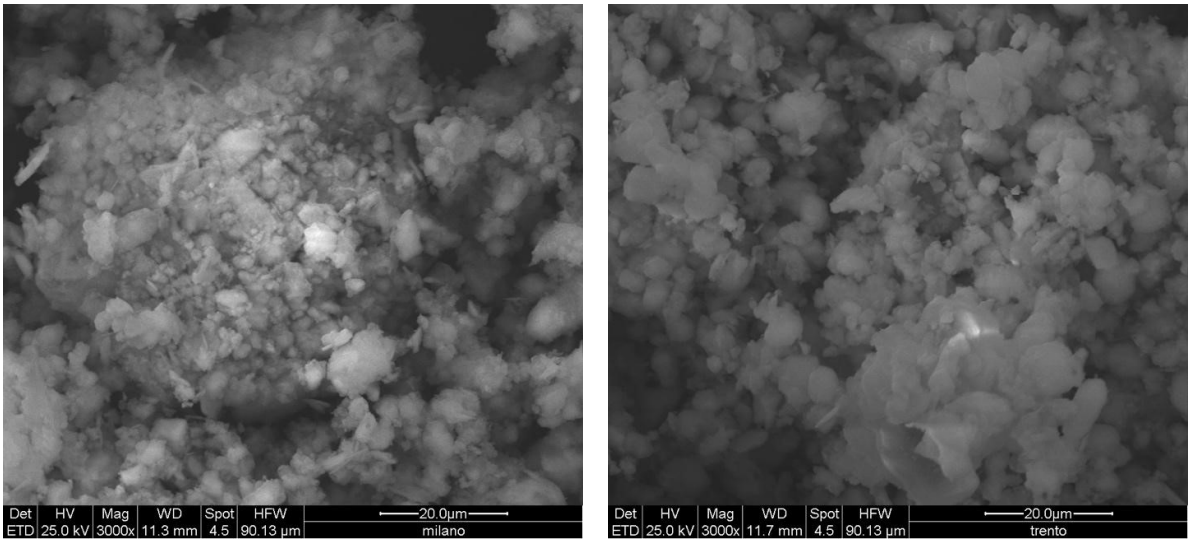

(a) *(b)*

Figure 3. Scanning electron micrographs at 3000x for a) Milano sludge and b) Trento sludge.

Table 3. EDS-microanalysis results for Milano sample.

	Na	Mg	Al	Si	S	K	Ca	Fe	Total
Spectrum 1	0.38	2.27	5.74	21.91	3.40	0.92	60.76	4.63	100.00
Spectrum 2	0.46	2.32	5.82	23.97	3.22	0.85	60.47	2.89	100.00
Spectrum 3	0.61	1.63	6.73	24.31	3.84	0.89	59.39	2.59	100.00
MEAN	**0.48**	**2.08**	**6.09**	**23.40**	**3.48**	**0.89**	**60.21**	**3.37**	**100.00**
STD. DEV.	**0.12**	**0.38**	**0.55**	**1.30**	**0.32**	**0.03**	**0.72**	**1.10**	

Table 4. EDS-microanalysis results for Milano sample.

	Na	Mg	Al	Si	S	K	Ca	Fe	Total
Spectrum 1	n.d.	1.57	4.02	20.36	1.71	0.23	69.01	3.10	100.00
Spectrum 2	n.d.	1.33	5.16	25.47	2.78	0.62	60.60	4.04	100.00
Spectrum 3	n.d.	1.52	8.15	29.56	2.15	1.54	54.02	3.06	100.00
MEAN	n.d.	**1.47**	**5.77**	**25.13**	**2.21**	**0.80**	**61.21**	**3.40**	**100.00**
STD. DEV.	n.d.	**0.13**	**2.13**	**4.61**	**0.54**	**0.68**	**7.52**	**0.56**	

Thermo-gravimetric analysis

Thermo-gravimetric analysis (TG-DTA) was involved to measure the mass change of the sample with temperature and time. In particular, it was used to provide information on physical (phase transitions, absorption, desorption) and chemical (thermal decomposition, solid-gas reactions) phenomena. The instrument used for this characterization was the TG/DTA/FTIR STA 449 F3 Jupiter

Thermal Analysis by Netzsch. A heat ramp from 25°C to 1400°C and a heating rate of 10°C/min were considered for the measure under nitrogen flux.

The results obtained for the Milano and Trento samples are shown in Figure 5 and Figure 6, respectively. In TG-DTA results, the red curve indicates how the mass of the sample changes over time as the temperature increases (TG), while the blue curve provides information on phase transitions (DSC).

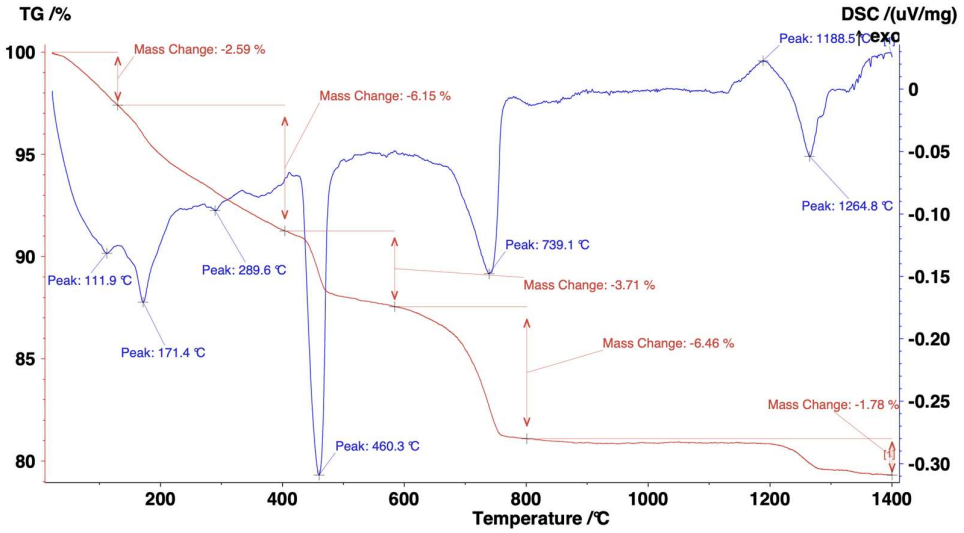

Figure 4. Thermogravimetric (TG-DTA) results for Milano sludge sample. In red curve the percentual mass loss (TG) and in blue curve the differential scanning calorimetry curve (DSC).

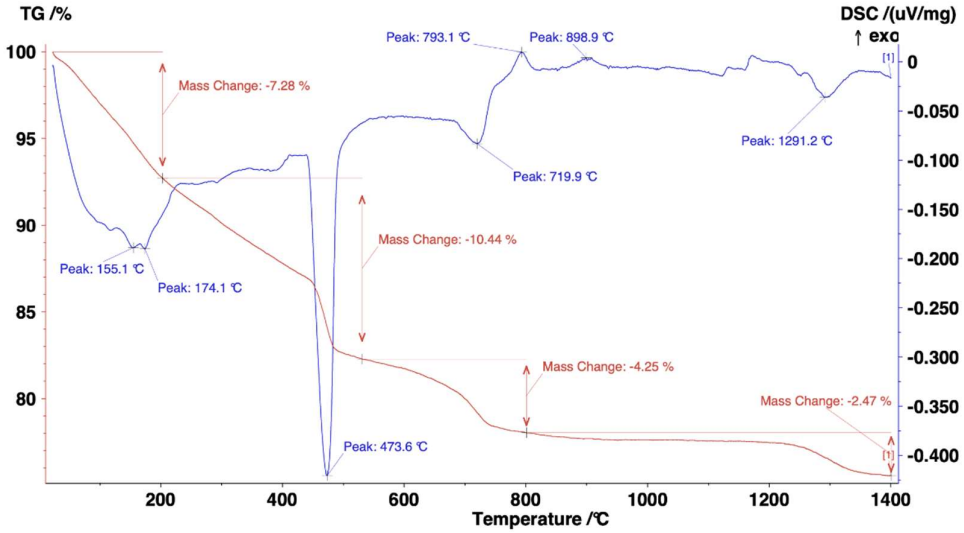

Figure 6. Thermogravimetric (TG-DTA) results for Trento sludge sample. In red curve the percentual mass loss (TG) and in blue curve the differential scanning calorimetry curve (DSC).

The analysis of the thermogravimetric results allows associating a jump in mass loss to a corresponding physic-chemical phenomenon highlighted by a peak in the DSC curve. A comparison with the literature data led to the following conclusions:

- 100-200 °C: water loss of hydrated compounds, gypsum and ettringite [20].

▪ 400-500 °C: water loss of Portlandite. The mass loss in this range is significantly higher for the Trento sample (-10.44%) as it has a high amount of Portlandite.

▪ 600-800 °C: decomposition of the carbonates (Calcite and Dolomite). The mass loss in this range is greater for the Milano sample (-6.46% as opposed to -4.25% for the Trento) as it was rich in carbonate phases, whereas they are not found in the Trento (unseasoned). The fact that the TG-DTA registered a mass loss in this temperature range even for the Trento sample means that traces of carbonates are present in it, but in too small a quantity to be seen through the mineralogical analysis.

Particle size distribution

The test was performed as in § 4.3.
The Milano sample displayed a bimodal trend. The first peak was at around 7 µm and the second at around 30 µm. While the Trento sample showed a monomodal trend with a single peak at around 9-10 µm.
A comparison of the main particle size distribution indexes (d_{10}, d_{50} and d_{90}) of the two samples is reported in Table 5. It is shown that for fine particles (diameters d_{10} and d_{50}) the two samples are very similar, while for coarser particles d_{90} the Trento sample is much finer (almost half) than the Milano. This aspect is important to consider when the powder is added to a mixture of traditional ceramic materials.

Table 5. Particle size distribution indexes of the Milano and Trento sludges.

	d_{10}	d_{50}	d_{90}
MILANO	2.550 µm	10.202 µm	44.097 µm
TRENTO	2.084 µm	8.309 µm	24.917 µm

Chlorides and sulphates content

A detection of soluble chlorides and sulphates in the Milano and Trento powders was performed to avoid degradation problems, such as expansion and cracking of concrete potentially produced by sulphates, and corrosion of reinforcement, produced by chlorides.

The sulphate and chloride content in the two sludges was evaluated to assess their possible use in the production of new concretes or cements. Two standards were considered for the test. The UNI EN 12457-2:2004 was used as a reference for the release test on sewage sludge, solid waste, and other similar matrices, while the UNI EN ISO 10304-1:2009 was used as a reference for determining dissolved anions. According to the latter, the allowed limit contents (valid for aggregates) to consider where Sulphates (SO_4^{2-}) < 250 mg/kg and Chlorides (Cl^-) < 100 mg/kg.

Table 6. Sulphate and chloride contents in the Milano and Trento sludges.

	unit	Sulphates	Chlorides
MILANO	mg/kg	271	1844
TRENTO	mg/kg	128	1335

As can be seen from Table 6, both samples exceeded the chloride content limit. On the other hand, the Milano sample also exceeded the sulphate content limit. In conclusion, the two sludges under

consideration cannot be considered as secondary raw materials for cementitious products and will not discuss in the later sections. Before considering the addition of these sludges into cementitious materials, a reduction of these values should be targeted through chemical treatment and precipitation. Otherwise, their recycling could be considered in other materials or applications.

11. Annex B – Particle size distribution of the binder components

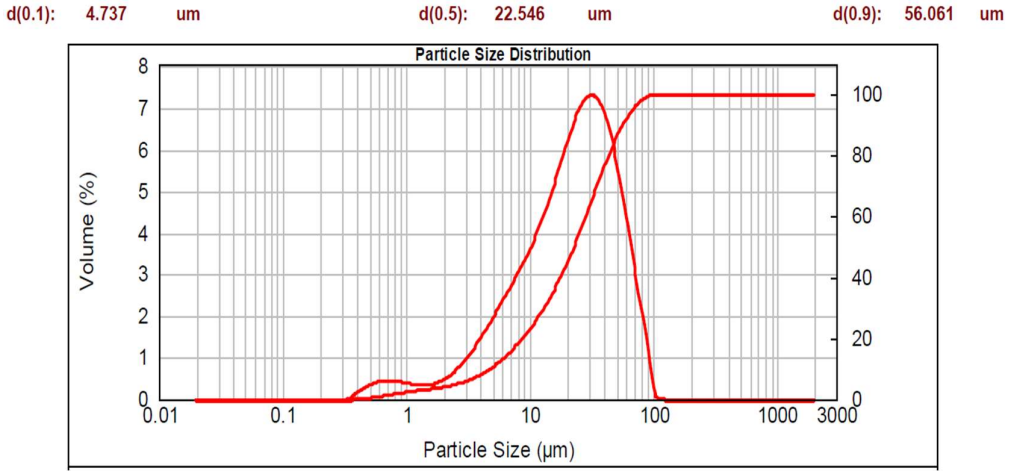

Figure 1. Particle size distribution of cement CEMI 42.5.

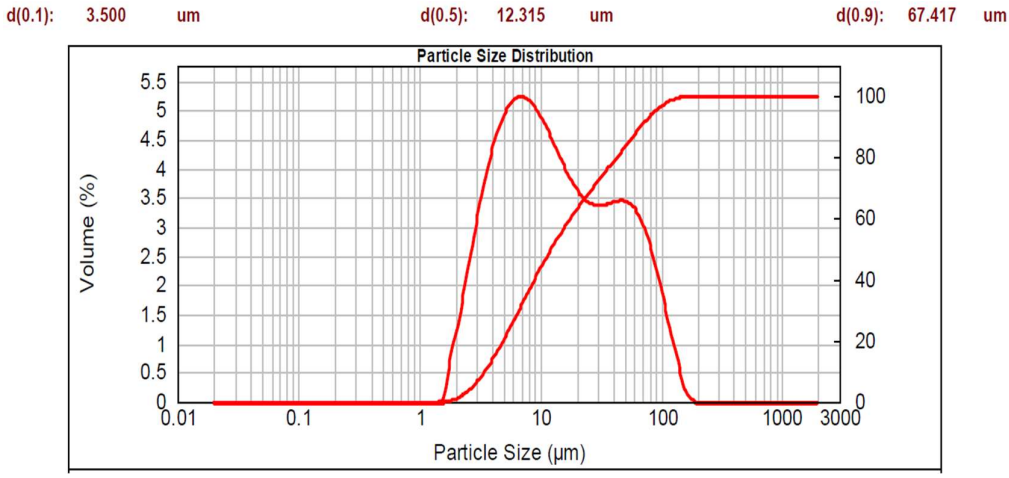

Figure 2. Particle size distribution of calcium hydroxide.

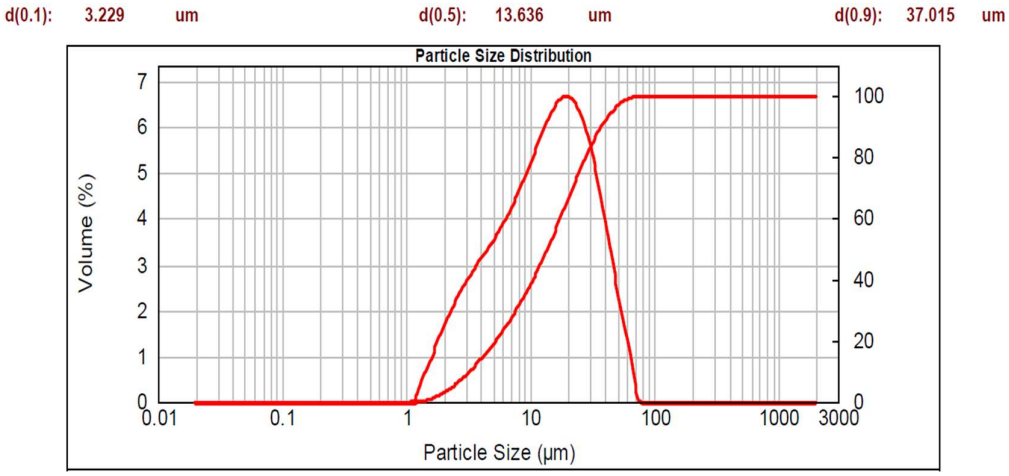

Figure 3. Particle size distribution of calcined clay.

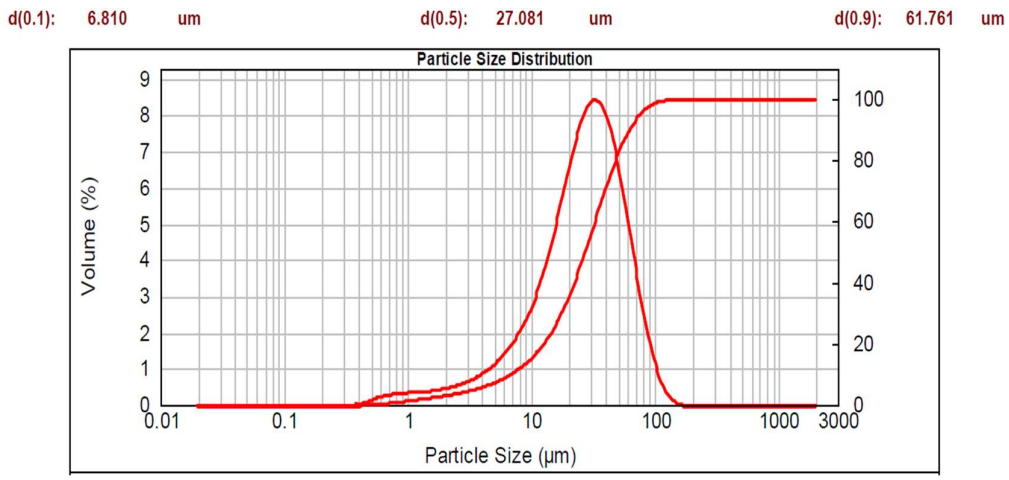

Figure 4. Particle size distribution of gypsum.

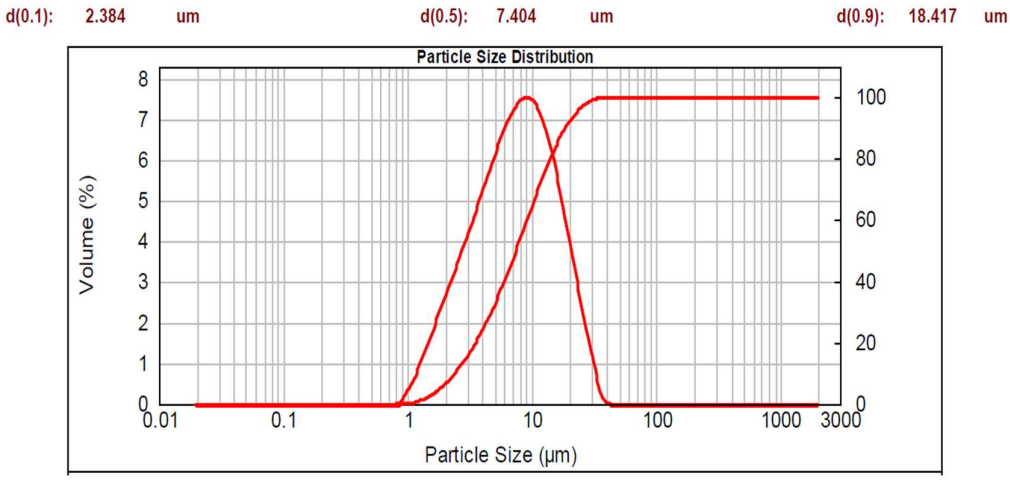

Figure 5. Particle size distribution of limestone.

Acknowledgements

My sincere thanks go to Professor Cristina Siligardi for getting me passionate about construction materials for the first time. Her dedication and passion for teaching, as well as her enthusiasm and energy in establishing collaborations with local companies were a source of inspiration for me. I thank her for having glimpsed in me the potential to undertake a doctoral program and for always supporting me on my way.
I sincerely thank Professor Paolo Pozzi for the invaluable practical knowledge he transmitted to me and for introducing me to the polymer and composite materials world. His experience and strong collaboration with companies allowed me to broaden my knowledge, curiosity and interdisciplinarity attitude.
I thank Prof. Siligardi and Prof. Pozzi for reposing great trust in my capabilities by leaving me free to build my own path. While supporting me at every step of the way, the independence they gave me provided me with a lot of awareness and responsibility and directly exposed me to the possibility of managing projects with companies and other research groups. Both of them have been reference points for my journey and I thank them for supporting each of my choices and helping me to shape my academic path.

I thank my colleagues Camila, Caterina, Erika, Marco, Mariangela, and Paola for sharing these three years of research, knowledge and personal growth.

I sincerely thank prof. Karen Scrivener from LMC, EPFL (Lausanne) for giving me the incredible opportunity to join her research group and make a difference towards carbon neutrality in the construction industry. Her commitment to research and achievements are inspiring to me.

I thank all those I had the pleasure of collaborating with and learning from. Luckily, it is a long list. DIEF: Prof. L. Lanzoni, Prof. I. Lancellotti, Prof. L. Barbieri, Prof. Nobili, Dr. C. Signorini, Dr. A. Sola, Dr. F. Andreola, Dr. M. Hanuskova, Prof. Antonio Zippo, Eng. G. Pagazzi. DISMI: Prof. L. Orazi, Prof. B. Reggiani, Dr. R. Pelaccia. Kerakoll: G. Grana Castagnetti, V. Liuzzi, Dr. P. Girardello. EPFL: Dr. A.E. Teixeira Pita, Dr. Q. Wang, Dr. F. Boscaro, Dr. H. Hafez, Dr. F. Zunino, Dr. E. Bohem Couriault, M. Schneider, H. Junmei, J. E. Packham, L. Sofia, J. Dieas Rego, J. Maxwell, A. Costarella.

I thank my family for allowing me to follow my dream of studying and doing research. Their support and love, even if they are not aware of it, have always been my safe harbor in stormy times. Thank you for always believing in my potential and making me dream big.

I fondly thank my partner Xhemsi for always standing by my side, supporting and encouraging me since our very first year at university, then through our first professional experience and throughout our PhDs in different countries. His constant presence has given me strength in difficult times and the confidence to make important decisions for my future and career. Thank you for always believing in my abilities and motivating me to constantly improve my and our life.